Chapter 9

Stimulated Brillouin and Stimulated Rayleigh Scattering

9.1. Stimulated Scattering Processes

We saw in Section 8.1 that light scattering can occur only as the result of fluctuations in the optical properties of a material system. A light-scattering process is said to be *spontaneous* if the fluctuations (typically in the dielectric constant) that cause the light-scattering are excited by thermal or by quantum-mechanical zero-point effects. In contrast, a light-scattering process is said to be *stimulated* if the fluctuations are induced by the presence of the light field. Stimulated light scattering is typically very much more efficient than spontaneous light scattering. For example, approximately one part in 10^5 of the power contained in a beam of visible light would be scattered out of the beam by spontaneous scattering in passing through 1 cm of liquid water.* In this chapter, we shall see that when the intensity of the incident light is sufficiently large, essentially 100% of a beam of light can be scattered in a 1-cm path as the result of stimulated scattering processes.

In the present chapter we study stimulated light scattering resulting from induced density variations of a material system. The most important example of such a process is stimulated Brillouin scattering (SBS), which is illustrated schematically in Fig. 9.1.1. This figure shows an incident laser beam of frequency ω_L scattering from the refractive index variation associated with a sound wave of frequency Ω. Since the acoustic wavefronts are moving away from the incident laser wave, the scattered light is shifted downward in frequency to the Stokes frequency $\omega_S = \omega_L - \Omega$. The reason why this interaction can lead to stimulated light scattering is that the interference of the laser

* Recall that the scattering coefficient R is of the order of 10^{-6} cm^{-1} for water.

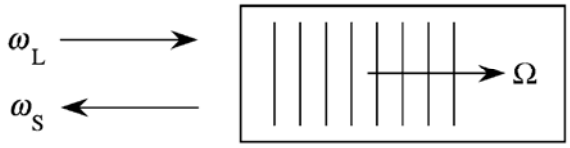

FIGURE 9.1.1 Stimulated Brillouin scattering.

and Stokes fields contains a frequency component at the difference frequency $\omega_L - \omega_S$, which of course is equal to the frequency Ω of the sound wave. The response of the material system to this interference term can act as a source that tends to increase the amplitude of the sound wave. Thus the beating of the laser wave with the sound wave tends to reinforce the Stokes wave, whereas the beating of the laser wave and Stokes waves tends to reinforce the sound wave. Under proper circumstances, the positive feedback described by these two interactions leads to exponential growth of the amplitude of the Stokes wave. SBS was first observed experimentally by Chiao *et al.* (1964).

There are two different physical mechanisms by which the interference of the laser and Stokes waves can drive the acoustic wave. One mechanism is electrostriction—that is, the tendency of materials to become more dense in regions of high optical intensity; this process is described in detail in the next section. The other mechanism is optical absorption. The heat evolved by absorption in regions of high optical intensity tends to cause the material to expand in those regions. The density variation induced by this effect can excite an acoustic disturbance. Absorptive SBS is less commonly used than electrostrictive SBS, since it can occur only in lossy optical media. For this reason we shall treat the electrostrictive case first and return to the case of absorptive coupling in Section 9.6.

There are two conceptually different configurations in which SBS can be studied. One is the SBS generator shown in part (a) of Fig. 9.1.2. In this configuration only the laser beam is applied externally, and both the Stokes and acoustic fields grow from noise within the interaction region. The noise process that initiates SBS is typically the scattering of laser light from thermally generated phonons. For the generator configuration, the Stokes radiation is created at frequencies near that for which the gain of the SBS process is largest. We shall see in Section 9.3 how to calculate this frequency.

Part (b) of Fig. 9.1.2 shows an SBS amplifier. In this configuration both the laser and Stokes fields are applied externally. Strong coupling occurs in this case only if the frequency of the injected Stokes wave is approximately equal to the frequency that would be created by an SBS generator.

In Figs. 9.1.1 and 9.1.2, we have assumed that the laser and Stokes waves are counterpropagating. In fact, the SBS process leads to amplification of a

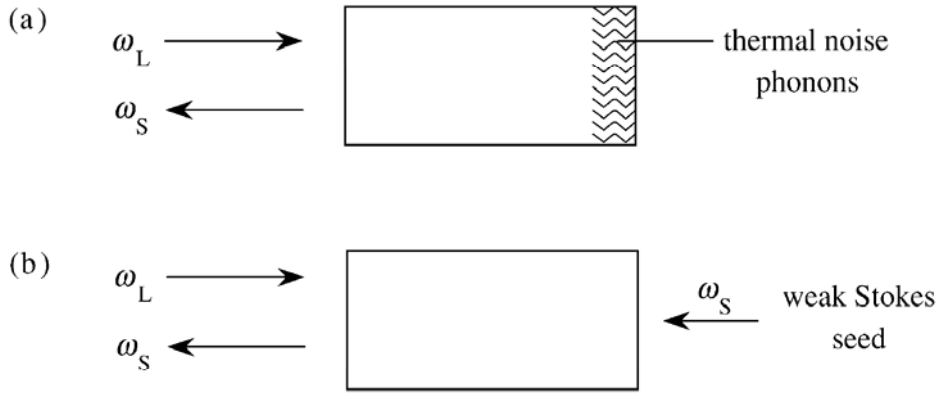

FIGURE 9.1.2 (a) SBS generator; (b) SBS amplifier.

Stokes wave propagating in any direction except for the propagation direction of the laser wave.* However, SBS is usually observed only in the backward direction, because the spatial overlap of the laser and Stokes beams is largest under these conditions.

9.2. Electrostriction

Electrostriction is the tendency of materials to become compressed in the presence of an electric field. Electrostriction is of interest both as a mechanism leading to a third-order nonlinear optical response and as a coupling mechanism that leads to stimulated Brillouin scattering.

The origin of the effect can be explained in terms of the behavior of a dielectric slab placed in the fringing field of a plane-parallel capacitor. As illustrated in part (a) of Fig. 9.2.1, the slab will experience a force tending to pull it into the region of maximum field strength. The nature of this force can be understood either globally or locally.

We can understand the origin of the electrostrictive force from a global point of view as being a consequence of the maximization of stored energy. The potential energy per unit volume of a material located in an electric field of field strength E is changed with respect to its value in the absence of the field by the amount

$$u = \tfrac{1}{2}\epsilon\epsilon_0 E^2, \tag{9.2.1}$$

where ϵ is the relative dielectric constant of the material and ϵ_0 is the permittivity of free space. Consequently the total energy of the system, $\int u\, dV$, is

* We shall see in Section 9.3 that copropagating laser and Stokes waves could interact only by means of acoustic waves of infinite wavelength, which cannot occur in a medium of finite spatial extent.

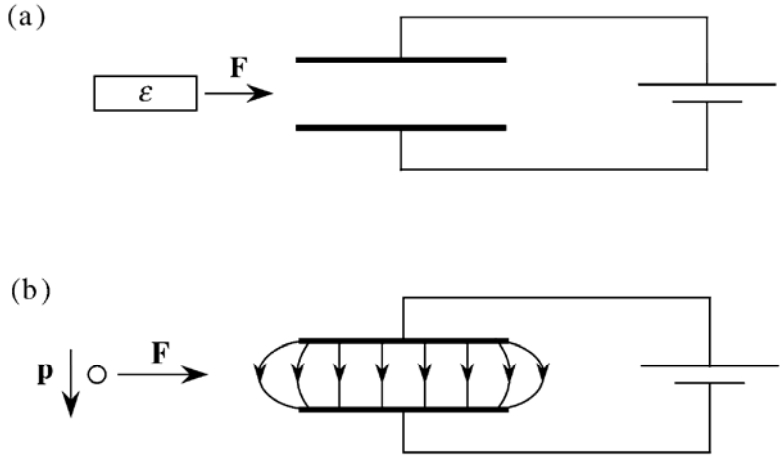

FIGURE 9.2.1 Origin of electrostriction: (a) a dielectric slab near a parallel plate capacitor; (b) a molecule near a parallel plate capacitor.

maximized by allowing the slab to move into the region between the capacitor plates where the field strength is largest.

From a microscopic point of view, we can consider the force acting on an individual molecule placed in the fringing field of the capacitor, as shown in part (b) of Fig. 9.2.1. In the presence of the field $\mathbf{E}$, the molecule develops the dipole moment $\mathbf{p} = \epsilon_0 \alpha \mathbf{E}$, where α is the molecular polarizability. The energy stored in the polarization of the molecule is given by

$$U = -\int_0^{\mathbf{E}} \mathbf{p} \cdot d\mathbf{E}' = -\int_0^{\mathbf{E}} \epsilon_0 \alpha \mathbf{E}' \cdot d\mathbf{E}' = -\tfrac{1}{2}\epsilon_0 \alpha \mathbf{E} \cdot \mathbf{E} \equiv -\tfrac{1}{2}\epsilon_0 \alpha E^2. \tag{9.2.2}$$

The force acting on the molecule is then given by

$$\mathbf{F} = -\nabla U = \tfrac{1}{2}\epsilon_0 \alpha \nabla\left(E^2\right). \tag{9.2.3}$$

We see that each molecule is pulled into the region of increasing field strength.

Next we consider the situation illustrated in Fig. 9.2.2, in which the capacitor is immersed in the dielectric liquid. Molecules are pulled from the surrounding medium into the region between the capacitor plates, thus increasing the density in this region by an amount that we shall call $\Delta\rho$. We calculate the value of $\Delta\rho$ by means of the following argument: As a result of the increase in density of the material, its dielectric constant changes from its original value ϵ to the value $\epsilon + \Delta\epsilon$, where

$$\Delta\epsilon = \left(\frac{\partial \epsilon}{\partial \rho}\right)\Delta\rho. \tag{9.2.4}$$

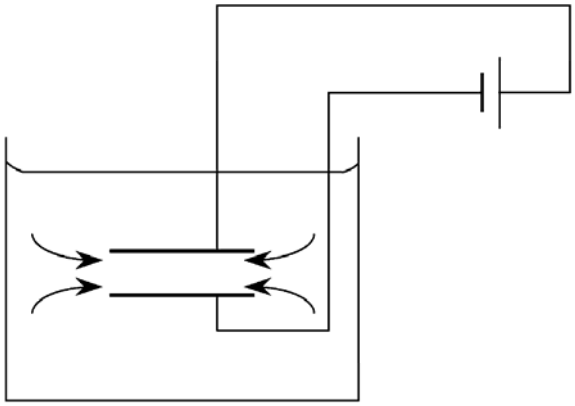

FIGURE 9.2.2 Capacitor immersed in a dielectric liquid.

Consequently, the field energy density changes by the amount

$$\Delta u = \tfrac{1}{2}\epsilon_0 E^2 \Delta\epsilon = \tfrac{1}{2}\epsilon_0 E^2 \left(\frac{\partial\epsilon}{\partial\rho}\right)\Delta\rho. \tag{9.2.5}$$

However, according to the first law of thermodynamics, this change in energy Δu must be equal to the work performed in compressing the material; the work done per unit volume is given by

$$\Delta w = p_{\text{st}}\frac{\Delta V}{V} = -p_{\text{st}}\frac{\Delta\rho}{\rho}. \tag{9.2.6}$$

Here the strictive pressure p_{st} is the contribution to the pressure of the material that is due to the presence of the electric field. Since $\Delta u = \Delta w$, by equating Eqs. (9.2.5) and (9.2.6), we find that the electrostrictive pressure is given by

$$p_{\text{st}} = -\tfrac{1}{2}\epsilon_0\rho\left(\frac{\partial\epsilon}{\partial\rho}\right)E^2 \equiv -\tfrac{1}{2}\epsilon_0\gamma_e E^2, \tag{9.2.7}$$

where $\gamma_e = \rho(\partial\epsilon/\partial\rho)$ is known as the electrostrictive constant (see also Eq. (8.3.6)). Since p_{st} is negative, the total pressure is reduced in regions of high field strength. The fluid tends to be drawn into these regions, and the density increases. We calculate the change in density as $\Delta\rho = -(\partial\rho/\partial p)\Delta p$, where we equate Δp with the electrostrictive pressure of Eq. (9.2.7). We write this result as

$$\Delta\rho = -\rho\left(\frac{1}{\rho}\frac{\partial\rho}{\partial p}\right)p_{\text{st}} \equiv -\rho C p_{\text{st}}, \tag{9.2.8}$$

where $C = \rho^{-1}(\partial\rho/\partial p)$ is the compressibility. Combining this result with Eq. (9.2.7), we find that

$$\Delta\rho = \tfrac{1}{2}\epsilon_0\rho C\gamma_e E^2. \tag{9.2.9}$$

This equation describes the change in material density $\Delta\rho$ induced by an applied electric field of strength E.

The derivation of this expression for $\Delta\rho$ has implicitly assumed that the electric field E is a static field. In such a case, the derivatives that appear in the expressions for C and γ_e are to be performed with the temperature T held constant. However, our primary interest is for the case in which E represents an optical frequency field; in such a case Eq. (9.2.9) should be replaced by

$$\Delta\rho = \tfrac{1}{2}\epsilon_0 \rho C \gamma_e \langle \tilde{\mathbf{E}} \cdot \tilde{\mathbf{E}} \rangle, \tag{9.2.10}$$

where the angular brackets denote a time average over an optical period. If $\tilde{\mathbf{E}}(t)$ contains more than one frequency component so that $\langle \tilde{\mathbf{E}} \cdot \tilde{\mathbf{E}} \rangle$ contains both static components and hypersonic components (as in the case of SBS), C and γ_e should be evaluated at constant entropy to determine the response for the hypersonic components and at constant temperature to determine the response for the static components.

Let us consider the modification of the optical properties of a material system that occurs as a result of electrostriction. We represent the change in the susceptibility in the presence of an optical field as $\Delta\chi = \Delta\epsilon$, where $\Delta\epsilon$ is calculated as $(\partial\epsilon/\partial\rho)\Delta\rho$, with $\Delta\rho$ given by Eq. (9.2.10). We thus find that

$$\Delta\chi = \tfrac{1}{2}\epsilon_0 C \gamma_e^2 \langle \tilde{\mathbf{E}} \cdot \tilde{\mathbf{E}} \rangle. \tag{9.2.11}$$

For the present, let us consider the case of a monochromatic applied field

$$\tilde{\mathbf{E}}(t) = \mathbf{E} e^{-i\omega t} + \text{c.c.}; \tag{9.2.12}$$

the case in which $\tilde{\mathbf{E}}(t)$ contains two frequency components that differ by approximately the Brillouin frequency is treated in the following section on SBS. Then, since $\langle \tilde{\mathbf{E}} \cdot \tilde{\mathbf{E}} \rangle = 2\mathbf{E} \cdot \mathbf{E}^*$, we see that

$$\Delta\chi = \epsilon_0 C_T \gamma_e^2 \mathbf{E} \cdot \mathbf{E}^*. \tag{9.2.13}$$

The complex amplitude of the nonlinear polarization that results from this change in the susceptibility can be represented as $\mathbf{P} = \Delta\chi\mathbf{E}$—that is, as

$$\mathbf{P} = \epsilon_0 C_T \gamma_e^2 |\mathbf{E}|^2 \mathbf{E}. \tag{9.2.14}$$

If we write this result in terms of a conventional third-order susceptibility, defined through

$$\mathbf{P} = 3\epsilon_0 \chi^{(3)}(\omega = \omega + \omega - \omega)|\mathbf{E}|^2 \mathbf{E}, \tag{9.2.15}$$

we find that

$$\chi^{(3)}(\omega = \omega + \omega - \omega) = \tfrac{1}{3}\epsilon_0 C_T \gamma_e^2. \tag{9.2.16}$$

For simplicity, we have suppressed the tensor nature of the nonlinear susceptibility in the foregoing discussion. However, we can see from the form of Eq. (9.2.14) that, for an isotropic material, the nonlinear coefficients of Maker and Terhune (see Eq. (4.2.10)) have the form $A = C_T \gamma_e^2$ and $B = 0$.

Let us estimate the numerical value of $\chi^{(3)}$. We saw in Eq. (8.3.12) that for a dilute gas the electrostrictive constant $\gamma_e \equiv \rho(\partial\epsilon/\partial\rho)$ is given by $\gamma_e = n^2 - 1$. More generally, we can estimate γ_e through use of the Lorentz–Lorenz law (Eq. (3.8.8a)), which leads to the prediction

$$\gamma_e = \left(n^2 - 1\right)\left(n^2 + 2\right)/3. \tag{9.2.17}$$

This result shows that γ_e is of the order of unity for condensed matter. The compressibility $C_T = \rho^{-1}(\partial\rho/\partial p)$ is approximately equal to 10^{-9} $\mathrm{m}^2\,\mathrm{Nt}^{-1}$ for CS_2 and is of the same order of magnitude for all condensed matter. We thus find that $\chi^{(3)}(\omega = \omega + \omega - \omega)$ is of the order of 3×10^{-21} $\mathrm{m}^2\ \mathrm{V}^{-2}$ for condensed matter. For ideal gases, the compressibility C_T is equal to $1/p$, where at 1 atmosphere $p = 10^5$ $\mathrm{Nt/m}^2$. The electrostrictive constant $\gamma_e = n^2 - 1$ for air at 1 atmosphere is approximately equal to 6×10^{-4}. We thus find that $\chi^{(3)}(\omega = \omega + \omega - \omega)$ is of the order of 1×10^{-23} $\mathrm{m}^2\,\mathrm{V}^{-2}$ for gases at 1 atmosphere of pressure.

A very useful, alternative expression for $\chi^{(3)}(\omega = \omega + \omega - \omega)$ can be deduced from expression (9.2.16) by expressing the electrostrictive constant through use of Eq. (9.2.17) and by expressing the compressibility in terms of the material density and velocity of sound through use of Eq. (8.3.21), such that $C_s = 1/v^2\rho$. Similarly, the isothermal compressibility is given by $C_T = \gamma C_s$ where γ is the usual thermodynamic adiabatic index. One thus finds that

$$\chi^{(3)}(\omega = \omega + \omega - \omega) = \frac{\epsilon_0 \gamma}{3v^2\rho}\left[\frac{(n^2 - 1)(n^2 + 2)}{3}\right]^2. \tag{9.2.18}$$

For pulses sufficiently short that heat flow during the pulse is negligible, the factor of γ in the numerator of this expression is to be replaced by unity. As usual, the nonlinear refractive index coefficient n_2 for electrostriction can be deduced from this expression and the result $n_2 = (3/4n_0^2\epsilon_0 c)\chi^{(3)}$ obtained earlier (Eq. (4.1.19)).

In comparison with other types of optical nonlinearities, the value of $\chi^{(3)}$ resulting from electrostriction is not usually large. However, it can make an appreciable contribution to total measured nonlinearity for certain optical materials. For the case of optical fibers, Buckland and Boyd (1996, 1997) found that electrostriction can make an approximately 20% contribution to the third-order susceptibility. Moreover, we shall see in the next section that elec-

trostriction provides the nonlinear coupling that leads to stimulated Brillouin scattering, which is often an extremely strong process.

9.3. Stimulated Brillouin Scattering (Induced by Electrostriction)

Our discussion of spontaneous Brillouin scattering in Chapter 8 presupposed that the applied optical fields are sufficiently weak that they do not alter the acoustic properties of the material system. Spontaneous Brillouin scattering then results from the scattering of the incident radiation off the sound waves that are thermally excited.*

For an incident laser field of sufficient intensity, even the spontaneously scattered light can become quite intense. The incident and scattered light fields can then beat together, giving rise to density and pressure variations by means of electrostriction. The incident laser field can then scatter off the refractive index variation that accompanies these density variations. The scattered light will be at the Stokes frequency and will add constructively with the Stokes radiation that produced the acoustic disturbance. In this manner, the acoustic and Stokes waves mutually reinforce each other's growth, and each can grow to a large amplitude. This circumstance is depicted in Fig. 9.3.1. Here an incident wave of amplitude E_1, angular frequency ω_1, and wavevector $\mathbf{k}_1$ scatters off a retreating sound wave of amplitude ρ, frequency Ω, and wavevector $\mathbf{q}$ to form a scattered wave of amplitude E_2, frequency ω_2, and wavevector $\mathbf{k}_2$.†

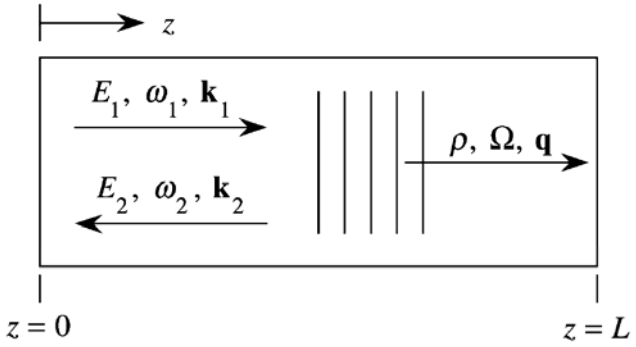

FIGURE 9.3.1 Schematic representation of the stimulated Brillouin scattering process.

* Stimulated Brillouin scattering can also be induced by absorptive effects. This less commonly studied case is examined in Section 9.6.

† We denote the field frequencies as ω_1 and ω_2 rather than ω_L and ω_S so that we can apply the results of the present treatment to the case of anti-Stokes scattering by identifying ω_1 with ω_{aS} and ω_2 with ω_L. The treatment of the present section assumes only that $\omega_2 < \omega_1$.

Let us next deduce the frequency ω_2 of the Stokes field that is created by the SBS process for the case of an SBS generator (see also part (a) of Fig. 9.1.2). Since the laser field at frequency ω_1 is scattered from a retreating sound wave, the scattered radiation will be shifted downward in frequency to

$$\omega_2 = \omega_1 - \Omega_B. \tag{9.3.1}$$

Here Ω_B is called the Brillouin frequency, and we shall now see how to determine its value. The Brillouin frequency is related to the acoustic wavevector $\mathbf{q}_B$ by the phonon dispersion relation

$$\Omega_B = |\mathbf{q}_B| v, \tag{9.3.2}$$

where v is the velocity of sound. By assumption, this sound wave is driven by the beating of the laser and Stokes fields, and its wavevector is therefore given by

$$\mathbf{q}_B = \mathbf{k}_1 - \mathbf{k}_2. \tag{9.3.3}$$

Since the wavevectors and frequencies of the optical waves are related in the usual manner, that is, by $|\mathbf{k}_i| = n\omega_i/c$, we can use Eq. (9.3.3) and the fact that the laser and Stokes waves are counterpropagating to express the Brillouin frequency of Eq. (9.3.2) as

$$\Omega_B = \frac{v}{c/n}(\omega_1 + \omega_2). \tag{9.3.4}$$

Equations (9.3.1) and (9.3.4) are now solved simultaneously to obtain an expression for the Brillouin frequency in terms of the frequency ω_1 of the applied field only—that is, we eliminate ω_2 from these equations to obtain

$$\Omega_B = \frac{\frac{2v}{c/n}\omega_1}{1 + \frac{v}{c/n}}. \tag{9.3.5}$$

However, since v is very much smaller than c/n for all known materials, it is an excellent approximation to take the Brillouin frequency to be simply

$$\Omega_B = \frac{2v}{c/n}\omega_1. \tag{9.3.6}$$

At this same level of approximation, the acoustic wavevector is given by

$$\mathbf{q}_B = 2\mathbf{k}_1. \tag{9.3.7}$$

For the case of the SBS amplifier configuration (see part (b) of Fig. 9.1.2), the Stokes wave is imposed externally and its frequency ω_2 is known *a priori*. The frequency of the driven acoustic wave is then given by

$$\Omega = \omega_1 - \omega_2, \tag{9.3.8}$$

which in general will be different from the Brillouin frequency of Eq. (9.3.6). As we shall see below, the acoustic wave will be excited efficiently under these circumstances only when ω_2 is chosen such that the frequency difference $|\Omega - \Omega_B|$ is less than or of the order of the Brillouin linewidth Γ_B, which is defined in Eq. (9.3.14b).

Let us next see how to treat the nonlinear coupling among the three interacting waves. We represent the optical field within the Brillouin medium as $\tilde{E}(z,t) = \tilde{E}_1(z,t) + \tilde{E}_2(z,t)$, where

$$\tilde{E}_1(z,t) = A_1(z,t)e^{i(k_1 z - \omega_1 t)} + \text{c.c.} \tag{9.3.9a}$$

and

$$\tilde{E}_2(z,t) = A_2(z,t)e^{i(-k_2 z - \omega_2 t)} + \text{c.c.} \tag{9.3.9b}$$

Similarly, we describe the acoustic field in terms of the material density distribution

$$\tilde{\rho}(z,t) = \rho_0 + \big[\rho(z,t)e^{i(qz-\Omega t)} + \text{c.c.}\big], \tag{9.3.10}$$

where $\Omega = \omega_1 - \omega_2$, $q = 2k_1$, and ρ_0 denotes the mean density of the medium.

We assume that the material density obeys the acoustic wave equation (see also Eq. (8.3.17))

$$\frac{\partial^2 \tilde{\rho}}{\partial t^2} - \Gamma' \nabla^2 \frac{\partial \tilde{\rho}}{\partial t} - v^2 \nabla^2 \tilde{\rho} = \nabla \cdot \mathbf{f}, \tag{9.3.11}$$

where v is the velocity of sound and Γ' is a damping parameter given by Eq. (8.3.23). The source term on the right-hand side of this equation consists of the divergence of the force per unit volume $\mathbf{f}$, which is given explicitly by

$$\mathbf{f} = \nabla p_{\text{st}}, \quad p_{\text{st}} = -\tfrac{1}{2}\epsilon_0 \gamma_e \langle \tilde{E}^2 \rangle. \tag{9.3.12}$$

For the fields given by Eq. (9.3.9), this source term is given by

$$\nabla \cdot \mathbf{f} = \epsilon_0 \gamma_e q^2 \big[A_1 A_2^* e^{i(qz-\Omega t)} + \text{c.c.}\big]. \tag{9.3.13}$$

If we now introduce Eqs. (9.3.10) and (9.3.13) into the acoustic wave equation (9.3.11) and assume that the acoustic amplitude varies slowly (if at all) in space and time, we obtain the result

$$-2i\Omega \frac{\partial \rho}{\partial t} + \big(\Omega_B^2 - \Omega^2 - i\Omega\Gamma_B\big)\rho - 2iqv^2 \frac{\partial \rho}{\partial z} = \epsilon_0 \gamma_e q^2 A_1 A_2^*, \tag{9.3.14a}$$

where we have introduced the Brillouin linewidth

$$\Gamma_B = q^2 \Gamma'; \tag{9.3.14b}$$

its reciprocal $\tau_p = \Gamma_B^{-1}$ gives the phonon lifetime.

Equation (9.3.14a) can often be simplified substantially by omitting the last term on its left-hand side. This term describes the propagation of phonons. However, hypersonic phonons are strongly damped and thus propagate only over very short distances before being absorbed.* Since the phonon propagation distance is typically small compared to the distance over which the source term on the right-hand side of Eq. (9.3.14a) varies significantly, it is conventional to drop the term containing $\partial\rho/\partial z$ in describing SBS. This approximation can break down, however, as discussed by Chiao (1965) and by Kroll and Kelley (1971). If we drop the spatial derivative term in Eq. (9.3.14a) and assume steady-state conditions so that $\partial\rho/\partial t$ also vanishes, we find that the acoustic amplitude is given by

$$\rho(z,t) = \epsilon_0 \gamma_e q^2 \frac{A_1 A_2^*}{\Omega_B^2 - \Omega^2 - i\Omega\Gamma_B}. \tag{9.3.15}$$

The spatial evolution of the optical fields is described by the wave equation

$$\frac{\partial^2 \tilde{E}_i}{\partial z^2} - \frac{1}{(c/n)^2}\frac{\partial^2 \tilde{E}_i}{\partial t^2} = \frac{1}{\epsilon_0 c^2}\frac{\partial^2 \tilde{P}_i}{\partial t^2}, \quad i = 1, 2. \tag{9.3.16}$$

The total nonlinear polarization, which gives rise to the source term in this equation, is given by

$$\tilde{P} = \epsilon_0 \Delta\chi \tilde{E} = \epsilon_0 \Delta\epsilon \tilde{E} = \epsilon_0 \rho_0^{-1} \gamma_e \tilde{\rho} \tilde{E}. \tag{9.3.17}$$

We next determine those parts of $\tilde{P}$ that can act as phase-matched source terms for the laser and Stokes fields. These contributions are given by

$$\tilde{P}_1 = p_1 e^{i(k_1 z - \omega_1 t)} + \text{c.c.}, \qquad \tilde{P}_2 = p_2 e^{i(k_2 z - \omega_2 t)} + \text{c.c.}, \tag{9.3.18}$$

where

$$p_1 = \epsilon_0 \gamma_e \rho_0^{-1} \rho A_2, \qquad p_2 = \epsilon_0 \gamma_e \rho_0^{-1} \rho^* A_1. \tag{9.3.19}$$

We introduce Eqs. (9.3.9) into the wave equation (9.3.16) along with Eqs. (9.3.18) and (9.3.19), make the slowly-varying amplitude approximation, and obtain the equations

$$\frac{\partial A_1}{\partial z} + \frac{1}{c/n}\frac{\partial A_1}{\partial t} = \frac{i\omega\gamma_e}{2nc\rho_0}\rho A_2, \tag{9.3.20a}$$

$$-\frac{\partial A_2}{\partial z} + \frac{1}{c/n}\frac{\partial A_2}{\partial t} = \frac{i\omega\gamma_e}{2nc\rho_0}\rho^* A_1. \tag{9.3.20b}$$

* We can estimate this distance as follows: According to Eq. (8.3.30), the sound absorption coefficient is given by $\alpha_s = \Gamma_B/v$, whereby in Eqs. (8.3.23) and (8.3.28) Γ_B is of the order of $\eta_s q^2/\rho_0$. For the typical values $v = 1 \times 10^3$ m/sec, $\eta_s = 10^{-9}$ N m/sec^2, $q = 4\pi \times 10^6$ m^{-1}, and $\rho_0 = 10$ kg m^{-3}, we find that $\Gamma_B = 1.6 \times 10^8$ sec^{-1} and $\alpha_s^{-1} = 6.3$ μm.

In these equations ρ is given by the solution to Eq. (9.3.14a). Furthermore, we have dropped the distinction between ω_1 and ω_2 by setting $\omega = \omega_1 \simeq \omega_2$.

Let us now consider steady-state conditions. In this case the time derivatives appearing in Eqs. (9.3.20) can be dropped, and ρ is given by Eq. (9.3.15). The coupled-amplitude equations then become

$$\frac{dA_1}{dz} = \frac{i\epsilon_0 \omega q^2 \gamma_e^2}{2nc\rho_0} \frac{|A_2|^2 A_1}{\Omega_B^2 - \Omega^2 - i\Omega\Gamma_B}, \tag{9.3.21a}$$

$$\frac{dA_2}{dz} = \frac{-i\epsilon_0 \omega q^2 \gamma_e^2}{2nc\rho_0} \frac{|A_1|^2 A_2}{\Omega_B^2 - \Omega^2 + i\Omega\Gamma_B}. \tag{9.3.21b}$$

We see from the form of these equations that SBS is a pure gain process, that is, that the SBS process is automatically phase-matched. For this reason, it is possible to introduce coupled equations for the intensities of the two interacting optical waves. Defining the intensities as $I_i = 2n\epsilon_0 c A_i A_i^*$, we find from Eqs. (9.3.21) that

$$\frac{dI_1}{dz} = -gI_1 I_2 \tag{9.3.22a}$$

and

$$\frac{dI_2}{dz} = -gI_1 I_2. \tag{9.3.22b}$$

In these equations g is the SBS gain factor, which to good approximation is given by

$$g = g_0 \frac{(\Gamma_B/2)^2}{(\Omega_B - \Omega)^2 + (\Gamma_B/2)^2}, \tag{9.3.23}$$

where the line-center gain factor is given by

$$g_0 = \frac{\gamma_e^2 \omega^2}{nvc^3 \rho_0 \Gamma_B}. \tag{9.3.24}$$

The solution to Eqs. (9.3.22) under general conditions will be described below. Note, however, that in the constant-pump limit $I_1 = \text{constant}$, the solution to Eq. (9.3.22b) is

$$I_2(z) = I_2(L) e^{gI_1(L-z)}. \tag{9.3.25}$$

In this limit a Stokes wave injected into the medium at $z = L$ experiences exponential growth as it propagates through the medium. It should be noted

TABLE 9.3.1 Properties of stimulated Brillouin scattering for a variety of materials [a]

Substance	$\Omega_B/2\pi$ (MHz)	$\Gamma_B/2\pi$ (MHz)	g_0 (m/GW)	$g_B^a(\max)/\alpha$ (cm^2/MW)
CS_2	5850	52.3	1.5	0.14
Acetone	4600	224	0.2	0.022
Toluene	5910	579	0.13	
CCl_4	4390	520	0.06	0.013
Methanol	4250	250	0.13	0.013
Ethanol	4550	353	0.12	0.010
Benzene	6470	289	0.18	0.024
H_2O	5690	317	0.048	0.0008
Cyclohexane	5550	774	0.068	
CH_4 (1400 atm)	150	10	1	
Optical glasses	15,000–26,000	10–106	0.04–0.25	
SiO_2	25,800	78	0.045	

[a] Values are quoted for a wavelength of 0.694 μm. The quantity $\Gamma_B/2\pi$ is the full width at half maximum in ordinary frequency units of the SBS gain spectrum. The last column gives a parameter used to describe the process of absorptive SBS, which is discussed in Section 9.6. To convert to other laser frequencies ω, recall that Ω_B is proportional to ω, Γ is proportional to ω^2, g_0 is independent of ω, and g_B^a (max) is proportional to ω^{-3}.

that the line-center gain factor g_0 of Eq. (9.3.24) is independent of the laser frequency ω, because the Brillouin linewidth Γ_B is proportional to ω^2 (recall that, according to Eq. (8.3.28), Γ_B is proportional to q^2 and that q is proportional to ω). An estimate of the size of g_0 for the case of CS_2 at a wavelength of 1 μm can be made as follows: $\omega = 2\pi \times 3 \times 10^{14}$ rad/sec, $n = 1.67$, $v = 1.1 \times 10^3$ m/sec, $\rho_0 = 1.26$ g/cm^3 $= 1.26 \times 10^3$ kg/m^3, $\gamma_e = 2.4$, and $\tau_p = \Gamma_B^{-1} = 4 \times 10^{-9}$ sec, giving $g_0 = 1.5$ m/GW, which in conventional laboratory units becomes $g_0 = 0.15$ cm/MW. The Brillouin gain factors and spontaneous linewidths $\Delta\nu = \Gamma_B/2\pi$ are listed in Table 9.3.1 for a variety of materials.

The theoretical treatment just presented can also be used to describe the propagation of a wave at the anti-Stokes frequency, $\omega_{aS} = \omega_L + \Omega_B$. Equations (9.3.22) were derived for the geometry of Fig. 9.3.1 under the assumption that $\omega_1 > \omega_2$. We can treat anti-Stokes scattering by identifying ω_1 with ω_{aS} and ω_2 with ω_S. We then find that the constant-pump approximation corresponds to the case $I_2(z) =$ constant and that the solution to Eq. (9.3.22a) is $I_1(z) = I_1(0)e^{-gI_2z}$. Since the anti-Stokes wave at frequency ω_1 propagates in the positive z direction, we see that it experiences attenuation due to the SBS process.

9.3.1. Pump Depletion Effects in SBS

We have seen (Eq. (9.3.25)) that, in the approximation in which the pump intensity is taken to be spatially invariant, the Stokes wave experiences exponential growth as it propagates through the Brillouin medium. Once the Stokes wave has grown to an intensity comparable to that of the pump wave, significant depletion of the pump wave must occur, and under these conditions we must solve the coupled-intensity equations (9.3.22) simultaneously in order to describe the SBS process. To find this simultaneous solution, we first note that $dI_1/dz = dI_2/dz$ and thus

$$I_1(z) = I_2(z) + C, \tag{9.3.26}$$

where the value of the integration constant C depends on the boundary conditions. Using this result, Eq. (9.3.22b) can be expressed as

$$\frac{dI_2}{I_2(I_2 + C)} = -g\,dz. \tag{9.3.27}$$

This equation can be integrated formally as

$$\int_{I_2(0)}^{I_2(z)} \frac{dI_2}{I_2(I_2 + C)} = -\int_0^z g\,dz', \tag{9.3.28}$$

which implies that

$$\ln\left\{\frac{I_2(z)[I_2(0) + C]}{I_2(0)[I_2(z) + C]}\right\} = -gCz. \tag{9.3.29}$$

Since we have specified the value of I_1 at $z = 0$, it is convenient to express the constant C defined by Eq. (9.3.26) as $C = I_1(0) - I_2(0)$. Equation (9.3.29) is now solved algebraically for $I_2(z)$, yielding

$$I_2(z) = \frac{I_2(0)[I_1(0) - I_2(0)]}{I_1(0)\exp\{gz[I_1(0) - I_2(0)]\} - I_2(0)}. \tag{9.3.30a}$$

According to Eq. (9.3.26), $I_1(z)$ can be found in terms of this expression as

$$I_1(z) = I_2(z) + I_1(0) - I_2(0). \tag{9.3.30b}$$

Equations (9.3.30) give the spatial distribution of the field intensities in terms of the boundary values $I_1(0)$ and $I_2(0)$. However, the boundary values that are known physically are $I_1(0)$ and $I_2(L)$; see Fig. 9.3.2. In order to find the unknown quantity $I_2(0)$ in terms of the known quantities $I_1(0)$ and $I_2(L)$, we set z equal to L in Eq. (9.3.30a) and write the resulting expression as follows:

$$I_2(L) = \frac{I_1(0)[I_2(0)/I_1(0)][1 - I_2(0)/I_1(0)]}{\exp\{gI_1(0)L[1 - I_2(0)/I_1(0)]\} - I_2(0)/I_1(0)}. \tag{9.3.31}$$

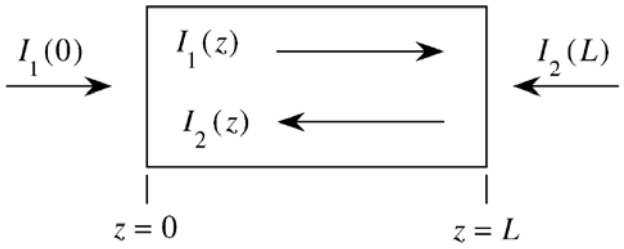

FIGURE 9.3.2 Geometry of an SBS amplifier. The boundary values $I_1(0)$ and $I_2(L)$ are known.

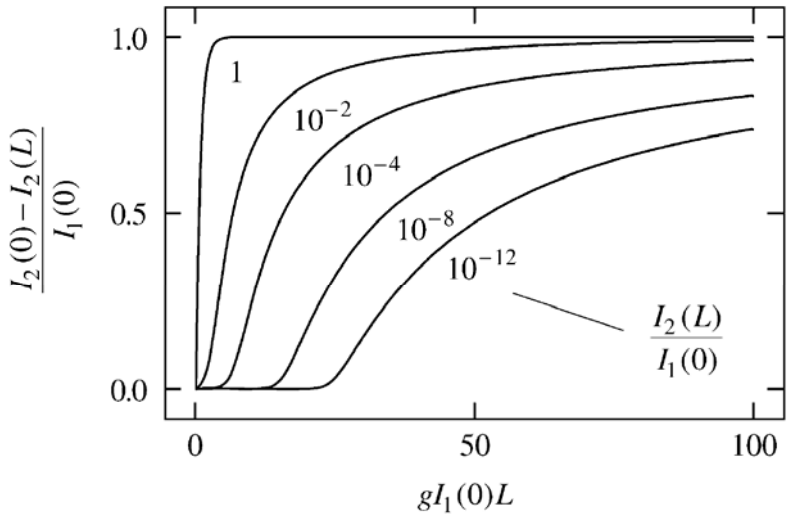

FIGURE 9.3.3 Intensity transfer characteristics of an SBS amplifier.

This expression is a transcendental equation giving the unknown quantity $I_2(0)/I_1(0)$ in terms of the known quantities $I_1(0)$ and $I_2(L)$.

The results given by Eqs. (9.3.30) and (9.3.31) can be used to analyze the SBS amplifier shown in Fig. 9.3.2. The transfer characteristics of such an amplifier are illustrated in Fig. 9.3.3. Here the vertical axis gives the fraction of the laser intensity that is transferred to the Stokes wave, and the horizontal axis is the quantity $G = gI_1(0)L$, which gives the exponential gain experienced by a *weak* Stokes input. The various curves are labeled according to the ratio of input intensities, $I_2(L)/I_1(0)$. For sufficiently large values of the exponential gain, essentially complete transfer of the pump energy to the Stokes beam is possible.

9.3.2. SBS Generator

For the case of an SBS generator, no Stokes field is injected externally into the interaction region, and thus the value of the Stokes intensity near the Stokes

input face $z = L$ is not known *a priori*. In this case, the SBS process is initiated by Stokes photons that are created by spontaneous Brillouin scattering involving the laser beam near its exit plane $z = L$. We therefore expect that the effective Stokes input intensity $I_2(L)$ will be proportional to the local value of the laser intensity $I_1(L)$; we designate the constant of proportionality as f so that

$$I_2(L) = f I_1(L). \tag{9.3.32}$$

We estimate the value of f as follows: We first consider the conditions that apply below the threshold for the occurrence of SBS, such that the SBS reflectivity $R = I_2(0)/I_1(0)$ is much smaller than unity. Under these conditions the laser intensity is essentially constant throughout the medium, and the Stokes output intensity is related to the Stokes input intensity by $I_2(0) = I_2(L)e^G$, where $G = gI_1(0)L$. However, since $I_2(L) = fI_1(0)$ (because $I_1(z)$ is constant), the SBS reflectivity can be expressed as

$$R \equiv \frac{I_2(0)}{I_1(0)} = fe^G. \tag{9.3.33}$$

Laboratory experience has shown that the SBS process displays an apparent threshold. One often defines the SBS threshold as the condition that the reflectivity R reach some prescribed value R_{th}; the value $R_{\text{th}} = 0.01$ is a convenient choice. This reflectivity occurs for the specific value G_{th} of the gain parameter $G = gI_1(0)L$. For a wide variety of materials and laser wavelengths, it is found that G_{th} typically lies in the fairly narrow range of 25 to 30. The actual value of G_{th} for a particular situation can be deduced theoretically from a consideration of the thermal fluctuations that initiate the SBS process; see, for instance, Boyd *et al.* (1990) for details. Since G_{th} is approximately 25–30, we see from Eq. (9.3.33) that f is of the order of $\exp(-G_{\text{th}})$, or approximately 10^{-12} to 10^{-11}. An order-of-magnitude estimate based on the properties of spontaneous scattering performed by Zel'dovich *et al.* (1985) reaches the same conclusion.

We next calculate the SBS reflectivity R for the general case $G > G_{\text{th}}$ (i.e., above threshold) through use of Eq. (9.3.31), which we write as

$$\frac{I_2(L)}{I_1(0)} = \frac{R(1-R)}{\exp[G(1-R)] - R}. \tag{9.3.34}$$

To good approximation, $-R$ can be dropped from the denominator of the right-hand side of this equation. In order to determine the ratio $I_2(L)/I_1(0)$ that appears on the left-hand side of Eq. (9.3.34), we express Eq. (9.3.30b) as

$$I_1(L) - I_2(L) = I_1(0) - I_2(0).$$

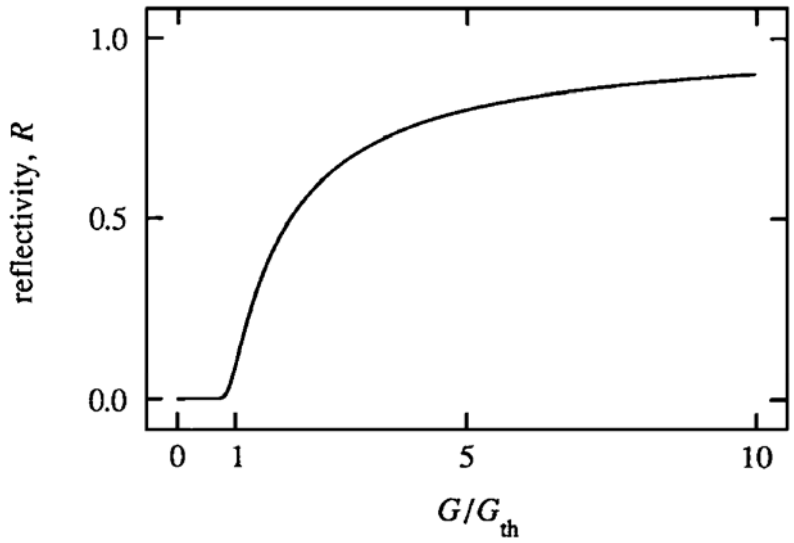

FIGURE 9.3.4 Dependence of the SBS reflectivity on the weak-signal gain $G = gI_1(0)L$.

Through use of Eq. (9.3.32) and the smallness of f, we can replace the left-hand side of this equation by $f^{-1}I_2(L)$. We now multiply both sides of the resulting equation by $f/I_1(0)$ to obtain the result $I_2(L)/I_1(0) = f(1 - R)$. This expression is substituted for the left-hand side of Eq. (9.3.34), which is then solved for G, yielding the result

$$\frac{G}{G_{\text{th}}} = \frac{G_{\text{th}}^{-1} \ln R + 1}{1 - R}, \tag{9.3.35}$$

where we have substituted G_{th} for $-\ln f$.

The nature of this solution is illustrated in Fig. 9.3.4, where the SBS reflectivity $R = I_2(0)/I_1(0)$ is shown plotted as a function of $G = gI_1(0)L$ for the value $G_{\text{th}} = 25$. We see that essentially no Stokes light is created for G less than G_{th} and that the reflectivity rises rapidly for laser intensities slightly above this threshold value. In addition, for $G \gg G_{\text{th}}$ the reflectivity asymptotically approaches 100%. Well above the threshold for SBS (i.e., for $G \gtrsim 3G_{\text{th}}$), Eq. (9.3.35) can be approximated as $G/G_{\text{th}} \simeq 1/(1 - R)$, which shows that the SBS reflectivity in this limit can be expressed as

$$R = 1 - \frac{1}{G/G_{\text{th}}} \quad (\text{for} \quad G \gg G_{\text{th}}). \tag{9.3.36}$$

Since the intensity $I_1(L)$ of the transmitted laser beam is given by $I_1(L) =$

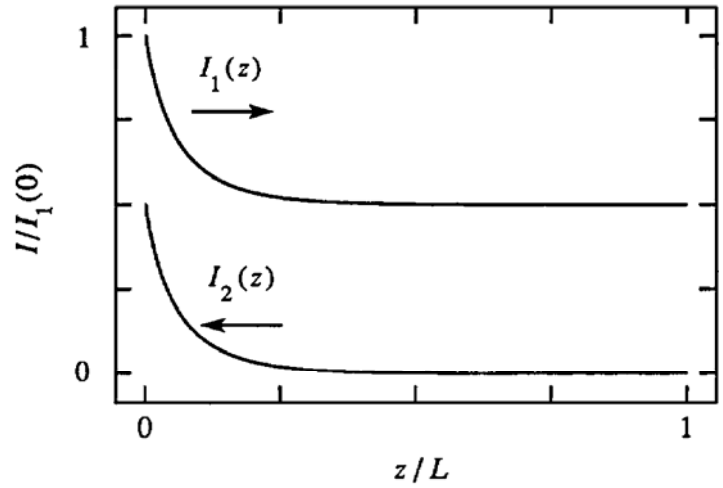

FIGURE 9.3.5 Distribution of the laser and Stokes intensities within the interaction region of an SBS generator.

$I_1(0)(1-R)$, in the limit of validity of Eq. (9.3.36) the intensity of the transmitted beam is given by

$$I_1(L) = \frac{G_{\text{th}}}{gL}; \tag{9.3.37}$$

here G_{th}/gL can be interpreted as the input laser intensity at the threshold for SBS. Hence the transmitted intensity is "clamped" at the threshold value for the occurrence of SBS.

Once the value of the Stokes intensity at the plane $z = 0$ is known from Eq. (9.3.35), the distributions of the intensities within the interaction region can be obtained from Eqs. (9.3.20). Figure 9.3.5 shows the distribution of intensities within an SBS generator.*

Let us estimate the minimum laser power P_{th} required to excite SBS under optimum conditions. We assume that a laser beam having a gaussian transverse profile is focused tightly into a cell containing a Brillouin-active medium. The characteristic intensity of such a beam at the beam waist is given by $I = P/\pi w_0^2$, where w_0 is the beam waist radius. The interaction length L is limited to the characteristic diffraction length $b = 2\pi w_0^2/\lambda$ of the beam. The product $G = gIL$ is thus given by $G = 2gP/\lambda$, and by equating this expression with the threshold value G_{th} we find that the minimum laser power

* Figure 9.3.5 is plotted for the case $G_{\text{th}} = 10$. The physically realistic case of $G_{\text{th}} = 25$ produces a much less interesting graph because the perceptible variation in intensities occurs in a small region near $z = 0$.

required to excite SBS is of the order of

$$P_{\text{th}} = \frac{G_{\text{th}}\lambda}{2g}. \tag{9.3.38}$$

For $\lambda = 1.06$ μm, $G_{\text{th}} = 25$, and $g = 0.15$ cm/MW (the value for CS_2) we find that P_{th} is equal to 9 kW. For other organic liquids the minimum power is approximately 10 times larger.

9.3.3. Transient and Dynamical Features of SBS

The phonon lifetime for stimulated Brillouin scattering in liquids is of the order of several nanoseconds. Since Q-switched laser pulses have a duration of the order of several nanoseconds, and mode-locked laser pulses can be much shorter, it is normal for experiments on SBS to be performed in the transient regime. The nature of transient SBS has been treated by Kroll (1965), Pohl *et al.* (1968), and Pohl and Kaiser (1970).

The SBS equations can be solved including the transient nature of the phonon field. This was done first by Carman *et al.* (1970) and the results have been summarized by Zel'dovich *et al.* (1985). One finds that

$$I_S(L,T) \simeq \begin{cases} I_N \exp(-2\Gamma_{\text{B}}T + 2\sqrt{2(gIL)(\Gamma_{\text{B}}T)} & \Gamma_{\text{B}}T < gIL/2, \\ I_N \exp(gIL) & \Gamma_{\text{B}}T > gIL/2. \end{cases} \tag{9.3.39}$$

Here I_N is the effective noise input that initiates the SBS process, gIL is the usual single pass gain, Γ_{B} is the phonon damping rate, and T is the laser pulse duration.

We can use this result to predict how the SBS threshold intensity I_{th} is increased through use of a short laser pulse. We require that in either limit given above the single pass amplification must equal the threshold value, which we take to be exp (25). We then find that

$$gI_{\text{th}}l = \begin{cases} (12.5 + 2\Gamma_{\text{B}}T)^2/2\Gamma_{\text{B}}T & \Gamma_{\text{B}}T < 12.5, \\ 25 & \Gamma_{\text{B}}T > 12.5. \end{cases} \tag{9.3.40}$$

This functional dependence is illustrated in Fig. 9.3.6. Note that even for laser pulses as long as twice the phonon lifetime, the threshold for SBS is raised by a factor of approximately two.

The SBS process is characterized by several different time scales, including the transit time of light through the interaction region, the laser pulse duration, and the phonon lifetime. Consequently, the SBS process can display

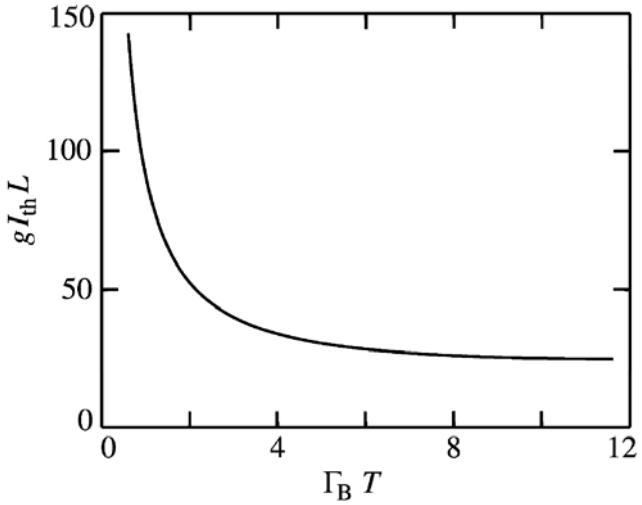

FIGURE 9.3.6 Dependence of the SBS threshold intensity I_{th} on the laser pulse duration T.

quite rich dynamical effects. One of these effects is pulse compression, the tendency of the SBS Stokes pulse to be shorter (at times very much shorter) than the incident laser pulse. This process is described in Problem 5 at the end of this chapter. When SBS is excited by a multi-longitudinal-mode laser, new types of dynamical behavior can occur. Here the various laser modes beat together leading to modulation in time of the laser intensity within the interaction region. This situation has been analyzed by Narum *et al.* (1986). In addition, the stochastic properties of SBS have been studied in considerable detail. SBS is initiated by noise in the form of thermally excited phonons. Since the SBS process involves nonlinear amplification (nonlinear because of pump depletion effects) in a medium with an effectively nonlocal response (nonlocal because the Stokes and laser fields are counterpropagating), the stochastic properties of the SBS output can be quite different from those of the phonon noise field that initiates SBS. These properties have been studied, for instance, by Gaeta and Boyd (1991). In addition, when SBS is excited by two counterpropagating pump fields, it can display even more complex behavior, including instability and chaos, as studied by Narum *et al.* (1988), Gaeta *et al.* (1989), and Kulagin *et al.* (1991).

9.4. Phase Conjugation by Stimulated Brillouin Scattering

It was noted even in the earliest experiments on stimulated Brillouin scattering (SBS) that the Stokes radiation was emitted in a highly collimated beam in the backward direction. In fact, the Stokes radiation was found to be so well

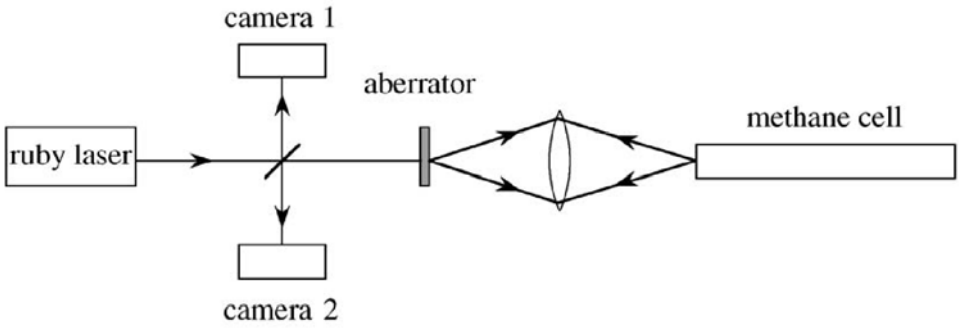

FIGURE 9.4.1 Setup of first experiment on phase conjugation by stimulated Brillouin scattering.

collimated that it was efficiently fed back into the exciting laser, often leading to the generation of new spectral components in the output of the laser (Goldblatt and Hercher, 1968). These effects were initially explained as a purely geometrical effect resulting from the long but thin shape of the interaction region.

The first indication that the backscattered light was in fact the phase conjugate of the input was provided by an experiment of Zel'dovich *et al.* (1972). The setup used in this experiment is shown in Fig. 9.4.1. The output of a single-mode ruby laser was focused into a cell containing methane gas at a pressure of 125 atmospheres. This cell was constructed in the shape of a cylindrical, multimode waveguide and served to confine the radiation in the transverse dimension. A strong SBS signal was generated from within this cell. A glass plate that had been etched in hydrofluoric acid was placed in the incident beam to serve as an aberrator. Two cameras were used to monitor the transverse intensity distributions of the incident laser beam and of the Stokes return.

The results of this experiment are summarized in the photographs taken by V.V. Ragulsky that are reproduced in Fig. 9.4.2. Part (a) of this figure shows the laser beam shape as recorded by camera 1, and part (b) shows the Stokes beam shape as recorded by camera 2. The similarity of the spot sizes and shapes indicates that the return beam is the phase conjugate of the incident beam. These highly elongated beam shapes are a consequence of the unusual mode pattern of the laser used in these experiments. Part (c) of the figure shows the spot size recorded by camera 2 when the SBS cell had been replaced by a conventional mirror. The spot size in this case is very much larger than that of the incident beam; this result shows the severity of the distortions impressed on the beam by the aberrator. Part (d) of the figure shows the spot size of the return beam when the aberrator was removed from the beam path.

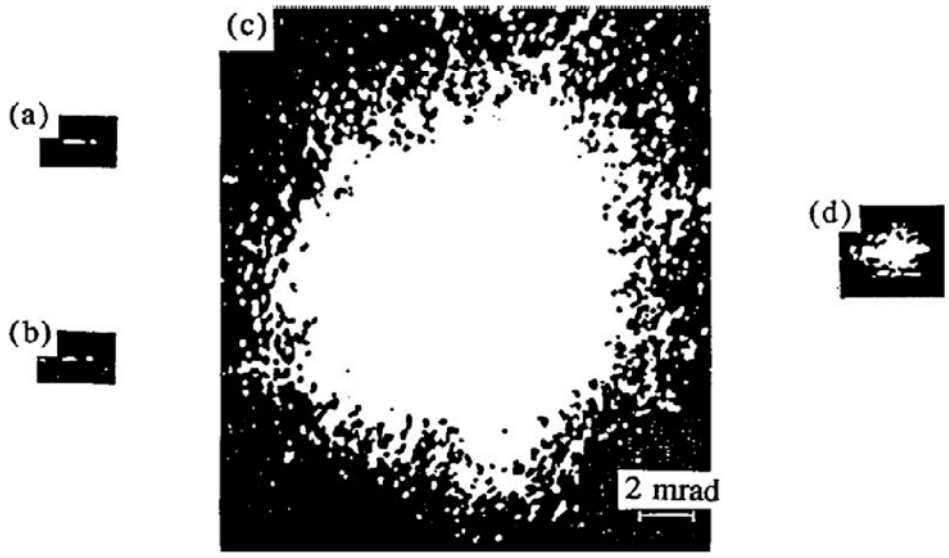

FIGURE 9.4.2 Results of the first experiment demonstrating SBS phase conjugation.

This spot size is larger than that shown in part (b). This result shows that SBS forms a more accurate conjugate of the incident light when the beam is highly distorted than when the beam is undistorted.*

The results of the experiment of Zel'dovich *et al.* are somewhat surprising, because it is not clear from inspection of the coupled-amplitude equations that describe the SBS process why SBS should lead to phase conjugation. We recall that the reason why degenerate four-wave mixing leads to phase conjugation is that the source term driving the output wave A_4 in the coupled-amplitude equations describing four-wave mixing (see, for example, Eq. (7.2.31b)) is proportional to the complex conjugate of the input wave amplitude, that is, to A_3^*. However, for the case of SBS, Eq. (9.3.21b) shows that the output wave amplitude A_2 is driven by a term proportional to $|A_1|^2 A_2$, which contains no information regarding the phase of the input wave A_1.

The reason why SBS leads to the generation of a phase-conjugate wave is in fact rather subtle (Zel'dovich *et al.*, 1972; Sidorovich, 1976). As illustrated in Fig. 9.4.3, we consider a badly aberrated optical wave that is focused into the SBS interaction region. Since the wave is highly aberrated, a highly nonuniform intensity distribution (i.e., a volume speckle pattern) is created in the focal region of the wave. Since the gain experienced by the Stokes wave depends on the local value of the laser intensity (see, for example, Eq. (9.3.22b)), a nonuniform gain distribution for the Stokes wave is therefore present in the

* The conclusion that SBS forms a better phase conjugate of an aberrated beam than of an unaberrated beam is not true in all cases, and appears to be a consequence of the details of the geometry of the experiment of Zel'dovich *et al.*

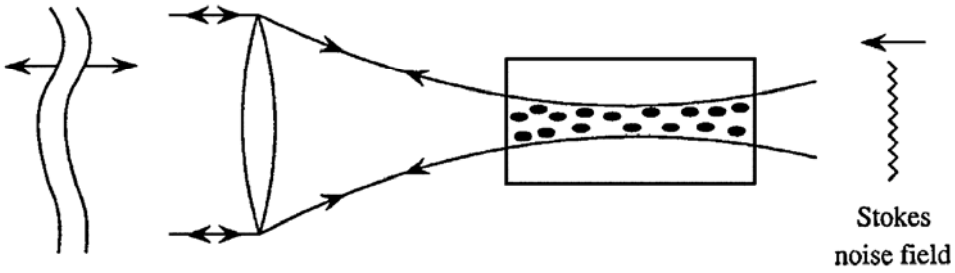

FIGURE 9.4.3 Origin of phase conjugation by SBS. The highly aberrated incident wavefront produces a highly nonuniform intensity distribution (and thus a nonuniform gain distribution) in the focal region of the lens.

focal volume. We recall that SBS is initiated by noise—that is, by spontaneously generated Stokes photons. The noise field that leads to SBS initially contains all possible spatial Fourier components. However, the portion of the noise field that experiences the maximum amplification is the portion whose intensity distribution best matches the nonuniform gain distribution. This portion of the noise field must have wavefronts that match those of the incident laser beam, and thus corresponds to the phase conjugate of the incident laser field.

In order to make this argument more precise, we consider the intensity equation satisfied by the Stokes field (see also Eq. (9.3.22b)),

$$\frac{dI_S}{dz} = -gI_L I_S. \tag{9.4.1}$$

Since we are now considering the case where I_L and I_S possess nonuniform transverse distributions, it is useful to consider the total power in each wave (at fixed z), defined by

$$P_L = \int I_L \, dA, \qquad P_S = \int I_S \, dA, \tag{9.4.2}$$

where the integrals are to be carried out over an area large enough to include essentially all of the power contained in each beam. Equation (9.4.1) can then be rewritten in the form

$$\frac{dP_S}{dz} = -g\frac{P_L P_S}{A}C, \tag{9.4.3}$$

where $A = \int dA$ and where

$$C = \frac{\langle I_L I_S \rangle}{\langle I_L \rangle \langle I_S \rangle} \tag{9.4.4}$$

represents the normalized spatial cross-correlation function of the laser and Stokes field intensity distributions. Here the angular brackets are defined so that $\langle x \rangle = \int x\, dA/A$, where x denotes I_L, I_S, or the product $I_L I_S$.

We see that the power gain experienced by the Stokes wave depends not only on the total power of the laser wave, but also on the degree of correlation between the laser and Stokes wave intensity distributions. If I_L and I_S are completely uncorrelated, so that $\langle I_L I_S \rangle = \langle I_L \rangle \langle I_S \rangle$, the correlation function C takes on the value unity. C is equal to unity also for the case in which both I_L and I_S are spatially uniform. However, if I_L and I_S are correlated, for example, because the laser and Stokes fields are phase conjugates of one another, the correlation function can be greater than unity.

A limiting case is that in which the laser field is so badly aberrated that the transverse variations in the complex field amplitude obey gaussian statistics. In such a case, the probability density function for the laser intensity is given by (see, for example, Goodman, 1985)

$$P(I) = \frac{1}{I_0} e^{-I/I_0}. \tag{9.4.5}$$

The moments of this distribution are given in general by $\langle I^n \rangle = n \langle I \rangle^n$, and in particular the second moment is given by

$$\langle I^2 \rangle = 2 \langle I \rangle^2. \tag{9.4.6}$$

For that portion of the Stokes field that is the phase conjugate of the laser field, the intensity I_S will be proportional to I_L, and we see from Eqs. (9.4.4) and (9.4.6) that C will be equal to 2. Hence, the exponential gain $G \equiv g P_L C L/A$ experienced by the phase-conjugate portion of the noise field will be two times larger than that experienced by any other mode of the noise field. Since the threshold for SBS corresponds to G of the order of 30, the phase-conjugate portion of the SBS signal at threshold will be approximately exp (15) times larger than that of any other component.

On the basis of the argument just presented, we expect that high-quality phase conjugation will occur only if a large number of speckles of the laser intensity distribution are present within the interaction volume. We now determine the conditions under which the number of speckles will be large. We assume that in the focal region the incident laser field has transverse wavefront irregularities on a distance scale as small as a. Each such region will diffract the incident beam into a cone with a characteristic angular spread of $\theta = \lambda/a$. Hence, the speckle pattern will look appreciably different after the beam has propagated through the longitudinal distance Δz such that $\theta \Delta z = a$. These considerations show that $\Delta z = a^2/\lambda$. We hence expect that SBS will

lead to a high-quality phase-conjugate signal only if the transverse extent of the interaction region is much larger than a and if the longitudinal extent of the interaction region is much longer than Δz. In addition, the quality of the phase-conjugate signal can be degraded if there is poor spatial overlap of the various spatial Fourier components of the laser beam. For example, a highly aberrated beam will spread with a large angular divergence $\theta = \lambda/a$. If those components of the beam with large divergence angle θ fail to overlap the strong central portion of the beam, they will be reflected with low efficiency, leading to a degradation of the quality of the phase-conjugation process. To avoid the possibility of such effects, SBS phase conjugation is often performed using the waveguide geometry shown in Fig. 9.4.1.

One of the applications of SBS phase conjugation is in the design of high-power laser systems. Phase conjugation can be used to correct for aberrations caused, for instance, by thermal stresses induced in the laser gain medium. One example of a high-power laser system that makes use of SBS phase conjugation to maintain control of the polarization properties of the laser output has been described by Bowers *et al.* (1997).

9.5. Stimulated Brillouin Scattering in Gases

We next consider stimulated Brillouin scattering (SBS) in gases. We saw above (Eq. (9.3.24)) that the steady-state line-center gain factor for SBS is given by

$$g_0 = \frac{\gamma_e^2 \omega^2}{\rho_0 n v c^3 \Gamma_B}, \tag{9.5.1}$$

with the electrostrictive constant γ_e given by Eq. (8.3.12) and with the Brillouin linewidth given to good approximation by (see also Eqs. (8.3.23) and (9.3.14b))

$$\Gamma_B = (2\eta_s + \eta_d)\, q^2/\rho_0. \tag{9.5.2}$$

For the case of an ideal gas, we can readily predict the values of the material parameters appearing in these equations (Loeb, 1961). First, we can assume the validity of the Stokes relation (see also the discussion in Appendix Section 9.6.1), which states that the shear and dilation viscosity coefficients are related by $\eta_d = -\frac{2}{3}\eta_s$, and we thus find that

$$\Gamma_B = \tfrac{4}{3}\eta_s q^2/\rho_0. \tag{9.5.3}$$

The shear viscosity coefficient η_s can be shown from kinetic theory to be given by

$$\eta_s = \tfrac{1}{3} N m \bar{v} L, \tag{9.5.4}$$

where N is the atomic number density, m is the molecular mass, $\bar{v}$ is the mean molecular velocity given by $\bar{v} = (8kT/\pi m)^{1/2}$, and L is the mean free path given by $L = (\sqrt{2}\pi d^2 N)^{-1}$ with d denoting the molecular diameter. We hence find that the shear viscosity coefficient is given by

$$\eta_s = \frac{2}{3\pi^{3/2}} \frac{\sqrt{kTm}}{d^2}. \tag{9.5.5}$$

Note that the shear viscosity coefficient is independent of the molecular number density N. The measured (and theoretical) value of the shear viscosity coefficient for nitrogen gas at standard temperature and pressure is $\eta_s = 1.8 \times 10^{-4}$ dyne sec/cm^2.

By introducing expression (9.5.5) for the viscosity into Eq. (9.5.2) and replacing q by $2n\omega/c$, we find that the Brillouin linewidth is given by

$$\Gamma_{\mathrm{B}} = \frac{32}{9\pi^{3/2}} \frac{n^2\omega^2}{c^2} \frac{\sqrt{kT/m}}{d^2 N}. \tag{9.5.6}$$

If we assume that the incident optical radiation has a wavelength λ of 1.06 μm, we find that the Brillouin linewidth for nitrogen at standard temperature and pressure is equal to $\Gamma_{\mathrm{B}} = 2.77 \times 10^9$ rad/sec and thus that the Brillouin linewidth in ordinary frequency units is given by $\delta\nu(\mathrm{FWHM}) = \Gamma_{\mathrm{B}}/2\pi = 440$ MHz.

The velocity of sound v, which appears in Eq. (9.5.1), is given for an ideal gas by $v = (\gamma kT/m)^{1/2}$, where γ, the ratio of specific heats, is equal to 5/3 for a monatomic gas and 7/5 for a diatomic gas. In addition, the electrostrictive constant γ_e can be estimated as $\gamma_e = \rho(\partial\epsilon/\partial\rho)$ with $(\partial\epsilon/\partial\rho)$ taken as the essentially constant quantity $(\epsilon - 1)/\rho$.

The dependence of g_0 on material parameters can be determined by combining these results with Eq. (9.5.1) to obtain

$$g_0 = \frac{9\pi^{3/2} N^2 m^2 d^2 (\partial\epsilon/\partial\rho)^2}{32\gamma^{1/2} n^3 ckT}. \tag{9.5.7}$$

However, in order to obtain a numerical estimate of g_0, it is often more convenient to evaluate the expression (9.5.1) for g_0 directly with the numerical value of Γ_{B} obtained from Eq. (9.5.6). For N_2 gas at standard temperature and pressure and for a wavelength of 1.06 μm, we take the values $\omega = 1.8 \times 10^{15}$ rad/sec, $n = 1.0003$, $v = 330$ m/sec, $\gamma_e = n^2 - 1 = 6 \times 10^{-4}$,

TABLE 9.5.1 Gain factors, phonon lifetimes, and frequency shifts for some compressed Brillouin-active gases at a wavelength of 249 nm [a]

Gas	p (atm)	g_0 (m/GW)	τ (nsec)	$\Omega_B/2\pi$ (GHz)	g_R (m/GW)
SF_6	15.5	2.5×10^{-1}	1	0.9	3×10^{-3}
	10	0.9×10^{-1}	0.6		2×10^{-3}
Xe	39	4.4×10^{-1}	2	1.4	0
	10	1.8×10^{-2}	0.4		
Ar	10	1.5×10^{-3}	0.1	3	0
N_2	10	1.7×10^{-3}	0.2	3	3×10^{-4}
CH_4	10	8×10^{-3}	0.1	3	1×10^{-2}

[a] For comparison, the gain factor g_R for forward stimulated Raman scattering is also listed. (After Damzen and Hutchinson, 1983.)

and we thereby obtain

$$g_0 = 0.038 \frac{\text{m}}{\text{TW}}. \tag{9.5.8}$$

Note from Eq. (9.5.7) that g_0 scales quadratically with molecular density. Hence, at a pressure of 100 atmospheres the gain factor of N_2 is equal to $g_0 = 0.38$ m/GW, which is comparable to that of typical organic liquids.

One advantage of the use of gases as the active medium for Brillouin scattering is that the gain for SBS scales with molecular number density as N^2, whereas the gain for stimulated Raman scattering, which is often a competing process, scales as N (see, for example, Eqs. (9.3.19a), (9.3.19b), and (9.3.20)). At pressures greater than 10 atmospheres, the gain for SBS typically exceeds that of stimulated Raman scattering. Moreover, through the use of rare gases (which have no vibrational modes), it is possible to suppress the occurrence of stimulated Raman scattering altogether.

Some parameters relevant to SBS at the 249 nm wavelength of the KrF laser have been compiled by Damzen and Hutchinson (1983) and are presented in Table 9.5.1.

9.6. General Theory of Stimulated Brillouin and Stimulated Rayleigh Scattering

In this section we develop a theoretical model that can treat both stimulated Brillouin and stimulated Rayleigh scattering. These two effects can conveniently be treated together because they both entail the scattering of light from

inhomogeneities in thermodynamic quantities. For convenience, we choose the temperature T and density ρ to be the independent thermodynamic variables. The theory that we present incorporates both electrostrictive and absorptive coupling of the radiation to the material system. Our analysis therefore describes the following four scattering processes:

1. *Electrostrictive stimulated Brillouin scattering.* The scattering of light from sound waves that are driven by the interference of the laser and Stokes fields through the process of electrostriction.
2. *Thermal stimulated Brillouin scattering.* The scattering of light from sound waves that are driven by the absorption and subsequent thermalization of the optical energy, leading to temperature and hence to density variations within the medium.
3. *Electrostrictive stimulated Rayleigh scattering.* The scattering of light from isobaric density fluctuations that are driven by the process of electrostriction.
4. *Thermal stimulated Rayleigh scattering.* The scattering of light from isobaric density fluctuations that are driven by the process of optical absorption.

Our analysis is based on the three equations of hydrodynamics (Hunt, 1955; Kaiser and Maier, 1972). The first of these equations is the equation of continuity

$$\frac{\partial \tilde{\rho}_t}{\partial t} + \tilde{\mathbf{u}}_t \cdot \nabla \tilde{\rho}_t + \tilde{\rho}_t \nabla \cdot \tilde{\mathbf{u}}_t = 0, \tag{9.6.1}$$

where $\tilde{\rho}_t$ is the mass density of the fluid and $\tilde{\mathbf{u}}_t$ is the velocity of some small volume element of the fluid.* The second equation is the equation of momentum transfer. It is a generalization of the Navier–Stokes equation and is given by

$$\tilde{\rho}_t \frac{\partial \tilde{\mathbf{u}}_t}{\partial t} + \tilde{\rho}_t (\tilde{\mathbf{u}}_t \cdot \nabla)\tilde{\mathbf{u}}_t = \tilde{\mathbf{f}} - \nabla \tilde{p}_t + (2\eta_s + \eta_d)\nabla(\nabla \cdot \tilde{\mathbf{u}}_t) - \eta_s \nabla \times (\nabla \times \tilde{\mathbf{u}}_t). \tag{9.6.2}$$

Here $\tilde{\mathbf{f}}$ represents the force per unit volume of any externally imposed forces; for the case of electrostriction, $\tilde{\mathbf{f}}$ is given by (see also Eq. (9.3.12))

$$\tilde{\mathbf{f}} = -\tfrac{1}{2}\epsilon_0 \gamma_e \nabla \langle \tilde{\mathbf{E}} \cdot \tilde{\mathbf{E}} \rangle, \tag{9.6.3}$$

* The subscript t stands for *total*; we shall later linearize these equations to find the equations satisfied by the linearized quantities, which we shall designate by nonsubscripted symbols.

where $\tilde{\mathbf{E}}$ denotes the instantaneous value of the time-varying applied total electric field and γ_e represents the electrostrictive coupling constant

$$\gamma_e = \rho \frac{\partial \epsilon}{\partial \rho}. \tag{9.6.4}$$

The second term on the right-hand side of Eq. (9.6.2) denotes the force due to the gradient of the pressure $\tilde{p}_t$. In the third term, η_s denotes the shear viscosity coefficient and η_d denotes the dilational viscosity coefficient. When the Stokes relation is satisfied, as it is for example for an ideal gas, these coefficients are related by

$$\eta_d = -\tfrac{2}{3}\eta_s. \tag{9.6.5}$$

The coefficients are defined in detail in the Appendix at the end of this section.

The last of three principal equations of hydrodynamics is the equation of heat transport, given by

$$\tilde{\rho}_t C_v \frac{\partial \tilde{T}_t}{\partial t} + \tilde{\rho}_t c_v (\tilde{\mathbf{u}} \cdot \nabla \tilde{T}_t) + \tilde{\rho}_t c_v \left(\frac{\gamma - 1}{\beta_p} \right) (\nabla \cdot \tilde{\mathbf{u}}_t) = -\nabla \cdot \tilde{\mathbf{Q}} + \tilde{\phi}_\eta + \tilde{\phi}_{\text{ext}}. \tag{9.6.6}$$

Here $\tilde{T}_t$ denotes the local value of the temperature, c_v the specific heat at constant volume, $\gamma = c_p/c_v$ the adiabatic index, $\beta_p = -\tilde{\rho}^{-1}(\partial \tilde{\rho}/\partial \tilde{T})_p$ the thermal expansion coefficient, and $\tilde{\mathbf{Q}}$ the heat flux vector. For heat flow due to thermal conduction, $\tilde{\mathbf{Q}}$ satisfies the equation

$$\nabla \cdot \tilde{\mathbf{Q}} = -\kappa \nabla^2 \tilde{T}_t, \tag{9.6.7}$$

where κ denotes the thermal conductivity. $\tilde{\phi}_\eta$ denotes the viscous energy deposited within the medium per unit volume per unit time and is given by

$$\tilde{\phi}_\eta = \sum_{ij} (2\eta_s d_{ij} d_{ji} + \eta_d d_{ii} d_{jj}), \tag{9.6.8a}$$

where

$$d_{ij} = \frac{1}{2}\left(\frac{\partial \tilde{u}_i}{\partial x_j} + \frac{\partial \tilde{u}_j}{\partial x_i} \right) \tag{9.6.8b}$$

is the rate-of-dilation tensor. Finally, $\tilde{\phi}_{\text{ext}}$ gives the energy per unit time per unit volume delivered to the medium from external sources. Absorption of the optical wave provides the contribution

$$\tilde{\phi}_{\text{ext}} = \alpha n \epsilon_0 c \langle \tilde{E}^2 \rangle, \tag{9.6.9}$$

to this quantity, where α is the optical absorption coefficient.

The acoustic equations are now derived by linearizing the hydrodynamic equations about the nominal conditions of the medium. In particular, we take

$$\tilde{\rho}_t = \rho_0 + \tilde{\rho} \quad \text{with} \quad |\tilde{\rho}| \ll \rho_0, \tag{9.6.10a}$$

$$\tilde{T}_t = T_0 + \tilde{T} \quad \text{with} \quad |\tilde{T}| \ll T_0, \tag{9.6.10b}$$

$$\tilde{\mathbf{u}}_t = \tilde{\mathbf{u}} \quad \text{with} \quad |\tilde{\mathbf{u}}| \ll v, \tag{9.6.10c}$$

where v denotes the velocity of sound. Note that we have assumed that the medium is everywhere motionless in the absence of the acoustic disturbance. We can reliably use the linearized form of the resulting equations so long as the indicated inequalities are satisfied.

We substitute the expansions (9.6.10) into the hydrodynamic equations (9.6.1), (9.6.2), and (9.6.6), drop any term that contains more than one small quantity, and subtract the unperturbed, undriven solution containing only $\tilde{\rho}_0$ and $\tilde{T}_0$. The continuity equation (9.6.1) then becomes

$$\frac{\partial \tilde{\rho}}{\partial t} + \rho_0 \nabla \cdot \tilde{\mathbf{u}} = 0. \tag{9.6.11}$$

In order to linearize the momentum transport equation (9.6.2), we first express the total pressure $\tilde{p}_t$ as

$$\tilde{p}_t = p_0 + \tilde{p} \quad \text{with} \quad |\tilde{p}| \ll p_0. \tag{9.6.12}$$

Since we have taken T and ρ as the independent thermodynamic variables, we can express $\tilde{p}$ as

$$\tilde{p} = \left(\frac{\partial p}{\partial \rho}\right)_T \tilde{\rho} + \left(\frac{\partial p}{\partial T}\right)_\rho \tilde{T} \tag{9.6.13}$$

or as

$$\tilde{p} = \frac{v^2}{\gamma}(\tilde{\rho} + \beta_p \rho_0 \tilde{T}), \tag{9.6.14}$$

where we have expressed $(\partial p/\partial \rho)_T$ as $\gamma^{-1}(\partial p/\partial \rho)_s = v^2/\gamma$ with $v^2 = (\partial p/\partial \rho)_s$ representing the square of the velocity of sound, and where we have expressed $(\partial p/\partial T)_\rho$ as $\gamma^{-1}(\partial p/\partial \rho)_s(\partial \rho/\partial T)_p = v^2 \beta_p \rho_0/\gamma$ with β_p representing the thermal expansion coefficient at constant pressure. Through use of Eq. (9.6.14), the linearized form of Eq. (9.6.2) becomes

$$\rho_0 \frac{\partial \tilde{\mathbf{u}}}{\partial t} + \frac{v^2}{\gamma}\nabla\tilde{\rho} + \frac{v^2 \beta_p \rho_0}{\gamma}\nabla\tilde{T} - (2\eta_s + \eta_d)\nabla(\nabla \cdot \tilde{\mathbf{u}}) + \eta_s \nabla \times (\nabla \times \tilde{\mathbf{u}}) = \tilde{\mathbf{f}}. \tag{9.6.15}$$

Finally, the linearized form of the energy transport equation, Eq. (9.6.6), becomes

$$\rho_0 c_v \frac{\partial \tilde{T}}{\partial t} + \frac{\rho_0 c_v (\gamma - 1)}{\beta_p} (\nabla \cdot \tilde{\mathbf{u}}) - \kappa \nabla^2 \tilde{T} = \tilde{\phi}_{\text{ext}}. \tag{9.6.16}$$

Note that the viscous contribution to the heat input, $\tilde{\phi}_\eta$, does not contribute in the linear approximation.

Equations (9.6.11), (9.6.15), and (9.6.16) constitute the three linearized equations of hydrodynamics for the quantities $\tilde{\mathbf{u}}$, $\tilde{\rho}$, and $\tilde{T}$. The continuity equation in its linearized form (Eq. (9.6.11)) can be used to eliminate the variable $\tilde{\mathbf{u}}$ from the remaining two equations. To do so, we take the divergence of the equation of momentum transfer (9.6.15) and use Eq. (9.6.11) to eliminate the terms containing $\nabla \cdot \tilde{\mathbf{u}}$. We obtain

$$-\frac{\partial^2 \tilde{\rho}}{\partial t^2} + \frac{v^2}{\gamma} \nabla^2 \tilde{\rho} + \frac{v^2 \beta_p \rho_0}{\gamma} \nabla^2 \tilde{T} + \frac{2\eta_s + \eta_d}{\rho_0} \frac{\partial}{\partial t} \left(\nabla^2 \tilde{\rho} \right) = \tfrac{1}{2} \epsilon_0 \gamma_e \nabla^2 \langle \tilde{E}^2 \rangle, \tag{9.6.17}$$

where we have explicitly introduced the form of $\tilde{\mathbf{f}}$ from Eq. (9.6.3). Also, the energy transport equation (9.6.16) can then be expressed through use of Eqs. (9.6.9) and (9.6.11) as

$$\rho_0 c_v \frac{\partial \tilde{T}}{\partial t} - \frac{c_v (\gamma - 1)}{\beta_p} \frac{\partial \tilde{\rho}}{\partial t} - \kappa \nabla^2 \tilde{T} = n \epsilon_0 c \alpha \langle \tilde{E}^2 \rangle. \tag{9.6.18}$$

Equations (9.6.17) and (9.6.18) constitute two coupled equations for the thermodynamic variables $\tilde{\rho}$ and $\tilde{T}$, and they show how these quantities are coupled to one another and are driven by the applied optical field.

In the absence of the driving terms appearing on their right-hand sides, Eqs. (9.6.17) and (9.6.18) allow solutions of the form of damped, freely propagating acoustic waves

$$\tilde{F}(z, t) = F e^{-i\Omega(t - z/v)} e^{-\alpha_s z} + \text{c.c.}, \tag{9.6.19}$$

where F denotes either ρ or T, and where the sound absorption coefficient α_s is given for low frequencies ($\Omega \ll \rho_0 v^2/(2\eta_s + \eta_d)$) by

$$\alpha_s = \frac{\Omega^2}{2\rho_0 v^3} \left[(2\eta_s + \eta_d) + (\gamma - 1) \frac{\kappa}{c_p} \right]. \tag{9.6.20}$$

For details, see the article by Sette (1961).

We next study the nature of the solution to Eqs. (9.6.17) and (9.6.18) in the presence of their driving terms. We assume that the total optical field can be

represented as

$$\tilde{E}(z,t) = A_1 e^{i(k_1 z - \omega_1 t)} + A_2 e^{i(-k_2 z - \omega_2 t)} + \text{c.c.} \tag{9.6.21}$$

We first determine the response of the medium at the beat frequency between these two applied field frequencies. This disturbance will have frequency

$$\Omega = \omega_1 - \omega_2 \tag{9.6.22}$$

and wavenumber

$$q = k_1 + k_2 \tag{9.6.23}$$

and can be taken to be of the form

$$\tilde{\rho}(z,t) = \rho e^{i(qz - \Omega t)} + \text{c.c.}, \tag{9.6.24}$$

$$\tilde{T}(z,t) = T e^{i(qz - \Omega t)} + \text{c.c.} \tag{9.6.25}$$

For the present, we are interested only in the steady-state response of the medium, and thus we assume that the amplitudes A_1, A_2, ρ, and T are time-independent. We introduce the fields $\tilde{E}$, $\tilde{\rho}$, and $\tilde{T}$ given by Eqs. (9.6.21) through (9.6.25) into the coupled acoustic equations (9.6.17) and (9.6.18). The parts of these equations that oscillate at frequency Ω are given respectively by

$$-\left(\Omega^2 + i\Omega\Gamma_{\text{B}} - \frac{v^2 q^2}{\gamma}\right)\rho + \frac{v^2 \beta_p \rho_0 q^2}{\gamma} T = \epsilon_0 \gamma_e q^2 A_1 A_2^* \tag{9.6.26}$$

and

$$-\left(i\Omega - \frac{1}{2}\gamma\Gamma_R\right)T + \frac{i(\gamma - 1)\Omega}{\beta_p \rho_0}\rho = \frac{2n\epsilon_0 c\alpha}{c_v \rho_0} A_1 A_2^*. \tag{9.6.27}$$

Here we have introduced the Brillouin linewidth

$$\Gamma_{\text{B}} = (2\eta_s + \eta_d) q^2 / \rho_0, \tag{9.6.28}$$

whose reciprocal $\tau_p = \Gamma_{\text{B}}^{-1}$ is the phonon lifetime, and the Rayleigh linewidth

$$\Gamma_R = \frac{2\kappa q^2}{\rho_0 c_p}, \tag{9.6.29}$$

whose reciprocal $\tau_R = \Gamma_R^{-1}$ is characteristic decay time of the isobaric density disturbances that give rise to Rayleigh scattering.

In deriving Eqs. (9.6.26) and (9.6.27) we have ignored those terms that contain the spatial derivatives of ρ and T. This approximation is equivalent to assuming that the material excitations are strongly damped and hence do not

propagate over any appreciable distances. This approximation is valid so long as

$$q \gg \left|\frac{1}{\rho}\frac{\partial \rho}{\partial z}\right| \left|\frac{1}{T}\frac{\partial T}{\partial z}\right| \quad \text{and} \quad q^2 \gg \left|\frac{1}{\rho}\frac{\partial^2 \rho}{\partial z^2}\right| \left|\frac{1}{T}\frac{\partial^2 T}{\partial z^2}\right|.$$

These inequalities are usually satisfied. Recall that a similar approximation was introduced in Section 9.3 in the derivation of Eq. (9.3.15).

We next solve Eq. (9.6.27) algebraically for T and introduce the resulting expression into Eq. (9.6.26). We obtain the equation

$$\left[-\left(\Omega^2 + i\Omega\Gamma_{\mathrm{B}} - \frac{v^2q^2}{\gamma}\right) + \frac{v^2q^2\Omega(\gamma-1)}{\left(\Omega + \frac{1}{2}i\gamma\Gamma_R\right)\gamma}\right]\rho$$
$$= \left[\epsilon_0\gamma_e - \frac{i\gamma_a q v}{\Omega + \frac{1}{2}i\gamma\Gamma_R}\right]q^2 A_1 A_2^*, \tag{9.6.30}$$

where we have introduced the absorptive coupling constant

$$\gamma_a = \frac{8\pi\alpha n v^2 \epsilon_0 c\beta_p}{c_P \Omega_{\mathrm{B}}} \tag{9.6.31}$$

with $\Omega_{\mathrm{B}} = qv$. Equation (9.6.30) shows how the amplitude ρ of the acoustic disturbance depends on the amplitudes A_1 and A_2 of the two optical fields. Both Brillouin and Rayleigh contributions to ρ are contained in Eq. (9.6.30).

It is an empirical fact (see, for example, Fig. 8.1.1) that the spectrum for Brillouin scattering does not appreciably overlap that for Rayleigh scattering. Equation (9.6.30) can thus be simplified by considering the resonant contributions to the two processes separately. First, we consider the case of stimulated Brillouin scattering (SBS). In this case Ω^2 is approximately equal to $\Omega_{\mathrm{B}}^2 = v^2q^2$, and thus the denominator $\Omega + \frac{1}{2}i\gamma\Gamma_R$ is nonresonant. We can thus drop the contribution $\frac{1}{2}i\gamma\Gamma_R$ in comparison with Ω in these denominators. Equation (9.6.30) then shows that the Brillouin contribution to ρ is given by

$$\rho_{\mathrm{B}} = \frac{-(\epsilon_0\gamma_e - i\gamma_a)q^2}{4\pi(\Omega^2 + i\Omega\Gamma_{\mathrm{B}} - v^2q^2)} A_1 A_2^*. \tag{9.6.32}$$

The other resonance in Eq. (9.6.30) occurs at $\Omega = 0$ and leads to stimulated Rayleigh scattering (SRLS). For $|\Omega| \lesssim \Gamma_R$, the Brillouin denominator $\Omega^2 + i\Omega\Gamma_{\mathrm{B}} - v^2q^2/\gamma$ is nonresonant and can be approximated by $-v^2q^2/\gamma$. Equation (9.6.30) thus becomes

$$\rho_R = \left[\frac{\epsilon_0\gamma_e(\Omega + \frac{1}{2}i\gamma\Gamma_R) - i\gamma_a\Omega_{\mathrm{B}}}{\Omega + \frac{1}{2}i\Gamma_R}\right]\frac{1}{4\pi v^2} A_1 A_2^*. \tag{9.6.33}$$

We next calculate the nonlinear polarization as

$$\tilde{p}^{\mathrm{NL}} = \epsilon_0 \Delta\chi \tilde{E} = \epsilon_0 \Delta\epsilon \tilde{E} = \epsilon_0 \left(\frac{\partial \epsilon}{\partial \rho}\right)_T \tilde{\rho}\tilde{E} = \frac{\epsilon_0 \gamma_e}{\rho_0}\tilde{\rho}\tilde{E}, \tag{9.6.34}$$

where $\tilde{\rho}$ and $\tilde{E}$ are given by Eqs. (9.6.24) and (9.6.21), respectively. We represent the nonlinear polarization in terms of its complex amplitudes as

$$\tilde{P}^{\mathrm{NL}} = p_1 e^{i(k_1 z - \omega_1 t)} + p_2 e^{i(-k_2 z - \omega_2 t)} + \text{c.c.} \tag{9.6.35}$$

with

$$p_1 = \frac{\epsilon_0 \gamma_e}{\rho_0}\rho A_2, \qquad p_2 = \frac{\epsilon_0 \gamma_e}{\rho_0}\rho^* A_1. \tag{9.6.36}$$

This form of the nonlinear polarization is now introduced into the wave equation, which we write in the form (see also Eq. (2.1.22))

$$\nabla^2\left[A_n(\mathbf{r})\, e^{i\mathbf{k}_n\cdot\mathbf{r}}\right] + \frac{\epsilon(\omega_n)\omega_n^2}{c^2} A_n(\mathbf{r}) e^{i\mathbf{k}_n\cdot\mathbf{r}} = \frac{\omega_n^2}{\epsilon_0 c^2}\, p_n\, e^{i\mathbf{k}_n\cdot\mathbf{r}}. \tag{9.6.37}$$

We next make the slowly-varying amplitude approximation and find that the field amplitudes obey the equations

$$\left(\frac{d}{dz} + \tfrac{1}{2}\alpha\right) A_1 = \frac{i\omega}{2n\epsilon_0 c} p_1, \tag{9.6.38a}$$

$$\left(\frac{d}{dz} - \tfrac{1}{2}\alpha\right) A_2 = \frac{-i\omega}{2n\epsilon_0 c} p_2, \tag{9.6.38b}$$

where we have introduced the real part of the refractive index $n = \mathrm{Re}\sqrt{\epsilon}$ and the optical absorption coefficient $\alpha = (2\omega/c)\,\mathrm{Im}\sqrt{\epsilon}$. Equations (9.6.38) can be used to describe either SBS or SRLS, depending on whether form (9.6.32) or (9.6.33) is used to determine the factor ρ that appears in the expression (9.3.36) for the nonlinear polarization. Since in either case ρ is proportional to the product $A_1 A_2^*$, Eqs. (9.6.38) can be written as

$$\frac{dA_1}{dz} = \kappa |A_2|^2 A_1 - \tfrac{1}{2}\alpha A_1, \tag{9.6.39a}$$

$$\frac{dA_2}{dz} = \kappa^* |A_1|^2 A_2 + \tfrac{1}{2}\alpha A_2, \tag{9.6.39b}$$

where for SBS κ is given by

$$\kappa_{\mathrm{B}} = -\frac{q^2\omega}{2\rho_0 n c} \frac{i\gamma_e(\epsilon_0\gamma_e - i\gamma_a)}{(\Omega^2 + i\Omega\Gamma_{\mathrm{B}} - v^2 q^2)}, \tag{9.6.40a}$$

and for SRLS is given by

$$\kappa_R = \frac{i\gamma_e\omega}{2\rho_0 n c v^2}\left[\frac{\gamma_e\left(\Omega + \frac{1}{2}i\gamma\Gamma_R\right) - i\gamma_a\Omega_B}{\Omega + \frac{1}{2}i\Gamma_R}\right]. \tag{9.6.40b}$$

We now introduce the intensities

$$I_i = 2n\epsilon_0 c|A_i|^2 \tag{9.6.41}$$

of the two interacting optical waves and use Eqs. (9.6.39) to calculate the spatial rate of change of the intensities as

$$\frac{dI_1}{dz} = -gI_1I_2 - \alpha I_1, \tag{9.6.42a}$$

$$\frac{dI_2}{dz} = -gI_1I_2 + \alpha I_2, \tag{9.6.42b}$$

where we have introduced the gain factor

$$g = -\frac{1}{n\epsilon_0 c}\,\mathrm{Re}\,\kappa. \tag{9.6.43}$$

For the case of SBS, we find that the gain factor can be expressed as

$$g_B = g_B^e + g_B^a, \tag{9.6.44a}$$

where

$$g_B^e = \frac{\omega^2\gamma_e^2}{\rho_0 n v c^2 \Gamma_B}\,\frac{1}{1 + (2\Delta\Omega/\Gamma_B)^2} \tag{9.6.44b}$$

and

$$g_B^a = \frac{-\omega^2\gamma_e\gamma_a}{2\rho_0 n v c^2 \Gamma_B}\,\frac{4\Delta\Omega/\Gamma_B}{1 + (2\Delta\Omega/\Gamma_B)^2} \tag{9.6.44c}$$

denote the electrostrictive and absorptive contributions to the SBS gain factor, respectively. Here we have introduced the detuning from the Brillouin resonance given by $\Delta\Omega = \Omega_B - \Omega$, where $\Omega_B = qv = (k_1 + k_2)v$ and where $\Omega = \omega_1 - \omega_2$. The electrostrictive contribution is maximum for $\Delta\Omega = 0$, where it attains the value

$$g_B^e(\max) = \frac{\omega^2\gamma_e^2}{\rho_0 n v c^3 \Gamma_B}. \tag{9.6.45}$$

Since (according to Eq. (9.6.28)) Γ_B is proportional to q^2 and thus to ω^2, the gain for electrostrictive SBS is independent of the laser frequency. The absorptive contribution is maximum for $\Delta\Omega = -\Gamma_B/2$—that is, when the

Stokes wave (at frequency ω_2) is detuned by one-half the spontaneous Brillouin linewidth Γ_B to the low-frequency side of resonance. The maximum value of the gain for this process is

$$g_B^a(\max) = \frac{\omega^2 \gamma_e \gamma_a}{2\rho_0 n v c^3 \Gamma_B}. \tag{9.6.46}$$

Note that since Γ_B is proportional to q^2 and (according to Eq. (9.6.31)) γ_a is proportional to q^{-1}, the absorptive SBS gain factor is proportional to q^3 and hence depends on the laser frequency as ω^{-3}. Since the gain factor for thermal SBS is linearly proportional to the optical absorption coefficient α (by Eqs. (9.6.31) and (9.6.46)), the gain for thermal SBS can be made to exceed that for electrostrictive SBS by adding an absorber such as a dye to the Brillouin-active medium. As shown in Table 9.3.1, this effect occurs roughly for absorption coefficients greater than 1 cm^{-1}.*

The spectral dependence of the two contributions to the SBS gain is shown schematically in Fig. 9.6.1.

For the case of stimulated Rayleigh scattering, we can express the gain factor appearing in Eqs. (9.6.42) through use of Eqs. (9.6.40b) and (9.6.43) as

$$g_R = g_R^e + g_R^a, \tag{9.6.47}$$

where

$$g_R^e = \frac{-\omega \gamma_e^2 (\gamma - 1)}{4\rho_0 n^2 c^2 v^2} \left[\frac{4\Omega/\Gamma_R}{1 + (2\Omega/\Gamma_R)^2} \right] \tag{9.6.48}$$

and

$$g_R^a = \frac{\omega \gamma_e \gamma_a \Omega_B}{2\rho_0 n^2 c^2 v^2 \Gamma_R} \left[\frac{4\Omega/\Gamma_R}{1 + (2\Omega/\Gamma_R)^2} \right] \tag{9.6.49}$$

denote the electrostrictive and absorptive contributions to the gain factor, respectively. The contribution g_R^e gives rise to electrostrictive stimulated Rayleigh scattering. The gain factor for this process is maximum for $\Omega = -\Gamma_R/2$ and has the value

$$g_R^e(\max) = \frac{\omega \gamma_e^2 (\gamma - 1)}{4\rho_0 n^2 c^2 v^2}. \tag{9.6.50}$$

Note that this quantity scales linearly with laser frequency. The absorptive

* The quantity g_B^e (max) is designated g_0 in Table 9.3.1.

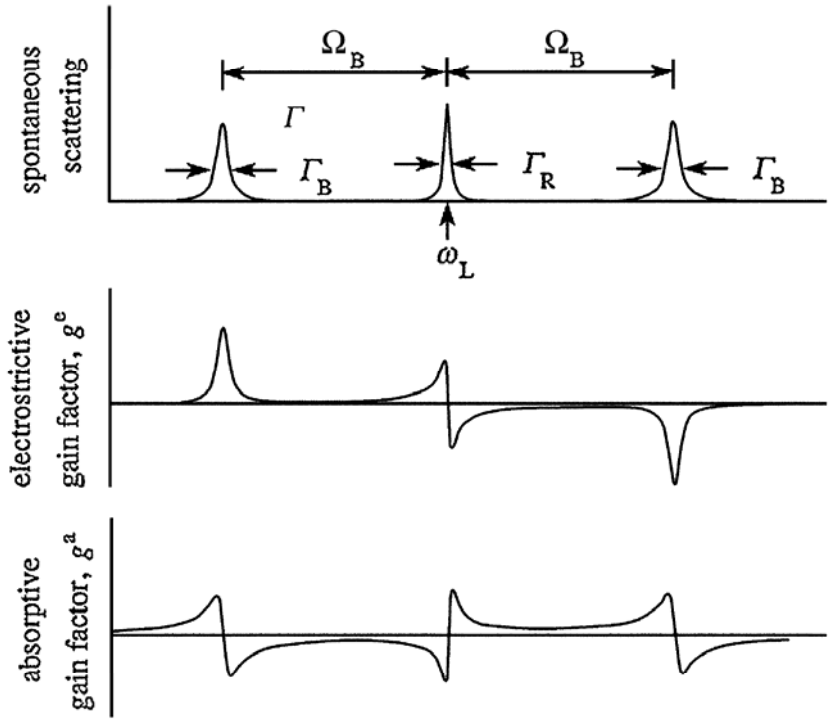

FIGURE 9.6.1 Gain spectra for stimulated Brillouin scattering and stimulated Rayleigh scattering, showing their electrostrictive and absorptive contributions. For comparison, the spectrum of spontaneous Brillouin and Rayleigh scattering is also shown.

contribution g_R^a gives rise to thermal SRLS. The gain for this process is maximum for $\Omega = \Gamma_R/2$ and has the value

$$g_R^a(\max) = \frac{\omega \gamma_e \gamma_a \Omega_B}{2\rho_0 n^2 c^2 v^2 \Gamma_R}. \tag{9.6.51}$$

Since Γ_R scales with the laser frequency as ω^2, γ_a scales as $1/\omega$, and Ω_B scales as ω, we see that the gain factor for thermal SRLS scales with the laser frequency as $1/\omega$.

As can be seen from Table 9.6.1, Γ_R is often of the order of 10 MHz, which is much narrower than the linewidths of pulsed lasers. In such cases, laser linewidth effects can often be treated in an approximate fashion by convolving the gain predicted by Eqs. (9.6.48) and (9.6.49) with the laser lineshape. If the laser linewidth Γ_L is much broader than Γ_R, the maximum gain for absorptive SRLS is then given by Eq. (9.6.51) with Γ_R replaced by Γ_L. Under these conditions g_R^a (max) is independent of the laser frequency.

We note by inspection of Table 9.6.1 that $g_R^a(\max)$ is very much larger than $g_R^e(\max)$ except for extremely small values of the absorption coefficient. The

TABLE 9.6.1 Properties of stimulated Rayleigh scattering for a variety of materials at a wavelength of 694 nm [a]

Substance	Gain Factor		Linewidth
	g_e(max) (cm/MW)	g_a(max)/α (cm^2/MW)	$\delta\nu_R$ (MHz)
CCl_4	2.6×10^{-4}	0.82	17
Methanol	8.4×10^{-4}	0.32	20
CS_2	6.0×10^{-4}	0.62	36
Benzene	2.2×10^{-4}	0.57	24
Acetone	2.0×10^{-4}	0.47	21
H_2O	0.02×10^{-4}	0.019	27.5
Ethanol		0.38	18

[a] After Kaiser and Maier (1972).

two gains become comparable for $\alpha \simeq 10^{-3}$ cm^{-1}, which occurs only for unusually pure materials.

We also see by comparison of Eqs. (9.6.51) and (9.6.46) that the ratio of the two thermal gain factors is given by

$$\frac{g_R^a(\text{max})}{g_B^a(\text{max})} = \frac{2\Gamma_B}{\Gamma_R}. \tag{9.6.52}$$

Comparison of Tables 9.3.1 and 9.6.1 shows that for a given material the ratio Γ_B/Γ_R is typically of the order of 100. Hence, when thermal stimulated scattering occurs, the gain for thermal SRLS is much larger than that for thermal SBS, and most of the energy is emitted by this process.

The frequency dependence of the gain for stimulated Rayleigh scattering is shown in Fig. 9.6.1. Note that electrostrictive SRLS gives rise to gain for Stokes shifted light but that thermal SRLS gives rise to gain for anti-Stokes scattering (Herman and Gray, 1967). This result can be understood from the point of view that n_2 is positive for electrostriction but is negative for the process of heating and subsequent thermal expansion. We saw in the discussion of two-beam coupling presented in Section 7.4 that the lower-frequency wave experiences gain for n_2 positive and loss for n_2 negative.

9.6.1. Appendix: Definition of the Viscosity Coefficients

The viscosity coefficients are defined as follows: The component t_{ij} of the stress tensor gives the i component of the force per unit area on an area element whose normal is in the j direction. We represent the stress tensor as

$$t_{ij} = -p\delta_{ij} + \sigma_{ij},$$

where p is the pressure and σ_{ij} is the contribution to the stress tensor due to viscosity. If we assume that σ_{ij} is linearly proportional to the rate of deformation

$$d_{ij} = \frac{1}{2}\left[\frac{\partial \tilde{u}_i}{\partial x_j} + \frac{\partial \tilde{u}_j}{\partial x_j}\right],$$

we can represent σ_{ij} as

$$\sigma_{ij} = 2\eta_s d_{ij} + \eta_d \delta_{ij} \sum_k d_{kk},$$

where η_s is the shear viscosity coefficient and η_d is the dilational viscosity coefficient. The quantity $\sum_k d_{kk}$ can be interpreted as follows:

$$\sum_k d_{kk} = \sum_k \frac{\partial \tilde{u}_k}{\partial x_k} = \nabla \cdot \tilde{\mathbf{u}}.$$

In general, η_s and η_d are independent parameters. However, for certain physical systems they are related to one another through a relationship first formulated by Stokes. This relationship results from the assumption that the viscous stress tensor σ_{ij} is traceless. In this case the trace of t_{ij} is unaffected by viscous effects; in other words, the mean pressure $-\frac{1}{3}\sum_i t_{ii}$ is unaffected by the effects of viscosity. Condition that σ_{ij} is traceless implies that the combination

$$\sum_i \sigma_{ii} = 2\eta_s \sum_i d_{ii} + 3\eta_d \sum_k d_{kk} = (2\eta_s + 3\eta_d) \sum_k d_{kk}$$

vanishes or that

$$\eta_d = -\tfrac{2}{3}\eta_s.$$

This result is known as the Stokes relation.

The viscosity coefficients η_s and η_d often appear in the combination $2\eta_s + \eta_d$, as they do in Eq. (9.6.2). When the Stokes relation is satisfied, this combination takes the value

$$2\eta_s + \eta_d = \tfrac{4}{3}\eta_s \quad \text{(Stokes relation valid)}.$$

Under general conditions, such that the Stokes relation is not satisfied, one often defines the bulk viscosity coefficient η_b by

$$\eta_b = \tfrac{2}{3}\eta_s + \eta_d,$$

in terms of which the quantity $2\eta_s + \eta_d$ can be represented as

$$2\eta_s + \eta_d = \tfrac{4}{3}\eta_s + \eta_b \quad \text{(in general)}.$$

Note that η_B vanishes identically when the Stokes relation is valid, for example, for the case of an ideal gas.

As an example of the use of these relations, we note that the Brillouin linewidth Γ_B introduced in Eqs. (8.3.23), (9.5.2), and (9.6.28) can be represented (ignoring the contribution due to thermal conduction) either as

$$\Gamma_B = (2\eta_s + \eta_d)q^2/\rho_0$$

or as

$$\Gamma_B = \left(\tfrac{4}{3}\eta_s + \eta_B\right)q^2/\rho_0.$$

Problems

1. *Lorentz–Lorenz prediction of the electrostrictive constant.* Verify Eq. (9.2.17).
2. *Angular dependence of SBS.* Generalize the discussion of Section 9.3 to allow the angle θ between the laser and Stokes propagation directions to be arbitrary. In particular, determine how the Brillouin frequency Ω_B, the steady-state line-center gain factor g_0, and the phonon lifetime τ_p depend on the angle θ.

   [Ans.:

   $$\Omega_B(\theta) = \Omega_B(\theta = 180^\circ)\sin\left(\tfrac{1}{2}\theta\right)$$

   $$g_0(\theta) = g_0(\theta = 180^\circ)/\sin\left(\tfrac{1}{2}\theta\right)$$

   $$\tau_p(\theta) = \tau_p(\theta = 180^\circ)/\sin^2\left(\tfrac{1}{2}\theta\right).]$$

3. *Transverse SBS.* Consider the possibility of exciting SBS in the transverse direction by a laser beam passing through a fused-silica window at near-normal incidence. Assume conditions appropriate to a high-energy laser. In particular, assume that the window is 70 cm in diameter and is uniformly filled with a laser pulse of 10-nsec duration at a wavelength of 350 nm. What is the minimum value of the laser pulse energy for which SBS can be excited? (In fact, transverse SBS has been observed under such conditions similar to those assumed in this problem; see, for example, Murray *et al.*, 1989.)

   [Ans.: $\sim$2 kJ.]
4. *Optical damage considerations and the study of SBS.* The threshold intensity for optical damage to fused silica is approximately 3 GW/cm^2 and is of the same order of magnitude for most optical materials. (See, for example, Lowdermilk and Milam, 1981.) Use this fact and the value of the

SBS gain factor at line center quoted in Table 9.3.1 to determine the minimum length of a cell utilizing fused-silica windows that can be used to excite SBS in acetone with a collimated laser beam. Assume that the laser intensity is restricted to 50% of the threshold intensity as a safety factor to avoid damage to the windows. If the laser pulse length is 20 nsec, what is the minimum value of the laser pulse energy per unit area that can be used to excite SBS? (SBS is often excited by tightly focused laser beams rather than by collimated beams to prevent optical damage to the windows of the cell.)

5. *Pulse compression by SBS*. Explain qualitatively why the Stokes radiation excited by SBS in the backward direction can be considerable shorter in duration than the exciting radiation. How must the physical length of the interaction region be related to the duration of the laser pulse in order to observe this effect? Write down the coupled-amplitude equations that are needed to describe this effect and, if you wish, solve these equations numerically by computer. What determines the minimum value of the duration of the output pulse?

   [Hint: Pulse compression by SBS is described in the scientific literature by Hon (1980) and by Gulidov *et al.* (1988).]

6. *Brillouin-enhanced four-wave mixing*. In addition to SBS, light beams can interact in a Brillouin medium by means of the process known as Brillouin-enhanced four-wave mixing (BEFWM), which is illustrated in the following figure.

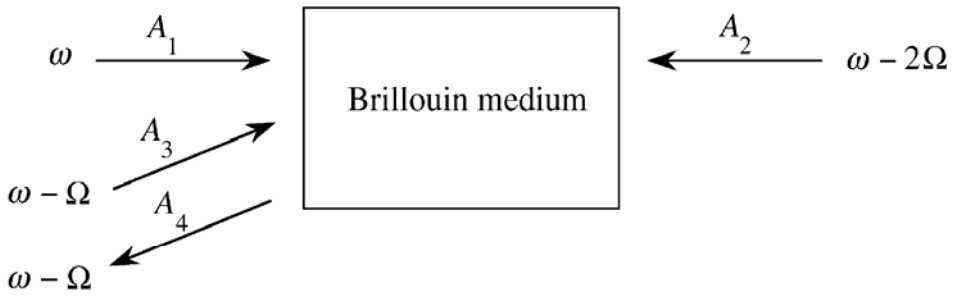

In this process, the incoming signal wave A_3 interferes with the backward-going pump wave A_2 to generate an acoustic wave propagating in the forward direction. The forward-going pump wave scatters from the acoustic wave to generate the phase-conjugate wave A_4. Since A_4 is at the Stokes sideband of A_1, it also undergoes amplification by the usual SBS process. Phase-conjugate reflectivities much larger than 100% have been observed in the BEFWM process. Using the general formalism outlined in

Section 9.3, derive the form of the four coupled-amplitude equations that describe BEFWM under steady-state conditions. Solve these equations analytically in the constant-pump approximation.

[Hint: BEFWM has been discussed in the scientific literature. See, for example, Skeldon *et al.* (1987).]

References

Reviews of Stimulated Light Scattering

Kaiser, W., Maier, M., 1972. In: Arecchi, F.T., Schulz-DuBois, E.O. (Eds.), *Laser Handbook*. North-Holland.

Zel'dovich, B.Ya., Pilipetsky, N.F., Shkunov, V.V., 1985. *Principles of Phase Conjugation*. Springer-Verlag, Berlin.

Further Reading on Stimulated Light Scattering

Fabelinskii, I.L., 1968. *Molecular Scattering of Light*. Plenum Press, New York.

Fabelinskii, I.L., 1975. In: Rabin, H., Tang, C.L. (Eds.), *Quantum Electronics: A Treatise, Vol. I*. Part A. Academic Press, New York.

Fisher, R.A. (Ed.), 1983. *Optical Phase Conjugation*. Academic Press, New York. Especially Chapters 6 and 7.

Shen, Y.R., 1984. *Principles of Nonlinear Optics*. Wiley, New York.

Stimulated Brillouin Scattering

Bowers, M.W., Boyd, R.W., Hankla, A.K., 1997. *Opt. Lett.* **22**, 360.

Boyd, R.W., Rzążewski, K., Narum, P., 1990. *Phys. Rev.* **A42**, 5514.

Buckland, E.L., Boyd, R.W., 1996. *Opt. Lett.* **21**, 1117.

Buckland, E.L., Boyd, R.W., 1997. *Opt. Lett.* **22**, 676.

Carman, R.L., Shimizu, F., Wang, C.S., Bloembergen, N., 1970. *Phys. Rev.* **A2**, 60.

Chiao, R.Y., *Ph.D. Dissertation*. Massachusetts Institute of Technology, 1965.

Chiao, R.Y., Townes, C.H., Stoicheff, B.P., 1964. *Phys. Rev. Lett.* **12**, 592.

Damzen, M.J., Hutchinson, H., 1983. *IEEE J. Quantum Electron.* **QE-19**, 7.

Gaeta, A.L., Boyd, R.W., 1991. *Phys. Rev.* **A44**, 3205.

Gaeta, A.L., Skeldon, M.D., Boyd, R.W., Narum, P., 1989. *J. Opt. Soc. Am.* **B6**, 1709.

Goldblatt, N., Hercher, M., 1968. *Phys. Rev. Lett.* **20**, 310.

Goodman, J.W., 1985. *Statistical Optics*. Wiley, New York.

Gulidov, S.S., Mak, A.A., Papernyi, S.B., 1988. *JETP Lett.* **47**, 394.

Herman, R.M., Gray, M.A., 1967. *Phys. Rev. Lett.* **19**, 824.

Hon, D.T., 1980. *Opt. Lett.* **5**, 516.

Hunt, F.V., 1955. *J. Acoust. Soc. Am.* **27**, 1019; see also *American Institute of Physics Handbook*. McGraw-Hill, New York, 1972. pp. 3–37.

Kroll, N.M., 1965. *Appl. Phys.* **36**, 34.

Kroll, N.M., Kelly, P.L., 1971. *Phys. Rev.* **A4**, 763.

Kulagin, O., Pasmanik, G.A., Gaeta, A.L., Moore, T.R., Benecke, G.J., Boyd, R.W., 1991. *J. Opt. Soc.* **B8**, 2155.

Loeb, L.B., 1961. *The Kinetic Theory of Gases*. Dover, New York.

Lowdermilk, W.H., Milam, D., 1981. *IEEE J. Quantum Electron.* **17**, 1888.

Murray, J.R., Smith, J.R., Ehrlich, R.B., Kyrazis, D.T., Thompson, C.E., Weiland, T.L., Wilcox, R.B., 1989. *J. Opt. Soc. Am.* **6**, 2402.

Narum, P., Skeldon, M.D., Boyd, R.W., 1986. *IEEE J. Quantum Electron.* **QE-22**, 2161.

Narum, P., Skeldon, M.D., Gaeta, A.L., Boyd, R.W., 1988. *J. Opt. Soc. Am.* **B5**, 623.

Pohl, D., Kaiser, W., 1970. *Phys. Rev.* **B1**, 31.

Pohl, D., Maier, M., Kaiser, W., 1968. *Phys. Rev. Lett.* **20**, 366.

Sette, D., 1961. In: *Handbuch der Physik, XI/1. Acoustics I*. Springer-Verlag, Berlin.

Sidorovich, V.G., 1976. *Sov. Phys. Tech. Phys.* **21**, 1270.

Skeldon, M.D., Narum, P., Boyd, R.W., 1987. *Opt. Lett.* **12**, 1211.

Zel'dovich, B.Ya., Popovichev, V.I., Ragulsky, V.V., Faizullov, F.S., 1972. *JETP Lett.* **15**, 109.

Chapter 10

Stimulated Raman Scattering and Stimulated Rayleigh-Wing Scattering

10.1. The Spontaneous Raman Effect

The spontaneous Raman effect was discovered by C.V. Raman in 1928. To observe this effect, a beam of light illuminates a material sample (which can be a solid, liquid, or gas), and the scattered light is observed spectroscopically, as illustrated in Fig. 10.1.1. In general, the scattered light contains frequencies different from those of the excitation source. Those new components shifted to lower frequencies are called Stokes components, and those shifted to higher frequencies are called anti-Stokes components. The Stokes components are typically orders of magnitude more intense than the anti-Stokes components.

These properties of Raman scattering can be understood through use of the energy level diagrams shown in Fig. 10.1.2. Raman Stokes scattering consists

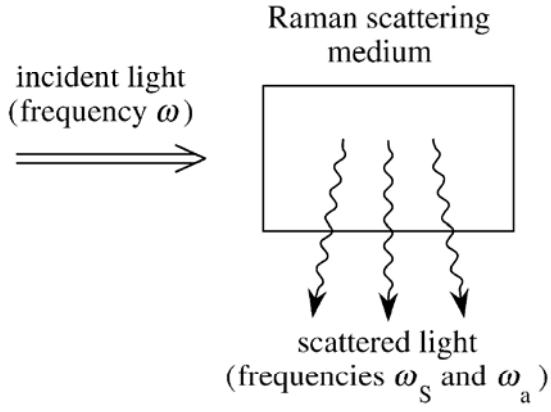

FIGURE 10.1.1 Spontaneous Raman scattering.

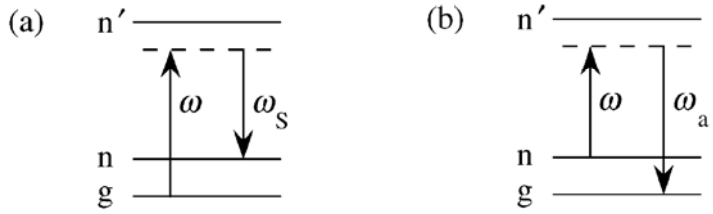

FIGURE 10.1.2 Energy level diagrams describing (a) Raman Stokes scattering and (b) Raman anti-Stokes scattering.

of a transition from the ground state g to the final state n by means of a virtual intermediate level associated with excited state n'. Raman anti-Stokes scattering entails a transition from level n to level g with n' serving as the intermediate level. The anti-Stokes lines are typically much weaker than the Stokes lines because, in thermal equilibrium, the population of level n is smaller than the population in level g by the Boltzmann factor $\exp(-\hbar\omega_{ng}/kT)$.

The Raman effect has important spectroscopic applications because transitions that are one-photon forbidden can often be studied using Raman scattering. For example, the Raman transitions illustrated in Fig. 10.1.2 can occur only if the matrix elements $\langle g|\hat{\mathbf{r}}|n'\rangle$ and $\langle n'|\hat{\mathbf{r}}|n\rangle$ are both nonzero, and this fact implies (for a material system that possesses inversion symmetry, so that the energy eigenstates possess definite parity) that the states g and n must possess the same parity. But under these conditions the $g \rightarrow n$ transition is forbidden for single-photon electric dipole transitions because the matrix element $\langle g|\hat{\mathbf{r}}|n\rangle$ must necessarily vanish.

10.2. Spontaneous versus Stimulated Raman Scattering

The spontaneous Raman scattering process described in the previous section is typically a rather weak process. Even for condensed matter, the scattering cross section per unit volume for Raman Stokes scattering is only approximately 10^{-6} cm^{-1}. Hence, in propagating through 1 cm of the scattering medium, only approximately 1 part in 10^6 of the incident radiation will be scattered into the Stokes frequency.

However, under excitation by an intense laser beam, highly efficient scattering can occur as a result of the stimulated version of the Raman scattering process. Stimulated Raman scattering is typically a very strong scattering process: 10% or more of the energy of the incident laser beam is often converted into the Stokes frequency. Another difference between spontaneous and stimulated Raman scattering is that the spontaneous process leads to emission in the form of a dipole radiation pattern, whereas the stimulated

process leads to emission in a narrow cone in the forward and backward directions. Stimulated Raman scattering was discovered by Woodbury and Ng (1962) and was described more fully by Eckhardt *et al.* (1962). The properties of stimulated Raman scattering have been reviewed by Bloembergen (1967), Kaiser and Maier (1972), Penzkofer *et al.* (1979), and Raymer and Walmsley (1990).

The relation between spontaneous and stimulated Raman scattering can be understood in terms of an argument (Hellwarth, 1963) that considers the process from the point of view of the photon occupation numbers of the various field modes. One postulates that the probability per unit time that a photon will be emitted into Stokes mode S is given by

$$P_S = Dm_L(m_S + 1). \tag{10.2.1}$$

Here m_L is the mean number of photons per mode in the laser radiation, m_S is the mean number of photons in Stokes mode S, and D is a proportionality constant whose value depends on the physical properties of the material medium. This functional form is assumed because the factor m_L leads to the expected linear dependence of the transition rate on the laser intensity, and the factor $m_S + 1$ leads to stimulated scattering through the contribution m_S and to spontaneous scattering through the contribution of unity. This dependence on the factor $m_S + 1$ is reminiscent of the stimulated and spontaneous contributions to the total emission rate for a single-photon transition of an atomic system as treated by the Einstein A and B coefficients. Equation (10.2.1) can be justified by more rigorous treatments; note, for example, that the results of the present analysis are consistent with those of the fully quantum-mechanical treatment of Raymer and Mostowski (1981).

By the definition of P_S as a probability per unit time for emitting a photon into mode S, the time rate of change of the mean photon occupation number for the Stokes mode is given by $dm_S/dt = P_S$ or through the use of Eq. (10.2.1) by

$$\frac{dm_S}{dt} = Dm_L(m_S + 1). \tag{10.2.2}$$

If we now assume that the Stokes mode corresponds to a wave traveling in the positive z direction at the velocity c/n, as illustrated in Fig. 10.2.1, we see that the time rate of change given by Eq. (10.2.2) corresponds to a spatial growth rate given by

$$\frac{dm_S}{dz} = \frac{1}{c/n}\,\frac{dm_S}{dt} = \frac{1}{c/n} Dm_L(m_S + 1). \tag{10.2.3}$$

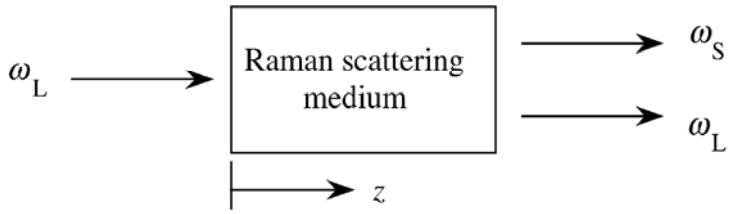

FIGURE 10.2.1 Geometry describing stimulated Raman scattering.

For definiteness, Fig. 10.2.1 shows the laser and Stokes beams propagating in the same direction; in fact, Eq. (10.2.3) applies even if the angle between the propagation directions of the laser and Stokes waves is arbitrary, as long as z is measured along the propagation direction of the Stokes wave.

It is instructive to consider Eq. (10.2.3) in the two opposite limits of $m_S \ll 1$ and $m_S \gg 1$. In the first limit, where the occupation number of the Stokes mode is much less than unity, Eq. (10.2.3) becomes simply

$$\frac{dm_S}{dz} = \frac{1}{c/n} D m_L \quad (\text{for } m_S \ll 1). \tag{10.2.4}$$

The solution to this equation for the geometry of Fig. 10.2.1 under the assumption that the laser field is unaffected by the interaction (and thus that m_L is independent of z) is

$$m_S(z) = m_S(0) + \frac{1}{c/n} D m_L z \quad (\text{for } m_S \ll 1), \tag{10.2.5}$$

where $m_S(0)$ denotes the photon occupation number associated with the Stokes field at the input to the Raman medium. This limit corresponds to spontaneous Raman scattering; the Stokes intensity increases in proportion to the length of the Raman medium and thus to the total number of molecules contained in the interaction region.

The opposite limiting case is that in which there are many photons in the Stokes mode. In this case Eq. (10.2.3) becomes

$$\frac{dm_S}{dz} = \frac{1}{c/n} D m_L m_S \quad (\text{for } m_S \gg 1), \tag{10.2.6}$$

whose solution (again under the assumption of an undepleted input field) is

$$m_S(z) = m_S(0) e^{Gz} \quad (\text{for } m_S \gg 1), \tag{10.2.7}$$

where we have introduced the Raman gain coefficient

$$G = \frac{D m_L}{c/n}. \tag{10.2.8}$$

Again $m_S(0)$ denotes the photon occupation number associated with the Stokes field at the input to the Raman medium. If no field is injected into the Raman medium, $m_S(0)$ represents the quantum noise associated with the vacuum state, which is equivalent to one photon per mode. Emission of the sort described by Eq. (10.2.7) is called stimulated Raman scattering. The Stokes intensity is seen to grow exponentially with propagation distance through the medium, and large values of the Stokes intensity are routinely observed at the output of the interaction region.

We see from Eq. (10.2.8) that the Raman gain coefficient can be related simply to the phenomenological constant D introduced in Eq. (10.2.1). However, we see from Eq. (10.2.5) that the strength of spontaneous Raman scattering is also proportional to D. Since the strength of spontaneous Raman scattering is often described in terms of a scattering cross section, it is thus possible to determine a relationship between the gain coefficient G for stimulated Raman scattering and the cross section for spontaneous Raman scattering. This relationship is derived as follows.

Since one laser photon is lost for each Stokes photon that is created, the occupation number of the laser field changes as the result of spontaneous scattering into one particular Stokes mode in accordance with the relation $dm_L/dz = -dm_S/dz$, with dm_S/dz given by Eq. (10.2.4). However, since the system can radiate into a large number of Stokes modes, the total rate of loss of laser photons is given by

$$\frac{dm_L}{dz} = -Mb\frac{dm_S}{dz} = \frac{-Dm_L Mb}{c/n}, \tag{10.2.9}$$

where M is the total number of modes into which the system can radiate and where b is a geometrical factor that accounts for the fact that the angular distribution of scattered radiation may be nonuniform and hence that the scattering rate into different Stokes modes may be different. Explicitly, b is the ratio of the angularly averaged Stokes emission rate to the rate in the direction of the particular Stokes mode S for which D (and thus the Raman gain coefficient) is to be determined. If $|f(\theta, \phi)|^2$ denotes the angular distribution of the Stokes radiation, b is then given by

$$b = \frac{\int |f(\theta, \phi)|^2 \, d\Omega/4\pi}{|f(\theta_S, \phi_S)|^2}, \tag{10.2.10}$$

where (θ_S, ϕ_S) gives the direction of the particular Stokes mode for which D is to be determined.

The total number of Stokes modes into which the system can radiate is given by the expression (see, for example, Boyd, 1983, Eq. (3.4.4))

$$M = \frac{V\omega_S^2 \Delta\omega}{\pi^2 (c/n)^3}, \tag{10.2.11}$$

where V denotes the volume of the region in which the modes are defined and where $\Delta\omega$ denotes the linewidth of the scattered Stokes radiation. The rate of loss of laser photons is conventionally described by the cross section σ for Raman scattering, which is defined by the relation

$$\frac{dm_L}{dz} = -N\sigma m_L, \tag{10.2.12}$$

where N is the number density of molecules. By comparison of Eqs. (10.2.9) and (10.2.12), we see that we can express the parameter D in terms of the cross section σ by

$$D = \frac{N\sigma(c/n)}{Mb}. \tag{10.2.13}$$

This expression for D, with M given by Eq. (10.2.11), is now substituted into expression (10.2.8) for the Raman gain coefficient to give the result

$$G = \frac{N\sigma\pi^2 c^3 m_L}{V\omega_S^2 \Delta\omega b n^3} \equiv \frac{N\pi^2 c^3 m_L}{V\omega_S^2 b n^3} \left(\frac{\partial\sigma}{\partial\omega}\right)_0, \tag{10.2.14}$$

where in obtaining the second form we have used the definition of the spectral density of the scattering cross section to express σ in terms of its line-center value $(\partial\sigma/\partial\omega)_0$ as

$$\sigma = \left(\frac{\partial\sigma}{\partial\omega}\right)_0 \Delta\omega. \tag{10.2.15}$$

Equation (10.2.14) gives the Raman gain coefficient in terms of the number of laser photons per mode, m_L. In order to express the gain coefficient in terms of the laser intensity, which can be measured directly, we assume the geometry shown in Fig. 10.2.2. The laser intensity I_L is equal to the number of photons contained in this region multiplied by the energy per photon and divided by the cross-sectional area of the region and by the transit time through the region—that is,

$$I_L = \frac{m_L \hbar\omega_L}{A(nL/c)} = \frac{m_L \hbar\omega_L c}{Vn}, \tag{10.2.16}$$

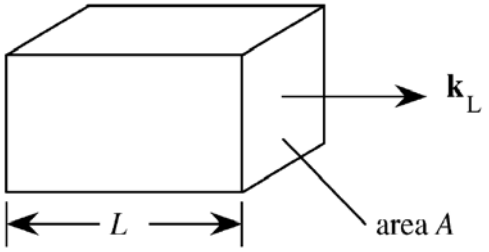

FIGURE 10.2.2 Geometry of the region within which the laser and Stokes modes are defined.

where $V = AL$. Through use of this result, the Raman gain coefficient of Eq. (10.2.14) can be expressed as

$$G = \frac{N\pi^2 c^2}{\omega_S^2 b n^2 \hbar \omega_L} \left(\frac{\partial \sigma}{\partial \omega} \right)_0 I_L. \tag{10.2.17}$$

It is sometimes convenient to express the Raman gain coefficient not in terms of the spectral cross section $(\partial\sigma/\partial\omega)_0$ but in terms of the differential spectral cross section $(\partial^2\sigma/\partial\omega\,\partial\Omega)_0$, where $d\Omega$ is an element of solid angle. These quantities are related by

$$\left(\frac{\partial \sigma}{\partial \omega} \right)_0 = 4\pi b \left(\frac{\partial^2 \sigma}{\partial \omega \partial \Omega} \right)_0, \tag{10.2.18}$$

where b is the factor defined in Eq. (10.2.10) that accounts for the possible nonuniform angular distribution of the scattered Stokes radiation. Through use of this relation, Eq. (10.2.17) becomes

$$G = \frac{4\pi^3 N c^2}{\omega_S^2 \hbar \omega_L n_S^2} \left(\frac{\partial^2 \sigma}{\partial \omega \partial \Omega} \right)_0 I_L. \tag{10.2.19}$$

Some of the parameters describing stimulated Raman scattering are listed in Table 10.2.1 for a number of materials.

10.3. Stimulated Raman Scattering Described by the Nonlinear Polarization

Here we develop a classical (that is, non-quantum-mechanical) model that describes stimulated Raman scattering (see also Garmire *et al.*, 1963). For conceptual clarity, our treatment is restricted to the scalar approximation. Treatments that include the tensor properties of Raman interaction are cited in the references listed at the end of this chapter.

We assume that the optical field interacts with a vibrational mode of a molecule, as illustrated in Fig. 10.3.1. We assume that the vibrational mode can

TABLE 10.2.1 Properties of stimulated Raman scattering for several materials [a]

Substance	Frequency Shift v_0 (cm^{-1})	Linewidth Δv (cm^{-1})	Cross Section $N(d\sigma/d\Omega)_0$ (10^{-6} m^{-1} sec^{-1})	Gain Factor [b] G/I_L (m/TW)
Liquid O_2	1552	0.117	0.48 ± 0.14	145 ± 40
Liquid N_2	2326.5	0.067	0.29 ± 0.09	160 ± 50
Benzene	992	2.15	3.06	28
CS_2	655.6	0.50	7.55	240
Nitrobenzene	1345	6.6	6.4	21
Bromobenzene	1000	1.9	1.5	15
Chlorobenzene	1002	1.6	1.5	19
Toluene	1003	1.94	1.1	12
$NiNbO_3$	256	23	381	89
	637	20	231	94
$Ba_2NaNb_5O_{15}$	650			67
$LiTaO_3$	201	22	238	44
SiO_2	467			08
Methane gas	2916		(10 atm) [c]	6.6
H_2 gas	4155		(>10 atm)	15
H_2 gas (rotat.)	450		(>0.5 atm)	5
Deuterium gas	2991		(>10 atm)	11
N_2 gas	2326		(10 atm) [c]	0.71
O_2 gas	1555		(10 atm) [c]	0.16

[a] After Kaiser and Maier (1972) and Simon and Tittel (1994). All transitions are vibrational except for the 450 cm^{-1} hydrogen transition which is rotational.

[b] Measured at 694 nm unless stated otherwise.

[c] Measured at 500 nm.

be described as a simple harmonic oscillator of resonance frequency ω_v and damping constant γ, and we denote by $\tilde{q}(t)$ the deviation of the internuclear distance from its equilibrium value q_0. The equation of motion describing the molecule vibration is thus

$$\frac{d^2\tilde{q}}{dt^2} + 2\gamma\frac{d\tilde{q}}{dt} + \omega_v^2\tilde{q} = \frac{\tilde{F}(t)}{m}, \tag{10.3.1}$$

where $\tilde{F}(t)$ denotes any force that acts on the vibrational mode and where m represents the reduced nuclear mass.

The key assumption of the theory is that the optical polarizability of the molecule (which is typically predominantly electronic in origin) is not constant, but depends on the internuclear separation $\tilde{q}(t)$ according to the equation

$$\tilde{\alpha}(t) = \alpha_0 + \left(\frac{\partial\alpha}{\partial q}\right)_0 \tilde{q}(t). \tag{10.3.2}$$

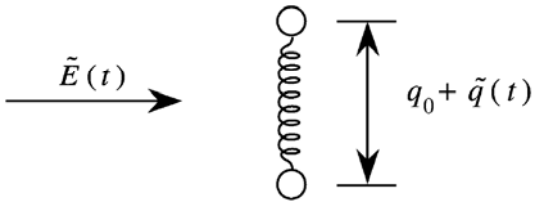

FIGURE 10.3.1 Molecular description of stimulated Raman scattering.

Here α_0 is the polarizability of a molecule in which the internuclear distance is held fixed at its equilibrium value. According to Eq. (10.3.2), when the molecule is set into oscillation its polarizability will be modulated periodically in time, and thus the refractive index of a collection of coherently oscillating molecules will be modulated in time in accordance with the relations

$$\tilde{n}(t) = \sqrt{\tilde{\epsilon}(t)} = \left[1 + N\tilde{\alpha}(t)\right]^{1/2}. \tag{10.3.3}$$

The temporal modulation of the refractive index will modify a beam of light as it passes through the medium. In particular, frequency sidebands separated from the laser frequency by $\pm\omega_v$ will be impressed upon the transmitted laser beam.

Next, we examine how molecular vibrations can be driven coherently by an applied optical field. In the presence of the optical field $\tilde{E}(z,t)$, each molecule will become polarized, and the induced dipole moment of a molecule located at coordinate z will be given by

$$\tilde{\mathbf{p}}(z,t) = \epsilon_0 \alpha \tilde{\mathbf{E}}(z,t). \tag{10.3.4}$$

The energy required to establish this oscillating dipole moment is given by

$$W = \tfrac{1}{2}\langle \tilde{\mathbf{p}}(z,t) \cdot \tilde{\mathbf{E}}(z,t) \rangle = \tfrac{1}{2}\epsilon_0 \alpha \langle \tilde{E}^2(z,t) \rangle, \tag{10.3.5}$$

where the angular brackets denote a time average over an optical period. The applied optical field hence exerts a force given by

$$\tilde{F} = \frac{dW}{dq} = \frac{\epsilon_0}{2}\left(\frac{d\alpha}{dq}\right)_0 \langle \tilde{E}^2(z,t) \rangle \tag{10.3.6}$$

on the vibrational degree of freedom. In particular, if the applied field contains two frequency components, Eq. (10.3.6) shows that the vibrational coordinate will experience a time-varying force at the beat frequency between the two field components.

The origin of stimulated Raman scattering can be understood schematically in terms of the interactions shown in Fig. 10.3.2. Part (a) of the figure shows how molecular vibrations modulate the refractive index of the medium

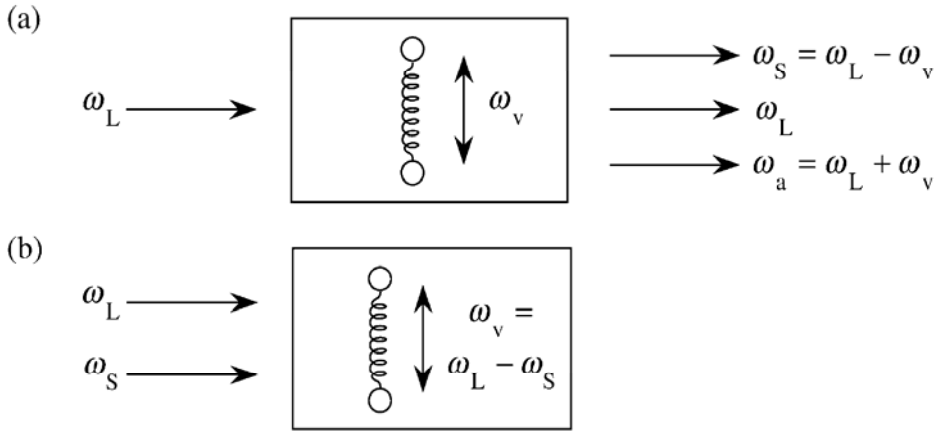

FIGURE 10.3.2 Stimulated Raman scattering.

at frequency ω_v and thereby impress frequency sidebands onto the laser field. Part (b) shows how the Stokes field at frequency $\omega_S = \omega_L - \omega_v$ can beat with the laser field to produce a modulation of the total intensity of the form

$$\tilde{I}(t) = I_0 + I_1 \cos(\omega_L - \omega_S)t. \tag{10.3.7}$$

This modulated intensity coherently excites the molecular oscillation at frequency $\omega_L - \omega_S = \omega_v$. The two processes shown in parts (a) and (b) of the figure reinforce one another in the sense that the interaction shown in part (b) leads to a stronger molecular vibration, which by the interaction shown in part (a) leads to a stronger Stokes field, which in turn leads to a stronger molecular vibration.

To make these ideas quantitative, let us assume that the total optical field can be represented as

$$\tilde{E}(z,t) = A_L e^{i(k_L z - \omega_L t)} + A_S e^{i(k_S z - \omega_S t)} + \text{c.c.} \tag{10.3.8}$$

According to Eq. (10.3.6) the time-varying part of the applied force is then given by

$$\tilde{F}(z,t) = \epsilon_0 \left(\frac{\partial \alpha}{\partial q}\right)_0 \left[A_L A_S^* e^{i(Kz - \Omega t)} + \text{c.c.}\right], \tag{10.3.9}$$

where we have introduced the notation

$$K = k_L - k_S \quad \text{and} \quad \Omega = \omega_L - \omega_S. \tag{10.3.10}$$

We next find the solution to Eq. (10.3.1) with a force term of the form of Eq. (10.3.9). We adopt a trial solution of the form

$$\tilde{q} = q(\Omega) e^{i(Kz - \Omega t)} + \text{c.c.} \tag{10.3.11}$$

We insert Eqs. (10.3.9) and (10.3.11) into Eq. (10.3.1), which becomes

$$-\omega^2 q(\Omega) - 2i\omega\gamma q(\Omega) + \omega_v^2 q(\Omega) = \frac{\epsilon_0}{m}\left(\frac{\partial\alpha}{\partial q}\right)_0 A_L A_S^*,$$

and we thus find that the amplitude of the molecular vibration is given by

$$q(\Omega) = \frac{(\epsilon_0/m)(\partial\alpha/\partial q)_0 A_L A_S^*}{\omega_v^2 - \Omega^2 - 2i\Omega\gamma}. \tag{10.3.12}$$

Since the polarization of the medium is given according to Eqs. (10.3.2) and (10.3.4) by

$$\begin{aligned}\tilde{P}(z,t) &= N\tilde{p}(z,t) = \epsilon_0 N\tilde{\alpha}(z,t)\tilde{E}(z,t)\\ &= \epsilon_0 N\left[\alpha_0 + \left(\frac{\partial\alpha}{\partial q}\right)_0 \tilde{q}(z,t)\right]\tilde{E}(z,t),\end{aligned} \tag{10.3.13}$$

the nonlinear part of the polarization is given by

$$\begin{aligned}\tilde{P}^{\mathrm{NL}}(z,t) = \epsilon_0 N\left(\frac{\partial\alpha}{\partial q}\right)_0 &\left[q(\Omega)e^{i(Kz-\Omega t)} + \text{c.c.}\right]\\ &\times\left[A_L e^{i(k_L z-\omega_L t)} + A_S e^{i(k_S z-\omega_S t)} + \text{c.c.}\right].\end{aligned} \tag{10.3.14}$$

The nonlinear polarization is thus seen to contain several different frequency components. The part of this expression that oscillates at frequency ω_S is known as the Stokes polarization and is given by

$$\tilde{P}_S^{\mathrm{NL}}(z,t) = P(\omega_S)e^{-i\omega_s t} + \text{c.c.} \tag{10.3.15}$$

with a complex amplitude given by

$$P(\omega_S) = N\epsilon_0\left(\frac{\partial\alpha}{\partial q}\right)_0 q^*(\Omega)A_L e^{ik_S z}. \tag{10.3.16}$$

By introducing the expression (10.3.12) for $q(\Omega)$ into this equation, we find that the complex amplitude of the Stokes polarization is given by

$$P(\omega_S) = \frac{(\epsilon_0^2 N/m)(\partial\alpha/\partial q)_0^2|A_L|^2 A_S}{\omega_v^2 - \Omega^2 + 2i\Omega\gamma}e^{ik_S z}. \tag{10.3.17}$$

We now define the Raman susceptibility through the expression

$$P(\omega_S) = 6\epsilon_0\chi_R(\omega_S)|A_L|^2 A_S e^{ik_S z}, \tag{10.3.18}$$

where for notational convenience we have introduced $\chi_R(\omega_S)$ as a shortened form of $\chi^{(3)}(\omega_S = \omega_S + \omega_L - \omega_L)$. By comparison of Eqs. (10.3.17) and

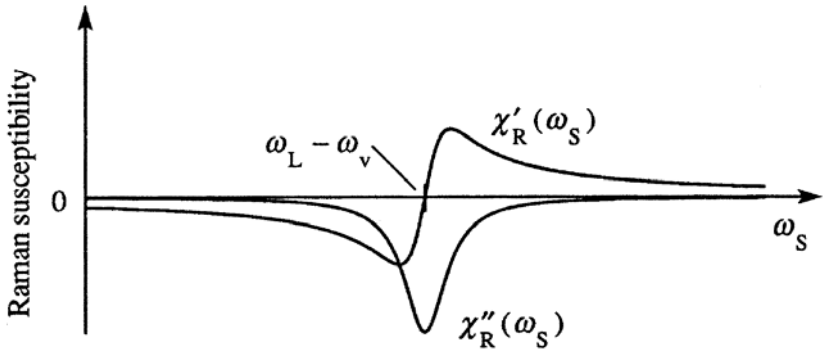

FIGURE 10.3.3 Resonance structure of the Raman susceptibility.

(10.3.18), we find that the Raman susceptibility is given by

$$\chi_R(\omega_S) = \frac{\epsilon_0(N/6m)(\partial\alpha/\partial q)_0^2}{\omega_v^2 - (\omega_L - \omega_S)^2 + 2i(\omega_L - \omega_S)\gamma}. \tag{10.3.19a}$$

The real and imaginary parts of $\chi_R(\omega_S) \equiv \chi'_R(\omega_S) + i\chi''_R(\omega_S)$ are illustrated in Fig. 10.3.3. Near the Raman resonance, the Raman susceptibility can be approximated as

$$\chi_R(\omega_S) = \frac{(\epsilon_0 N/12m\omega_v)(\partial\alpha/\partial q)_0^2}{[\omega_S - (\omega_L - \omega_v)] + i\gamma}. \tag{10.3.19b}$$

Note that, at the exact Raman resonance (that is, for $\omega_S = \omega_L - \omega_v$), the Raman susceptibility is negative imaginary. (We shall see below that consequently the Stokes wave experiences amplification.)

In order to describe explicitly the spatial evolution of the Stokes wave, we use Eqs. (10.3.8), (10.3.15), (10.3.18), and (9.3.19) for the nonlinear polarization appearing in the driven wave equation (2.1.17). We then find that the evolution of the field amplitude A_S is given in the slowly varying amplitude approximation by

$$\frac{dA_S}{dz} = -\alpha_S A_S, \tag{10.3.20}$$

where

$$\alpha_S = -3i\frac{\omega_S}{n_S c}\chi_R(\omega_S)|A_L|^2 \tag{10.3.21}$$

is the Stokes wave "absorption" coefficient. Since the imaginary part of $\chi_R(\omega_S)$ is negative, the real part of the absorption coefficient is negative, implying that the Stokes wave actually experiences exponential growth. Note that α_S depends only on the modulus of the complex amplitude of the laser field. Raman Stokes amplification is thus a process for which the phase-

matching condition is automatically satisfied. Alternatively, Raman Stokes amplification is said to be a pure gain process.

We can also predict the spatial evolution of a wave at the anti-Stokes frequency through use of the results of the calculation just completed. In the derivation of Eq. (10.3.19a), no assumptions were made regarding the sign of $\omega_L - \omega_S$. We can thus deduce the form of the anti-Stokes susceptibility by formally replacing ω_S by ω_a in Eq. (10.3.19a) to obtain the result

$$\chi_R(\omega_a) = \frac{\epsilon_0(N/6m)(\partial\alpha/\partial q)_0^2}{\omega_v^2 - (\omega_L - \omega_a)^2 + 2i(\omega_L - \omega_a)\gamma}. \tag{10.3.22}$$

Since ω_S and ω_a are related through

$$\omega_L - \omega_S = -(\omega_L - \omega_a), \tag{10.3.23}$$

we see that

$$\chi_R(\omega_a) = \chi_R(\omega_S)^*. \tag{10.3.24}$$

The relation between the Stokes and anti-Stokes Raman susceptibilities is illustrated in Fig. 10.3.4. Near the Raman resonance, Eq. (10.3.22) can be approximated by

$$\chi_R(\omega_a) = \frac{-(\epsilon_0 N/12m\omega_v)(\partial\alpha/\partial q)_0^2}{[\omega_a - (\omega_L + \omega_v)] + i\gamma}, \tag{10.3.25}$$

and at the exact resonance the Raman susceptibility is positive imaginary. The amplitude of the anti-Stokes wave hence obeys the propagation equation

$$\frac{dA_a}{dz} = -\alpha_a A_a, \tag{10.3.26}$$

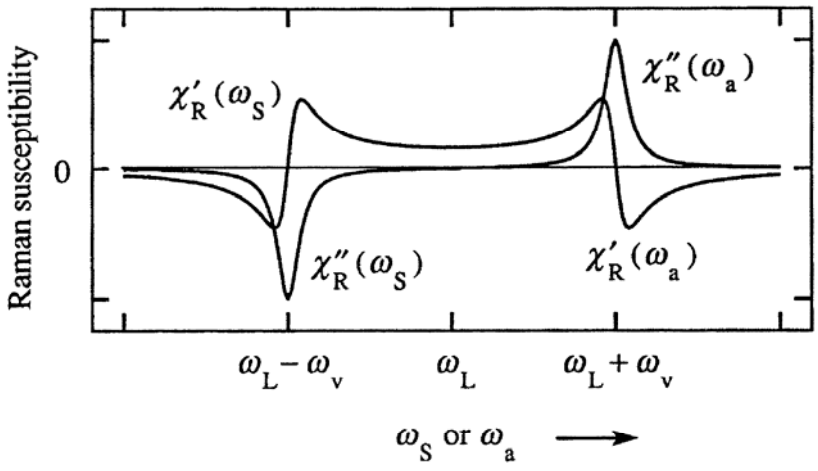

FIGURE 10.3.4 Relation between Stokes and anti-Stokes Raman susceptibilities.

where

$$\alpha_a = -3i\frac{\omega_a}{n_a c}\chi_R(\omega_a)|A_L|^2. \tag{10.3.27}$$

For a positive imaginary $\chi_R(\omega_a)$, α_a is positive real, implying that the anti-Stokes wave experiences attenuation.

However, it was found experimentally (Terhune, 1963) that the anti-Stokes wave is generated with appreciable efficiency, at least in certain directions. The origin of anti-Stokes generation is an additional contribution to the nonlinear polarization beyond that described by the Raman susceptibility of Eq. (10.3.25). Inspection of Eq. (10.3.14) shows that there is a contribution to the anti-Stokes polarization

$$\tilde{P}_a^{\mathrm{NL}}(z,t) = P(\omega_a)e^{-i\omega_a t} + \text{c.c.} \tag{10.3.28}$$

that depends on the Stokes amplitude and which is given by

$$P(\omega_a) = N\epsilon_0\left(\frac{\partial\alpha}{\partial q}\right)_0 q(\Omega)A_L = \frac{(N\epsilon_0^2/m)(\partial\alpha/\partial q)_0^2 A_L^2 A_S^*}{\omega_v^2 - \Omega^2 - 2i\Omega\gamma}e^{i(2k_L - k_S)z}. \tag{10.3.29}$$

(Recall that $\Omega \equiv \omega_L - \omega_S = \omega_a - \omega_L$.) This contribution to the nonlinear polarization can be described in terms of a four-wave mixing susceptibility $\chi_F(\omega_a) \equiv \chi^{(3)}(\omega_a = \omega_L + \omega_L - \omega_S)$, which is defined by the relation

$$P(\omega_a) = 3\epsilon_0\chi_F(\omega_a)A_L^2 A_S^* e^{i(2k_L - k_S)z}, \tag{10.3.30}$$

and which is hence equal to

$$\chi_F(\omega_a) = \frac{(N\epsilon_0/3m)(\partial\alpha/\partial q)_0^2}{\omega_v^2 - (\omega_L - \omega_a)^2 + 2i(\omega_L - \omega_a)\gamma}. \tag{10.3.31}$$

We can see by comparison with Eq. (10.3.22) that

$$\chi_F(\omega_a) = 2\chi_R(\omega_a). \tag{10.3.32}$$

The total polarization at the anti-Stokes frequency is the sum of the contributions described by Eqs. (10.3.22) and (10.3.31) and is thus given by

$$P(\omega_a) = 6\epsilon_0\chi_R(\omega_a)|A_L|^2 A_a e^{ik_a z} + 3\epsilon_0\chi_F(\omega_a)A_L^2 A_S^* e^{i(2k_L - k_s)z}. \tag{10.3.33}$$

Similarly, there is a four-wave mixing contribution to the Stokes polarization described by

$$\chi_F(\omega_S) = \frac{(N\epsilon_0/3m)(\partial\alpha/\partial q)_0^2}{\omega_v^2 - (\omega_L - \omega_a)^2 + 2i(\omega_L - \omega_S)\gamma} \tag{10.3.34}$$

so that the total polarization at the Stokes frequency is given by

$$P(\omega_S) = 6\epsilon_0 \chi_R(\omega_S)|A_L|^2 A_S e^{ik_S z} + 3\epsilon_0 \chi_F(\omega_S) A_L^2 A_a^* e^{i(2k_L - k_a)z}. \tag{10.3.35}$$

The Stokes four-wave mixing susceptibility is related to the Raman Stokes susceptibility by

$$\chi_F(\omega_S) = 2\chi_R(\omega_S) \tag{10.3.36}$$

and to the anti-Stokes susceptibility through

$$\chi_F(\omega_S) = \chi_F(\omega_a)^*. \tag{10.3.37}$$

The spatial evolution of the Stokes and anti-Stokes fields is now obtained by introducing Eqs. (10.3.33) and (10.3.35) into the driven wave Eq. (2.1.17). We assume that the medium is optically isotropic and that the slowly varying amplitude and constant-pump approximations are valid. We find that the field amplitudes obey the set of coupled equations

$$\frac{dA_S}{dz} = -\alpha_S A_S + \kappa_S A_a^* e^{i\Delta k z}, \tag{10.3.38a}$$

$$\frac{dA_a}{dz} = -\alpha_a A_a + \kappa_a A_S^* e^{i\Delta k z}, \tag{10.3.38b}$$

where we have introduced nonlinear absorption and coupling coefficients

$$\alpha_j = \frac{-3i\omega_j}{n_j c} \chi_R(\omega_j)|A_L|^2, \quad j = S, a, \tag{10.3.39a}$$

$$\kappa_j = \frac{3i\omega_j}{2n_j c} \chi_F(\omega_j) A_L^2, \qquad j = S, a, \tag{10.3.39b}$$

and have defined the wavevector mismatch

$$\Delta k = \Delta \mathbf{k} \cdot \hat{\mathbf{z}} = (2\mathbf{k}_L - \mathbf{k}_S - \mathbf{k}_a) \cdot \hat{z}. \tag{10.3.40}$$

The form of Eqs. (10.3.38) shows that each of the Stokes and anti-Stokes amplitudes is driven by a Raman gain or loss term (the first term on the right-hand side) and by a phase-matched four-wave mixing term (the second). The four-wave mixing term is an effective driving term only when the wavevector mismatch Δk is small. For a material with normal dispersion, the refractive index experienced by the laser wave is always less than the mean of those experienced by the Stokes and anti-Stokes waves, as illustrated in part (a) of Fig. 10.3.5. For this reason, perfect phase matching ($\Delta k = 0$) can always be achieved if the Stokes wave propagates at some nonzero angle with respect to the laser wave, as illustrated in part (b) of the figure. For angles appreciably

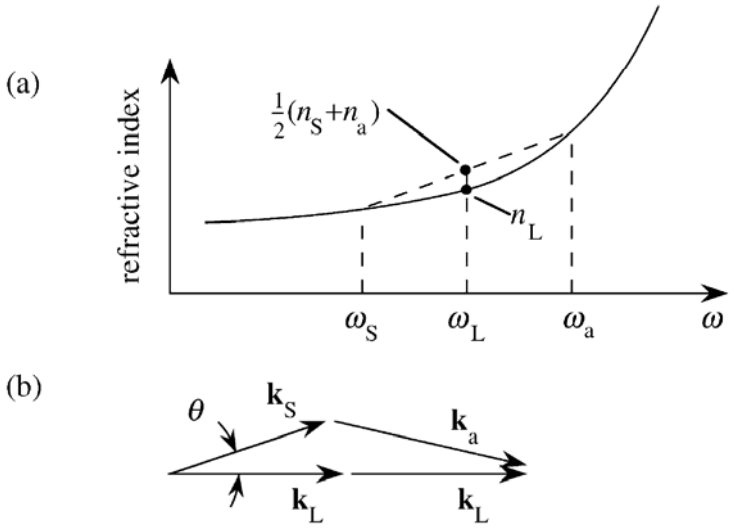

FIGURE 10.3.5 Phase-matching relations for Stokes and anti-Stokes coupling in stimulated Raman scattering.

different from this phase-matching angle, Δk is large, and only the first term on the right-hand side of each of Eqs. (10.3.38) is important. For these directions, the two equations decouple, and the Stokes sideband experiences gain and the anti-Stokes sideband experiences lose. However, for directions such that Δk is small, both driving terms on the right-hand sides of Eqs. (10.3.38) are important, and the two equations must be solved simultaneously. In the next section, we shall see how to solve these equations and shall see that both Stokes and anti-Stokes radiation can be generated in directions for which Δk is small.

10.4. Stokes–Anti-Stokes Coupling in Stimulated Raman Scattering

In this section, we study the nature of the solution to the equations describing the propagation of the Stokes and anti-Stokes waves. We have just seen that these equations are of the form

$$\frac{dA_1}{dz} = -\alpha_1 A_1 + \kappa_1 A_2^* e^{i\Delta kz}, \tag{10.4.1a}$$

$$\frac{dA_2^*}{dz} = -\alpha_2^* A_2^* + \kappa_2^* A_1 e^{-i\Delta kz}. \tag{10.4.1b}$$

In fact, equations of this form are commonly encountered in nonlinear optics and also describe, for example, any forward four-wave mixing process in the

constant-pump approximation. The ensuing discussion of the solution to these equations is simplified by first rewriting Eqs. (10.4.1) as

$$e^{-i\Delta kz/2}\left(\frac{dA_1}{dz}+\alpha_1 A_1\right)=\kappa_1 A_2^* e^{i\Delta kz/2}, \tag{10.4.2a}$$

$$e^{i\Delta kz/2}\left(\frac{dA_2^*}{dz}+\alpha_2^* A_2^*\right)=\kappa_2^* A_1 e^{-i\Delta kz/2}, \tag{10.4.2b}$$

from which it follows that the equations can be expressed as

$$\left(\frac{d}{dz}+\alpha_1+\frac{i\Delta k}{2}\right)A_1 e^{-i\Delta kz/2}=\kappa_1 A_2^* e^{i\Delta kz/2}, \tag{10.4.3a}$$

$$\left(\frac{d}{dz}+\alpha_2^*-\frac{i\Delta k}{2}\right)A_2^* e^{i\Delta kz/2}=\kappa_2^* A_1 e^{-i\Delta kz/2}. \tag{10.4.3b}$$

The form of these equations suggests that we introduce the new variables F_1 and F_2 defined by

$$F_1=A_1 e^{-i\Delta kz/2} \quad \text{and} \quad F_2^*=A_2^* e^{i\Delta kz/2}, \tag{10.4.4}$$

so that Eqs. (10.4.3) become

$$\left(\frac{d}{dz}+\alpha_1+i\frac{\Delta k}{2}\right)F_1=\kappa_1 F_2^*, \tag{10.4.5a}$$

$$\left(\frac{d}{dz}+\alpha_2^*-i\frac{\Delta k}{2}\right)F_2^*=\kappa_2^* F_1. \tag{10.4.5b}$$

We now eliminate F_2^* algebraically from this set of equations to obtain the single equation

$$\left(\frac{d}{dz}+\alpha_2^*-i\frac{\Delta k}{2}\right)\left(\frac{d}{dz}+\alpha_1+i\frac{\Delta k}{2}\right)F_1=\kappa_1\kappa_2^* F_1. \tag{10.4.6}$$

We solve this equation by adopting a trial solution of the form

$$F_1(z)=F_1(0)e^{gz}, \tag{10.4.7}$$

where g represents an unknown spatial growth rate. We substitute this form into Eq. (10.4.6) and find that this equation is satisfied by the trial solution if g satisfies the algebraic equation

$$\left(g+\alpha_2^*-\frac{i\Delta k}{2}\right)\left(g+\alpha_1+\frac{i\Delta k}{2}\right)=\kappa_1\kappa_2^*. \tag{10.4.8}$$

In general, this equation possesses two solutions, which are given by

$$g_\pm=-\tfrac{1}{2}(\alpha_1+\alpha_2^*)\pm\tfrac{1}{2}\left[\left(\alpha_1-\alpha_2^*+i\Delta k\right)^2+4\kappa_1\kappa_2^*\right]^{1/2}. \tag{10.4.9}$$

Except for special values of $\alpha_1, \alpha_2, \kappa_1, \kappa_2$, and Δk, the two values of g given by Eq. (10.4.9) are distinct. Whenever the two values of g are distinct, the general solution for F is given by

$$F_1 = F_1^+(0)e^{g_+ z} + F_1^-(0)e^{g_- z}, \tag{10.4.10}$$

and thus through the use of Eq. (10.4.4) we see that the general solution for A_1 is of the form

$$A_1(z) = \left(A_1^+ e^{g_+ z} + A_1^- e^{g_- z}\right)e^{i\Delta k z/2}. \tag{10.4.11}$$

Here A_1^+ and A_1^- are constants of integration whose values must be determined from the relevant boundary conditions. The general form of the solution for $A_2^*(z)$ is readily found by substituting Eq. (10.4.11) into Eq. (10.4.3a), which becomes

$$\left(g_+ + \alpha_1 + i\frac{\Delta k}{2}\right)A_1^+ e^{g_+ z} + \left(g_- + \alpha_1 + i\frac{\Delta k}{2}\right)A_1^- e^{g_- z} = \kappa_1 A_2^* e^{i\Delta k z/2}.$$

This equation is now solved for $A_2^*(z)$ to obtain

$$A_2^*(z) = \left[\left(\frac{g_+ + \alpha_1 + i\Delta k/2}{\kappa_1}\right)A_1^+ e^{g_+ z} + \left(\frac{g_- + \alpha_1 + i\Delta k/2}{\kappa_1}\right)A_1^- e^{g_- z}\right]e^{-i\Delta k z/2}. \tag{10.4.12}$$

If we define constants A_2^+ and A_2^- by means of the equation

$$A_2^*(z) = \left(A_2^{+*} e^{g_+ z} + A_2^{-*} e^{g_- z}\right)e^{-i\Delta k z/2}, \tag{10.4.13}$$

we see that the amplitudes $A_1^\pm$ and $A_2^\pm$ are related by

$$\frac{A_2^{\pm *}}{A_1^\pm} = \frac{g_\pm + \alpha_1 + i\Delta k/2}{\kappa_1}. \tag{10.4.14}$$

This equation shows how the amplitudes A_2^+ and A_1^+ are related in the part of the solution that grows as $\exp(g_+ z)$, and similarly how the amplitudes A_2^- and A_1^- are related in the part of the solution that grows as $\exp(g_- z)$. We can think of Eq. (10.4.14) as specifying the eigenmodes of propagation of the Stokes and anti-Stokes waves. As written, Eq. (10.4.14) appears to be asymmetric with respect to the roles of the ω_1 and ω_2 fields. However, this asymmetry occurs in appearance only. Since $g_\pm$ depends on $\alpha_1, \alpha_2, \kappa_1, \kappa_2$, and Δk, the right-hand side of Eq. (10.4.14) can be written in a variety of equivalent ways, some of which display the symmetry of the interaction more explicitly. We next rewrite Eq. (10.4.14) in such a manner.

One can show by explicit calculation using Eq. (10.4.9) that the quantities g_+ and g_- are related by

$$\left(g_+ + \alpha_1 + \frac{i\Delta k}{2}\right)\left(g_- + \alpha_1 + \frac{i\Delta k}{2}\right) = -\kappa_1\kappa_2^*. \tag{10.4.15}$$

In addition, one can see by inspection of Eq. (10.4.9) that their difference is given by

$$g_+ - g_- = \left[\left(\alpha_1 - \alpha_2^* + i\Delta k\right)^2 + 4\kappa_1\kappa_2^*\right]^{1/2}. \tag{10.4.16a}$$

By substitution of Eq. (10.4.9) into this last equation, it follows that

$$g_+ - g_- = \pm\left[2g_\pm + \left(\alpha_1 + \alpha_2^*\right)\right], \tag{10.4.16b}$$

where on the right-hand side either both pluses or both minuses must be used. Furthermore, one can see from Eq. (10.4.9) that

$$g_+ + g_- = -\left(\alpha_1 + \alpha_2^*\right). \tag{10.4.16c}$$

By rearranging this equation and adding $i\Delta k/2$ to each side, it follows that

$$\left(g_\pm + \alpha_1 + \frac{i\Delta k}{2}\right) = -\left(g_\mp + \alpha_2^* - \frac{i\Delta k}{2}\right), \tag{10.4.17a}$$

$$\left(g_\pm + \alpha_2^* + \frac{i\Delta k}{2}\right) = -\left(g_\mp + \alpha_1 + \frac{i\Delta k}{2}\right). \tag{10.4.17b}$$

Through the use of Eqs. (10.4.15) and (10.4.17a), Eq. (10.4.14) can be expressed as

$$\frac{A_2^{\pm *}}{A_1^\pm} = \frac{g_\pm + \alpha_1 + i\Delta k/2}{\kappa_1} = \frac{-\kappa_2^*}{g_\mp + \alpha_1 + i\Delta k/2} = \frac{\kappa_2^*}{g_\pm + \alpha_2^* - i\Delta k/2}.$$

By taking the geometric mean of the last and third-last forms of this expression, we find that the ratio $A_2^{\pm *}/A_1^\pm$ can be written as

$$\frac{A_2^{\pm *}}{A_1^\pm} = \left[\frac{\kappa_2^*(g_\pm + \alpha_1 + i\Delta k/2)}{\kappa_1(g_\pm + \alpha_2^* - i\Delta k/2)}\right]^{1/2}; \tag{10.4.19}$$

this form shows explicitly the symmetry between the roles of the ω_1 and ω_2 fields.

Next, we find the form of the solution when the boundary conditions are such that the input fields are known at the plane $z = 0$—that is, when $A_1(0)$ and $A_2^*(0)$ are given. We proceed by finding the values of the constants of integration A_1^+ and A_1^-. Equation (10.4.11) is evaluated at $z = 0$ to give the

result

$$A_1(0) = A_1^+ + A_1^-, \tag{10.4.20a}$$

and Eq. (10.4.12) is evaluated at $z = 0$ to give the result

$$A_2^*(0) = \left(\frac{g_+ + \alpha_1 + i\Delta k/2}{\kappa_1}\right)A_1^+ + \left(\frac{g_- + \alpha_1 + i\Delta k/2}{\kappa_1}\right)A_1^-. \tag{10.4.20b}$$

We rearrange Eq. (10.4.20a) to find that $A_1^- = A_1(0) - A_1^+$, and we substitute this form into Eq. (10.4.20b) to obtain

$$A_2^*(0) = \left(\frac{g_+ - g_-}{\kappa_1}\right)A_1^+ + \left(\frac{g_- + \alpha_1 + i\Delta k/2}{\kappa_1}\right)A_1(0).$$

We solve this equation for A_1^+ to obtain

$$A_1^+ = \left(\frac{\kappa_1}{g_+ - g_-}\right)A_2^*(0) - \left(\frac{g_- + \alpha_1 + i\Delta k/2}{g_+ - g_-}\right)A_1(0). \tag{10.4.21a}$$

If instead we solve Eq. (10.4.20a) for A_1^+ and substitute the result $A_1^+ = A_1(0) - A_1^-$ into Eq. (10.4.20b), we find that

$$A_2^*(0) = \left(\frac{g_- - g_+}{\kappa_1}\right)A_1^- - \left(\frac{g_+ + \alpha_1 + i\Delta k/2}{\kappa_1}\right)A_1(0),$$

which can be solved for A_1^- to obtain

$$A_1^- = -\left(\frac{\kappa_1}{g_+ - g_-}\right)A_2^*(0) + \left(\frac{g_+ + \alpha_1 + i\Delta k/2}{g_+ - g_-}\right)A_1(0). \tag{10.4.21b}$$

The expressions (10.4.21) for the constants A_1^+ and A_1^- are now substituted into Eqs. (10.4.11) and (10.4.12) to give the solution for the spatial evolution of the two interacting fields in terms of their boundary values as

$$\begin{aligned} A_1(z) = \frac{1}{g_+ - g_-}\Bigg\{&\left[\kappa_1 A_2^*(0) - \left(g_- + \alpha_1 + \frac{i\Delta k}{2}\right)A_1(0)\right]e^{g_+ z} \\ &- \left[\kappa_1 A_2^*(0) - \left(g_+ + \alpha_1 + \frac{i\Delta k}{2}\right)A_1(0)\right]e^{g_- z}\Bigg\}e^{i\Delta k z/2} \end{aligned} \tag{10.4.22}$$

and

$$A_2^*(z) = \frac{1}{g_+ - g_-}\left\{\left[\left(g_+ + \alpha_1 + \frac{i\Delta k}{2}\right)A_2^*(0) + \kappa_2^* A_1(0)\right]e^{g_+ z} - \left[\left(g_- + \alpha_1 + \frac{i\Delta k}{2}\right)A_2^*(0) + \kappa_2^* A_1(0)\right]e^{g_- z}\right\}e^{-i\Delta k z/2}. \tag{10.4.23}$$

Through use of Eqs. (10.4.17), the second form can be written in terms of α_2 instead of α_1 as

$$A_2^*(z) = \frac{1}{g_+ - g_-}\left\{\left[-\left(g_- + \alpha_2^* - \frac{i\Delta k}{2}\right)A_2^*(0) + \kappa_2^* A_1(0)\right]e^{g_+ z} + \left[\left(g_+ + \alpha_2^* - \frac{i\Delta k}{2}\right)A_2^*(0) - \kappa_2^* A_1(0)\right]e^{g_- z}\right\}e^{-i\Delta k z/2}. \tag{10.4.24}$$

Before applying the results of the derivation just performed to the case of stimulated Raman scattering, let us make sure that the solution makes sense by applying it to several specific limiting cases.

10.4.1. Dispersionless, Nonlinear Medium without Gain or Loss

For a medium without gain (or loss), we set $\alpha_1 = \alpha_2 = 0$. Also, for a medium that is lossless and dispersionless, $\chi^{(3)}(\omega_1 = 2\omega_0 - \omega_2)$ must equal $\chi^{(3)}(\omega_2 = 2\omega_0 - \omega_1)$, and thus the product $\kappa_1\kappa_2^*$ that appears in the solution is equal to

$$\kappa_1\kappa_2^* = \frac{9\omega_1\omega_2}{4n_1n_2c^2}\left|\chi^{(3)}(\omega_1 = 2\omega_0 - \omega_2)\right|^2|A_0|^4, \tag{10.4.25}$$

which is a real, positive quantity. We allow Δk to be arbitrary. Under these conditions, the coupled gain coefficient of Eq. (10.4.9) reduces to

$$g_\pm = \pm\left[\kappa_1\kappa_2^* - (\Delta k/2)^2\right]^{1/2}. \tag{10.4.26}$$

We see that, so long as Δk is not too large, the root g_+ will be a positive real number corresponding to amplification, whereas the root g_- will be a negative real number corresponding to attenuation. However, if the wavevector mismatch becomes so large that Δk^2 exceeds $4\kappa_1\kappa_2^*$, both roots will become pure imaginary, indicating that each eigensolution shows oscillatory spatial behavior. According to Eq. (10.4.14), the ratio of amplitudes corresponding

to each eigensolution is given by

$$\frac{A_2^{\pm *}}{A_1^{\pm}} = \frac{g_\pm + i\,\Delta k/2}{\kappa_1}. \tag{10.4.27}$$

The right-hand side of this expression simplifies considerably for the case of perfect phase matching ($\Delta k = 0$) and becomes $\pm(\kappa_2^*/\kappa_1)^{1/2}$. If we also choose our phase conventions so that A_0 is purely real, we find that expression reduces to

$$\frac{A_2^{\pm *}}{A_1^{\pm}} = \pm i\left(\frac{n_1\omega_2}{n_2\omega_1}\right)^{1/2} \simeq \pm i, \tag{10.4.28}$$

which shows that the two frequency sidebands are phased by $\pm\pi/2$ radians in each of the eigensolutions.

10.4.2. Medium without a Nonlinearity

One would expect on physical grounds that, for a medium in which $\chi^{(3)}$ vanishes, the solution would reduce to the usual case of the free propagation of the ω_1 and ω_2 waves. We now verify that our formal solution possesses this property. By setting $\kappa_1 = \kappa_2 = 0$ in Eq. (10.4.9), and assuming for simplicity that Δk vanishes, we find that

$$g_+ = -\alpha_2^* \quad \text{and} \quad g_- = -\alpha_1^*. \tag{10.4.29}$$

The eigenamplitudes are found most readily from Eq. (10.4.19). If we assume that κ_1 and κ_2 approach zero in such a manner that κ_2^*/κ_1 remains finite, we find from Eq. (10.4.19) that

$$\frac{A_2^{+*}}{A_1^{+}} = \infty, \qquad \frac{A_2^{-*}}{A_1^{-}} = 0. \tag{10.4.30}$$

Thus, the positive root corresponds to a wave at frequency ω_2, which propagates according to

$$A_2^*(z) = A_2^*(0)e^{g_+ z} = A_2^*(0)e^{-\alpha_2^* z}, \tag{10.4.31a}$$

whereas the negative root corresponds to a wave at frequency ω_1, which propagates according to

$$A_1(z) = A_1(0)e^{g_- z} = A_1(0)e^{-\alpha_1 z}. \tag{10.4.31b}$$

We thus see that each of the waves simply experiences free propagation.

10.4.3. Stokes–Anti-Stokes Coupling in Stimulated Raman Scattering

Let us now apply this analysis to the case of stimulated Raman scattering (see also Bloembergen and Shen, 1964). For definiteness, we associate ω_1 with the Stokes frequency ω_S and ω_2 with the anti-Stokes frequency ω_a. The nonlinear absorption coefficients α_S and α_a and coupling coefficients κ_S and κ_a are given by Eqs. (10.3.39) with the nonlinear susceptibilities given by Eqs. (10.3.19b), (10.3.25), (10.3.31), and (10.3.34). In light of the relations

$$\chi_F(\omega_S) = \chi_F(\omega_a)^* = 2\chi_R(\omega_S) = 2\chi_R(\omega_a)^* \tag{10.4.32}$$

among the various elements of the susceptibility, we find that the absorption and coupling coefficients can be related to each other as follows:

$$\alpha_a = -\alpha_S^*\left(\frac{n_S\omega_a}{n_a\omega_S}\right), \tag{10.4.33a}$$

$$\kappa_S = -\alpha_S e^{2i\phi_L}, \tag{10.4.33b}$$

$$\kappa_a = \alpha_S^*\left(\frac{n_S\omega_a}{n_a\omega_S}\right)e^{2i\phi_L}, \tag{10.4.33c}$$

where ϕ_L is the phase of the pump laser defined through

$$A_L = |A_L|e^{i\phi_L}, \tag{10.4.34}$$

and where the Stokes amplitude absorption coefficient is given explicitly by

$$\alpha_S = \frac{-i\omega_S N\epsilon_0^2(\partial\alpha/\partial q)_0^2|A_L|^2}{4mn_S c\omega_v[\omega_S - (\omega_L - \omega_v) + i\gamma]}. \tag{10.4.35}$$

If we now introduce the relations (10.4.33) into the expression (10.4.9) for the coupled gain coefficient, we find the gain eigenvalues are given by

$$g_\pm = -\tfrac{1}{2}\alpha_S\left(1 - \frac{n_S\omega_a}{n_a\omega_S}\right) \pm \frac{1}{2}\left\{\left[\alpha_S\left(1 + \frac{n_S\omega_a}{n_a\omega_S}\right) + i\Delta k\right]^2 - 4\alpha_S^2\frac{n_S\omega_a}{n_a\omega_S}\right\}^{1/2}. \tag{10.4.36}$$

It is usually an extremely good approximation to set the factor $n_S\omega_L/n_a\omega_S$ equal to unity. In this case Eq. (10.4.36) simplifies to

$$g_\pm = \pm\left[i\alpha_S\Delta k - (\Delta k/2)^2\right]^{1/2}. \tag{10.4.37}$$

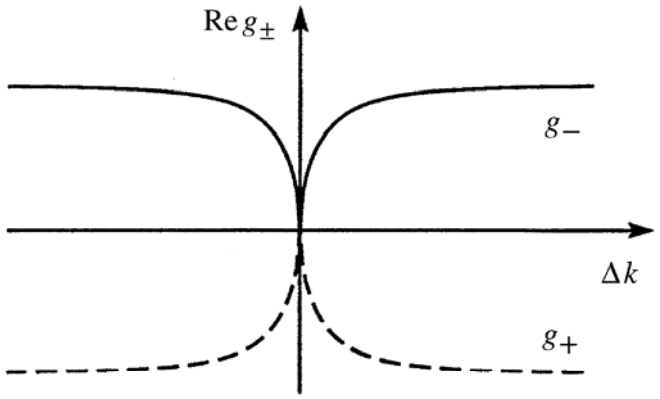

FIGURE 10.4.1 Dependence of the coupled gain on the wavevector mismatch.

The dependence of $g_\pm$ on the phase mismatch is shown graphically in Fig. 10.4.1.* Equation (10.4.37) leads to the perhaps surprising result that the coupled gain $g_\pm$ vanishes in the limit of perfect phase matching. The reason for this behavior is that, for sufficiently small Δk, the anti-Stokes wave (which normally experiences loss) is so strongly coupled to the Stokes wave (which normally experiences gain) that it prevents the Stokes wave from experiencing growth.

It is also instructive to study the expression (10.4.37) for the coupled gain in the limit in which $|\Delta k|$ is very large. For $|\Delta k| \gg |\alpha_S|$, Eq. (10.4.37) becomes

$$g_\pm = \pm i\frac{\Delta k}{2}\left(1 - \frac{4i\alpha_S}{\Delta k}\right) \simeq \pm\left(\alpha_S + \tfrac{1}{2}i\Delta k\right). \tag{10.4.38}$$

Through the use of Eq. (10.4.14), we find that the ratio of sidemode amplitudes associated with each of these gain eigenvalues is given by

$$\frac{A_a^{+*}}{A_S^+} = -2 - i\frac{\Delta k}{\alpha_S} \simeq i\frac{\Delta k}{\alpha_S}, \tag{10.4.39a}$$

$$\frac{A_a^{-*}}{A_S^-} = 0. \tag{10.4.39b}$$

Since we have assumed that $|\Delta k|$ is much larger than $|\alpha_S|$, we see that the $+$ mode is primarily anti-Stokes, whereas the $-$ mode is primarily Stokes.†

Let us now examine more carefully the nature of the decreased gain that occurs near $\Delta k = 0$. By setting $\Delta k = 0$ in the exact expression (10.4.36) for

* The graph has the same visual appearance whether the approximate form (10.4.37) or the exact form (10.4.36) is plotted.

† Recall that at resonance α_S is real and *negative*; hence $g_- = -\alpha_S - \frac{1}{2}i\Delta k$ has a positive real part and leads to amplification.

the coupled gain, we find that the gain eigenvalues become

$$g_+ = 0, \qquad g_- = -\alpha_S\left(1 - \frac{n_S\omega_a}{n_a\omega_S}\right). \tag{10.4.40}$$

Note that $|g_-|$ is much smaller than $|\alpha_S|$ but does not vanish identically. Note also that with the sign convention used here at resonance g_- is a negative quantity. We find from Eq. (10.4.14) that for a good approximation

$$\frac{A_a^{\pm *}}{A_S^{\pm}} = -1; \tag{10.4.41}$$

thus, each eigensolution is seen to be an equal combination of Stokes and anti-Stokes components, as mentioned in our discussion of Fig. 10.4.1.

Next, let us consider the spatial evolution of the field amplitudes under the assumptions that $\Delta k = 0$ and that their values are known at $z = 0$. We find from Eqs. (10.4.22) and (10.4.23) that

$$A_S(z) = \frac{-1}{1 - n_S\omega_a/n_a\omega_S}\left\{\left[A_a^*(0)e^{2i\phi_L} + \frac{n_S\omega_a}{n_a\omega_S}A_S(0)\right]\right.$$
$$\left. - \left[A_a^*(0)e^{2i\phi_L} + A_S(0)\right]e^{g-z}\right\}, \tag{10.4.42a}$$

$$A_a^*(z) = \frac{1}{1 - n_S\omega_a/n_a\omega_S}\left\{\left[A_a^*(0) + \frac{n_S\omega_a}{n_a\omega_S}A_S(0)e^{-2i\phi_L}\right]\right.$$
$$\left. - \frac{n_S\omega_a}{n_a\omega_S}\left[A_a^*(0) + A_S(0)e^{-2i\phi_L}\right]e^{g-z}\right\}. \tag{10.4.42b}$$

Note that, since g_- is negative, the second term in each expression experiences exponential decay, and as $z \to \infty$ the field amplitudes approach the asymptotic values

$$A_S(z \to \infty) = \frac{-1}{1 - n_S\omega_a/n_a\omega_S}\left[A_a^*(0)e^{2i\phi_L} + \frac{n_S\omega_a}{n_a\omega_S}A_S(0)\right], \tag{10.4.43a}$$

$$A_a^*(z \to \infty) = \frac{1}{1 - n_S\omega_a/n_a\omega_S}\left[A_a^*(0) + \frac{n_S\omega_a}{n_a\omega_S}A_S(0)e^{-2i\phi_L}\right]. \tag{10.4.43b}$$

Note that each field is amplified by the factor $(1 - n_S\omega_a/n_a\omega_S)^{-1}$. The nature of this amplification is illustrated in part (a) of Fig. 10.4.2. We see that after propagating through a distance of several times $1/g_-$, the field amplitudes attain constant values and no longer change with propagation distance.

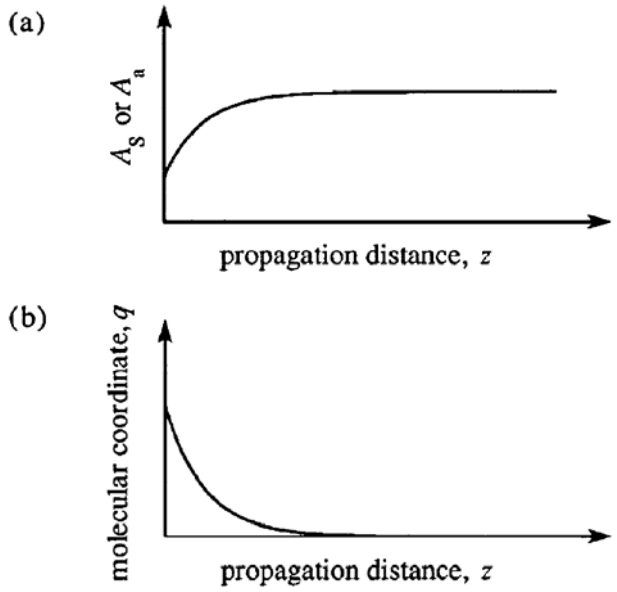

FIGURE 10.4.2 Nature of Raman amplification for the case of perfect phase matching ($\Delta k = 0$).

To see why field amplitudes remain constant, it is instructive to consider the nature of the molecule vibration in the simultaneous presence of the laser, Stokes, and anti-Stokes fields—that is, in the field

$$\tilde{E}(z,t) = A_L e^{i(k_L z - \omega_L t)} + A_S e^{i(k_S z - \omega_S t)} + A_a e^{i(k_a z - \omega_a t)} + \text{c.c.}, \quad (10.4.44)$$

where $k_L - k_S = k_a - k_L \equiv K$ and $\omega_L - \omega_S = \omega_a - \omega_L \equiv \Omega$. The solution to the equation of motion (10.3.1) for the molecular vibration with the force term given by Eqs. (10.3.6) and (10.4.44) is given by

$$\tilde{q}(z,t) = q(\Omega) e^{i(Kz - \Omega t)} + \text{c.c.},$$

where

$$g(\Omega) = \frac{(\epsilon_0/m)(\partial\alpha/\partial q)_0 (A_L A_S^* + A_a A_L^*)}{\omega_v^2 - \Omega^2 - 2i\Omega\gamma}. \quad (10.4.45)$$

We can see from Eqs. (10.4.43) that, once the field amplitudes have attained their asymptotic values, the combination $A_L A_S^* + A_a A_L^*$ vanishes, implying that the amplitude $q(\omega)$ of the molecular vibration also vanishes asymptotically, as illustrated in part (b) of Fig. 10.4.2.

10.5. Coherent Anti-Stokes Raman Scattering

In the previous sections of this chapter, we have discussed spontaneous Raman scattering and stimulated Raman scattering. These processes are represented symbolically in parts (a) and (b) of Fig. 10.5.1. In the notation of Section 10.3, stimulated Raman scattering is described by a nonlinear susceptibility of the form $\chi_R^{(3)}(\omega_S = \omega_S + \omega_L - \omega_L)$. We also saw in that section (see, for example, Eqs. (10.3.20) and (10.3.21)) that the Stokes wave at frequency ω_S tends to experience exponential growth, with a growth rate that scales as the product of the laser intensity and the imaginary part of $\chi_R^{(3)}$.

In the present section, we study two additional scattering processes, also shown in Fig. 10.5.1, known as coherent anti-Stokes Raman scattering (CARS) and coherent Stokes Raman scattering (CSRS). Our discussion will concentrate on the first of these processes, as it is the one most often used in laboratory investigations. In either of these processes, two laser beams at frequencies ω_1 and $\omega_2 < \omega_1$ are applied to the Raman medium, and a beam at a new frequency is generated by the interaction. In the process of coherent anti-Stokes Raman scattering (CARS), illustrated in part (c) of the figure, an output is created at frequency $2\omega_1 - \omega_2$ as a consequence of the susceptibility $\chi_F^{(3)}(\omega_a = \omega_1 - \omega_2 + \omega_1)$. In the process of coherent Stokes Raman scattering (CSRS), illustrated in part (d) of the figure, an output is created at frequency $2\omega_2 - \omega_1$ as a consequence of the susceptibility $\chi_F^{(3)}(\omega_S = \omega_2 + \omega_2 - \omega_1)$.

Let us now analyze more carefully the process of coherent anti-Stokes Raman scattering (CARS). We recall from Section 10.3 that the susceptibility describing this process is given according to Eqs. (10.3.25) and (10.3.32) for the current choice of frequencies by

$$\chi_F^{(3)}(\omega_a = \omega_1 - \omega_2 + \omega_1) = \frac{-(\epsilon_0 N/6m\omega_v)(\partial\alpha/\partial q)_0^2}{[(\omega_1 - \omega_2) - \omega_v)] + i\gamma}. \tag{10.5.1}$$

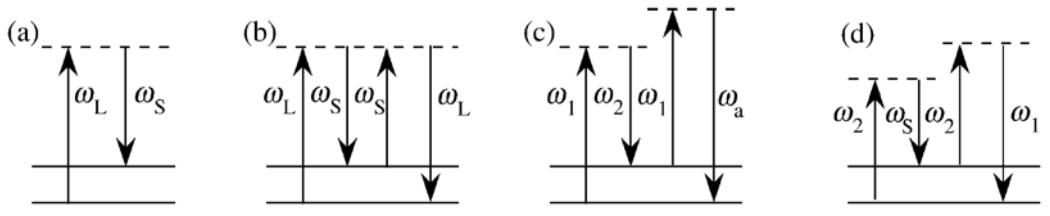

FIGURE 10.5.1 Various Raman scattering processes: (a) spontaneous Raman scattering; (b) stimulated Raman scattering; (c) coherent anti-Stokes Raman scattering (CARS); and (d) coherent Stokes Raman scattering (CSRS).

Note that the nonlinear response experiences a resonance whenever the input frequencies ω_1 and ω_2 are selected so that $\omega_1 - \omega_2$ is equal to a vibrational frequency ω_v of the material system. It is for this reason that CARS is particularly useful as a diagnostic tool for determining the presence of chemical species by means of their Raman vibrational modes. CARS is also useful as a probe of molecular structure because the resonance frequency ω_v and relaxation rate γ often depend sensitively upon the molecular environment.

The generation of the anti-Stokes wave is described by the coupled-amplitude equation Eq. (10.3.38b), which for the current situation becomes

$$\frac{dA_a}{dz} = -\alpha_a A_a + \kappa_a A_2^* e^{i\Delta kz}, \tag{10.5.2}$$

where

$$\alpha_a = \frac{-3i\omega_a}{n_a c}\chi_R(\omega_a)|A_1|^2, \qquad \kappa_a = \frac{3i\omega_a}{2n_a c}\chi_F(\omega_a)A_1^2, \tag{10.5.3}$$

and

$$\Delta k = \Delta\mathbf{k}\cdot\hat{\mathbf{z}} = (2\mathbf{k}_1 - \mathbf{k}_2 - \mathbf{k}_a)\cdot\hat{z}. \tag{10.5.4}$$

CARS is usually studied under conditions such that the generation of the anti-Stokes signal is dominated by the second term on the right-hand side of Eq. (10.5.2). This situation occurs whenever the gain of stimulated Raman scattering is small. Under this assumption and that of perfect phase matching ($\Delta k = 0$), the growth of the anti-Stokes wave can be expressed as

$$A_a(z) = \frac{3i\omega_a}{2n_a c}\chi_F(\omega_a)A_1^2 A_2^* z. \tag{10.5.5}$$

The spectral variation of the anti-Stokes generation as either of the two input frequencies is varied is given by $|\chi_F(\omega_a)|^2$, and thus is expected to have a Lorentzian line shape. However, it is found experimentally that the measured line shape is often highly distorted. An example of such a line shape is shown in Fig. 10.5.2. The explanation for this behavior is that in addition to the highly resonant molecular response described by Eq. 10.5.1 actual materials also exhibit a nonresonant background susceptibility $\chi_{\mathrm{NR}}^{(3)}$ due to electronic response and to nonresonant vibrational modes. The total susceptibility is then given by $\chi_{\mathrm{NR}}^{(3)} + \chi_F^{(3)}(\omega_a)$, and consequently the lineshape will be given by $|\chi_{\mathrm{NR}}^{(3)} + \chi_F^{(3)}(\omega_a)|^2$, which leads to a line shape of the sort shown in the figure.

The CARS effect was first observed experimentally by Maker and Terhune (1965). Significant early studies were those of Levenson *et al.* (1972) and Levenson and Bloembergen (1974). The subject of Raman spectroscopy is

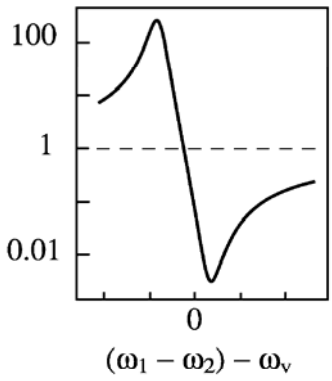

FIGURE 10.5.2 Typical CARS lineshape, such as that reported by Levenson and Bloembergen (1974).

covered well in the book by Levenson and Kano (1988). The use of CARS for imaging and for microscopy has been reviewed by Volkmer (2005).

10.6. Stimulated Rayleigh-Wing Scattering

Stimulated Rayleigh-wing scattering is the light-scattering process that results from the tendency of anisotropic molecules to become aligned along the electric field vector of an optical wave. Stimulated Rayleigh-wing scattering was described theoretically by Bloembergen and Lallemand (1966) and by Chiao *et al.* (1966), and was observed experimentally by Mash *et al.* (1965) and Cho *et al.* (1967). Other early studies were conducted by Denariez and Bret (1968) and by Foltz *et al.* (1968).

The molecular orientation effect was described in Section 4.4 for the case in which the applied optical field $\tilde{E}(t)$ contains a single frequency component, and it was found that the average molecular polarizability is modified by the presence of the applied field. The molecular polarizability can be expressed as

$$\langle \alpha \rangle = \alpha_0 + \alpha_{\mathrm{NL}}, \tag{10.6.1}$$

where the usual, weak-field polarizability is given by

$$\alpha_0 = \tfrac{1}{3}\alpha_{\parallel} + \tfrac{2}{3}\alpha_{\perp}, \tag{10.6.2}$$

where $\alpha_{\parallel}$ and $\alpha_{\perp}$ denote the polarizabilities measured parallel to the perpendicular to the symmetry axis of the molecule, respectively (see Fig. 10.6.1). In addition, the lowest-order nonlinear contribution to the polarizability is

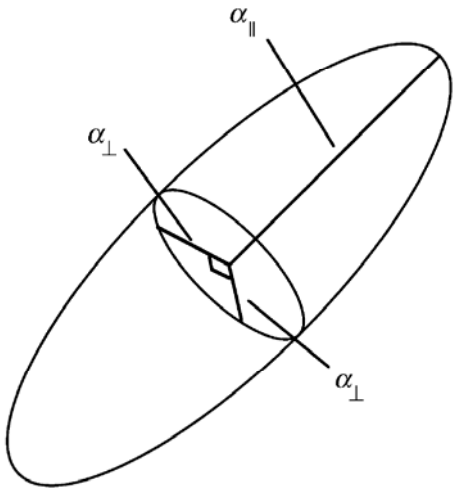

FIGURE 10.6.1 Illustration of the polarizabilities of an anisotropic molecule for the case $\alpha_\parallel > \alpha_\perp$.

given by

$$\alpha_{\mathrm{NL}} = \bar{\alpha}_2 \langle \tilde{E}^2 \rangle, \tag{10.6.3}$$

where

$$\bar{\alpha}_2 = \frac{2}{45 n_0} \frac{(\alpha_\parallel - \alpha_\perp)^2}{kT}. \tag{10.6.4}$$

In order to describe stimulated Rayleigh-wing scattering, we need to determine the response of the molecular system to an optical field that contains both laser and Stokes components, which we describe by the equation

$$\tilde{E}(\mathbf{r}, t) = A_L e^{i(k_L z - \omega_L t)} + A_S e^{i(-k_S z - \omega_S t)} + \text{c.c.} \tag{10.6.5}$$

For the present, we assume that the laser and Stokes waves are linearly polarized in the same direction and are counterpropagating. The analysis for the case in which the waves have arbitrary polarization and/or are copropagating is somewhat more involved and is discussed briefly below.

Since the intensity, which is proportional to $\langle \tilde{E}^2 \rangle$, now contains a component at the beat frequency $\omega_L - \omega_S$, the nonlinear contribution to the mean polarizability $\langle \alpha \rangle$ is no longer given by Eq. (10.6.3), which was derived for the case of a monochromatic field. We assume that, in general, α_{NL} is described by the equation

$$\tau \frac{d\alpha_{\mathrm{NL}}}{dt} + \alpha_{\mathrm{NL}} = \bar{\alpha}_2 \overline{\tilde{E}^2}. \tag{10.6.6}$$

TABLE 10.6.1 Properties of SRWS for several materials

Substance	G (m/TW)	τ (psec)	$\Delta\nu = 1/2\pi\tau$ (GHz)
CS_2	30	2	80
Nitrobenzene	30	48	3.3
Bromobenzene	14	15	10
Chlorobenzene	10	8	20
Toluene	10	2	80
Benzene	6	3	53

In this equation τ represents the molecular orientation relaxation time and is the characteristic response time of the SRWS process; see Table 10.6.1 for typical values of τ. Equation (10.6.6) has the form of a Debye relaxation equation; recall that we have studied equations of this sort in our general discussion of two-beam coupling in Section 7.4.

If Eq. (10.6.6) is solved in steady state with $\tilde{E}(t)$ given by Eq. (10.6.5), we find that the nonlinear contribution to the polarizability of a molecule located at position z is given by

$$\alpha_{\mathrm{NL}}(z,t) = 2\bar{\alpha}_2\left(A_L A_L^* + A_S A_S^*\right) + \left(\frac{2\bar{\alpha}_2 A_L A_S^* e^{iqz-\Omega t}}{1 - i\Omega\tau}\right) + \text{c.c.}, \quad (10.6.7)$$

where we have introduced the wavevector magnitude q and frequency Ω associated with the material excitation, which are given by

$$q = k_L + k_S \quad \text{and} \quad \Omega = \omega_L - \omega_S. \quad (10.6.8)$$

Note that because the denominator of the second term in the expression for $\alpha_{\mathrm{NL}}(z,t)$ is a complex quantity, the nonlinear response will in general be shifted in phase with respect to the intensity distribution associated with the interference of the laser and Stokes fields. We shall see below that this phase shift is the origin of the gain of the stimulated Rayleigh-wing scattering process.

We next derive the equation describing the propagation of the Stokes field. This derivation is formally identical to that presented in Section 7.4 in our general discussion of two-beam coupling. To apply that treatment to the present case, we need to determine the values of the refractive indices n_0 and n_2 that are relevant to the problem at hand. We find that n_0 is obtained from the usual Lorentz–Lorenz law (see also Eq. (3.8.8a)) as

$$\frac{n_0^2 - 1}{n_0^2 + 2} = \tfrac{1}{3} N\alpha_0 \quad (10.6.9a)$$

and that the nonlinear refractive index is given (see also Eqs. (4.1.18) and (4.4.26)) by

$$n_2 = \left(\frac{n_0^2+2}{3}\right)^4 \frac{1}{2n_0^2\epsilon_0 c} N\bar{\alpha}_2. \tag{10.6.9b}$$

Then, as in Eq. (7.4.15), we find that the spatial evolution of the Stokes wave is described by

$$\frac{dA_S}{dz} = \frac{2in_0n_2\omega_S}{c}\left(A_L A_L^* + A_S A_S^*\right)A_S + \frac{2in_0n_2\omega_S}{c}\frac{A_L A_L^* A_S}{1+i\Omega\tau}. \tag{10.6.10}$$

Here the first term on the right-hand side leads to a spatial variation of the phase of the Stokes, whereas the second term leads to both a phase variation and to amplification of the Stokes wave. The gain associated with stimulated Rayleigh-wing scattering can be seen more clearly in terms of the equation relating the intensities of the two waves, which are defined by

$$I_j = 2n_0\epsilon_0 c|A_j|^2, \quad j = L, S. \tag{10.6.11}$$

The spatial variation of the intensity of the Stokes wave is therefore described by

$$\frac{dI_S}{dz} = 2n_0\epsilon_0 c\left[A_S\frac{dA_S^*}{dz} + A_S^*\frac{dA_S}{dz}\right]. \tag{10.6.12}$$

Through use of Eq. (10.6.10), we can write this result as

$$\frac{dI_S}{dz} = g_{\mathrm{RW}} I_L I_S, \tag{10.6.13}$$

where we have introduced the gain factor g_{RW} for estimated Raleigh-wing scattering, which is given by

$$g_{\mathrm{RW}} = g_{\mathrm{RW}}^{(\max)}\left(\frac{2\Omega\tau}{1+\Omega^2\tau^2}\right), \tag{10.6.14a}$$

where $g_{\mathrm{RW}}^{(\max)}$ denotes the maximum value of the gain factor, which is given by

$$g_{\mathrm{RW}}^{(\max)} = \frac{n_2\omega_S}{c} = \left(\frac{n_0^2+2}{3}\right)^4 \frac{2\omega_S N(\alpha_\parallel - \alpha_\perp)^2}{45kTn_0^2\epsilon_0 c^2}. \tag{10.6.14b}$$

We have made use of Eqs. (10.6.4) and (10.6.9b) in obtaining the second form of the expression for $g_{\mathrm{RW}}^{(\max)}$.

The frequency dependence of the gain factor for stimulated Rayleigh-wing scattering as predicted by Eq. (10.6.14a) is illustrated in Fig. 10.6.2. We see

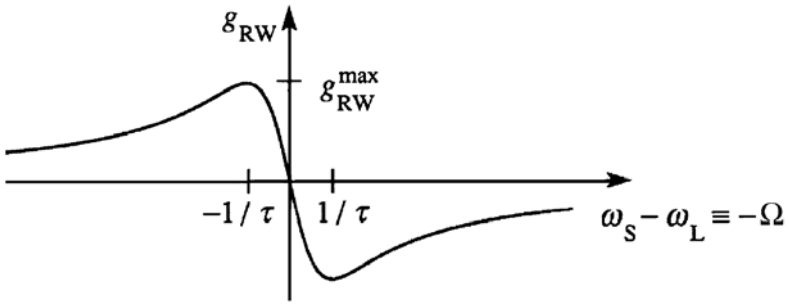

FIGURE 10.6.2 Frequency dependence of the gain factor for stimulated Rayleigh-wing scattering.

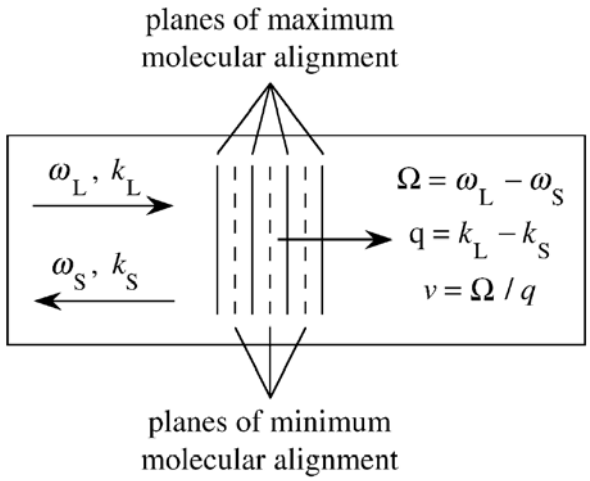

FIGURE 10.6.3 Nature of stimulated Rayleigh-wing scattering.

that amplification of the ω_S wave occurs for $\omega_S < \omega_L$ and that attenuation occurs for $\omega_S > \omega_L$. The maximum gain occurs when $\Omega \equiv \omega_L - \omega_S$ is equal to $1/\tau$.

The nature of the stimulated Rayleigh-wing scattering process is illustrated schematically in Fig. 10.6.3. The interference of the forward-going wave of frequency ω_L and wavevector magnitude k_L and the backward-going wave of frequency ω_S and wavevector magnitude k_S produces a fringe pattern that moves slowly through the medium in the forward direction with phase velocity $v = \Omega/q$. The tendency of the molecules to become aligned along the electric field vector of the total optical wave leads to planes of maximum molecular alignment alternating with planes of minimum molecular alignment. As mentioned above, these planes are shifted in phase with respect to the maxima and minima of the intensity distributions. The scattering of the laser field from this periodic array of aligned molecules leads to the generation of the Stokes wave. The scattered radiation is shifted to lower frequencies

because the material disturbance causing the scattering is moving in the forward direction. The scattering process shows gain because the generation of Stokes radiation tends to reinforce the modulated portion of the interference pattern, which leads to increased molecular alignment and thus to increased scattering of Stokes radiation.

10.6.1. Polarization Properties of Stimulated Rayleigh-Wing Scattering

A theoretical analysis of the polarization properties of stimulated Rayleigh-wing scattering has been conducted by Chiao and Godine (1969). The details of their analysis are quite complicated; here we shall simply quote some of their principal results.

In order to treat the polarization properties of stimulated Rayleigh-wing scattering, one must consider the tensor properties of the material response. The analysis of Chiao and Godine presupposes that the nonlinear contribution to the susceptibility obeys the equation of motion

$$\tau \frac{d}{dt} \Delta\chi_{ik} + \Delta\chi_{ik} = C\left(\langle \tilde{E}_i \tilde{E}_k \rangle - \tfrac{1}{3}\delta_{ik}\langle \tilde{\mathbf{E}} \cdot \tilde{\mathbf{E}} \rangle\right), \tag{10.6.15}$$

where, ignoring for the present local-field corrections, the proportionality constant C is given by

$$C = \frac{N\epsilon_0^2(\alpha_\parallel - \alpha_\perp)^2}{15kT}. \tag{10.6.16}$$

Note that the trace of the right-hand side of Eq. (10.6.15) vanishes, as required by the fact that Rayleigh-wing scattering is described by a traceless, symmetric permittivity tensor.

By requiring that the Stokes wave obey the wave equation with a susceptibility given by the solution to Eq. (10.6.15), and taking account of rotation of the pump laser polarization (see, for example, the discussion in Section 4.2), Chiao and Godine calculate the gain factor for stimulated Rayleigh-wing scattering for arbitrary polarization of the laser and Stokes fields. Some of their results for special polarization cases are summarized in Table 10.6.2.

For any state of polarization of the pump wave, some particular polarization of the Stokes wave will experience maximum gain. As a consequence of the large value of the gain required to observe stimulated light scattering ($g_{\mathrm{RW}} I_L L \simeq 25$), the light generated by stimulated Rayleigh-wing scattering will have a polarization that is nearly equal to that for which the gain is maximum. The relation between the laser polarization and the Stokes polarization for which the gain is maximum is illustrated in Table 10.6.3. Note that the

TABLE 10.6.2 Dependence of the gain factor for stimulated Rayleigh-wing scattering in the backward direction on the polarization of the laser and Stokes waves for the cases of linear and circular polarization [a]

Laser polarization				
Stokes polarization				
Gain factor	1	3/4	3/2	1/6

[a] The arrows on the circles denote the direction in which the electric field vector rotates in time at a fixed position in space. The gain factors are given relative to that given by Eqs. (10.5.14) for the case of linear and parallel polarization.

TABLE 10.6.3 Relation between laser polarization and the Stokes polarization experiencing maximum gain in backward stimulated Rayleigh-wing scattering

Laser			
Stokes			

generated wave will be nearly, but not exactly, the polarization conjugate (in the sense of vector phase conjugation, as discussed in Section 7.2) of the incident laser wave. In particular, the polarization ellipse of the generated wave will be rounder and tilted with respect to that of the laser wave.

Zel'dovich and Yakovleva (1980) have studied theoretically the polarization properties of stimulated Rayleigh-wing scattering for the case in which the pump radiation is partially polarized. They predict that essentially perfect vector phase conjugation can be obtained by stimulated Rayleigh-wing scattering for the case in which the pump radiation is completely depolarized in the sense that the state of polarization varies randomly over the transverse dimensions of the laser beam. The wavefront-reconstructing properties of stimulated Rayleigh-wing scattering have been studied experimentally by Kudriavtseva *et al.* (1978), and the vector phase conjugation properties have been studied experimentally by Miller *et al.* (1990).

The analysis of stimulated Rayleigh-wing scattering in the forward and near-forward direction is much more complicated than that of backward stimulated Rayleigh-wing scattering because the possibility of Stokes–anti-Stokes coupling (as described in Section 10.4 for stimulated Raman scattering) must be included in the analysis. This situation has been described by Chiao *et al.* (1966) and by Chiao and Godine (1969).

Problems

1. *Estimation of the properties of stimulated Raman scattering.* By making reasonable assumptions regarding the value of the parameter $(d\alpha/dq)$, perform an order-of-magnitude estimate of the gain factor for stimulated Raman scattering for condensed matter, and compare this value with the measured values given in Table 10.2.1.
2. *Polarization properties of stimulated Rayleigh-wing scattering.* By carrying out the prescription described in the first full paragraph following Eq. (10.6.16), verify that the entries in Table 10.6.2 are correct.

References

Stimulated Raman Scattering

Bloembergen, N., Shen, Y.R., 1964. *Phys. Rev. Lett.* **12**, 504.

Bloembergen, N., 1967. *Amer. J. Phys.* **35**, 989.

Boyd, R.W., 1983. *Radiometry and the Detection of Optical Radiation*. Wiley, New York.

Eckhardt, G., Hellwarth, R.W., McClung, F.J., Schwarz, S.E., Weiner, D., Woodbury, E.J., 1962. *Phys. Rev. Lett.* **9**.

Garmire, E., Pandarese, F., Townes, C.H., 1963. *Phys. Rev. Lett.* **11**, 160.

Hellwarth, R.W., 1963. *Phys. Rev.* **130**, 1850.

Kaiser, W., Maier, M., 1972. In: Arecchi, F.T., Schulz-DuBois, E.O. (Eds.), *Laser Handbook*. North-Holland.

Penzkofer, A., Laubereau, A., Kaiser, W., 1979. *Prog. Quantum Electron.* **6**, 55.

Raymer, M.G., Mostowski, J., 1981. *Phys. Rev.* **A24**, 1980.

Raymer, M.G., Walmsley, I.A., 1990. In: Wolf, E. (Ed.), *Progress in Optics, Vol. 28*. North-Holland, Amsterdam.

Simon, U., Tittel, F.K., 1994. In: Hulet, GU., Dunning, F.B. (Eds.), *Methods of Experimental Physics, Vol. III*. Academic Press, San Diego.

Terhune, R.W., 1963. *Bull. Am. Phys. Soc.* **8**, 359.

Woodbury, E.J., Ng, W.K., 1962. *Proc. I.R.E.* **50**, 2367.

Further Reading on Tensor Properties of Stimulated Raman Scattering

Happer, W., 1972. *Rev. Mod. Phys.* **44**, 169.
Holmes, R., Flusberg, A., 1988. *Phys. Rev.* **A37**, 1588.
Landau, L.D., Lifshitz, E.M., 1960. In: *Electrodynamics of Continuous Media*. Pergamon Press, Oxford, p. 383.
Pritchett, T., Smith, J., Mcintyre, G., Moore, T.R., Oldaker, B.G., 1999. *J. Mod. Optics* **46**, 949.
Venkin, G.V., Ilinskii, Y.A., Mikheev, G.M., 1985. *Kvantovaya Elektron. (Moscow)* **12**, 608. *Sov. J. Quantum Electron.* **15** (1985) 395.

Coherent Anti-Stokes Raman Scattering

Levenson, M.D., Flytzanis, C., Bloembergen, N., 1972. *Phys. Rev.* **B6**, 3962.
Levenson, M.D., Bloembergen, N., 1974. *Phys. Rev.* **B10**, 4447.
Levenson, M.D., Kano, S.S., 1988. *Introduction of Nonlinear Laser Spectroscopy*. Academic Press, Boston.
Maker, P.D., Terhune, R.W., 1965. *Phys. Rev.* **137**, **A**801.
Volkmer, A., 2005. *J. Phys.* **D38**, R59.

Stimulated Rayleigh-Wing Scattering

Bloembergen, N., Lallemand, P., 1966. *Phys. Rev. Lett.* **16**, 81.
Chiao, R.Y., Godine, J., 1969. *Phys. Rev.* **185**, 430.
Chiao, R.Y., Kelley, P.L., Garmire, E., 1966. *Phys. Rev. Lett.* **17**, 1158.
Cho, C.W., Foltz, N.D., Rank, D.H., Wiggins, T.A., 1967. *Phys. Rev. Lett.* **18**, 107.
Denariez, M., Bret, G., 1968. *Phys. Rev.* **177**, 171.
Foltz, N.D., Cho, C.W., Rank, D.H., Wiggins, T.A., 1968. *Phys. Rev.* **165**, 396.
Kudriavtseva, A.D., Sokolovskaia, A.I., Gazengel, J., Phu Xuan, N., Rivorc, G., 1978. *Opt. Commun.* **26**, 446.
Mash, D.I., Morozov, V.V., Starunov, V.S., Fabelinskii, I.L., 1965. *JETP Lett.* **2**, 25.
Miller, E.J., Malcuit, M.S., Boyd, R.W., 1990. *Opt. Lett.* **15**, 1189.
Zel'dovich, B.Ya., Yakovleva, T.V., 1980. *Sov. J. Quantum Electron.* **10**, 501.